CHALMERS
UNIVERSITY OF TECHNOLOGY

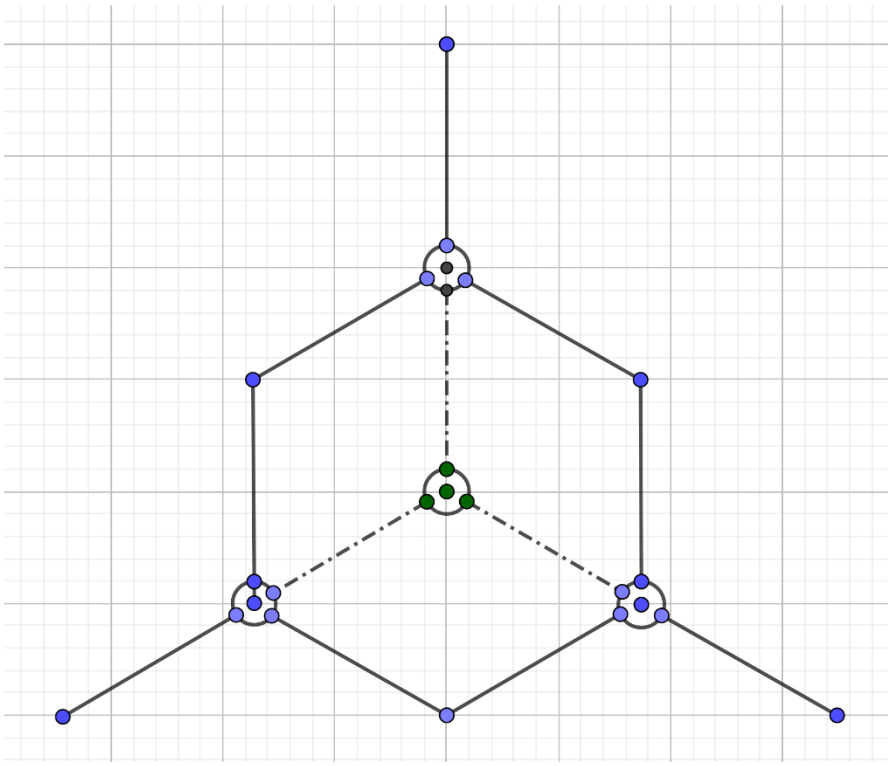

Efficient point absorbing wave energy converter configurations: influence of environment and array design

Master's thesis in the International Master´s Programme Naval Architecture and Ocean Engineering

CHARLENE VANCE

Department of Mechanics and Maritime Sciences
CHALMERS UNIVERSITY OF TECHNOLOGY
Gothenburg, Sweden 2018
Master's Thesis 2018/36

MASTER'S THESIS IN THE INTERNATIONAL MASTER'S PROGRAMME IN NAVAL ARCHITECTURE AND OCEAN ENGINEERING

Efficient point absorbing wave energy converter configurations: influence of environment and array design

CHARLENE VANCE

Department of Mechanics and Maritime Sciences

Division of Marine Technology

CHALMERS UNIVERSITY OF TECHNOLOGY

Göteborg, Sweden 2018

Efficient point absorbing wave energy converter configurations: influence of environment and array design
CHARLENE VANCE

Master's Thesis 2018/36
Department of Mechanics and Maritime Sciences
Division of Marine Technology
Chalmers University of Technology
SE - 412 96 Göteborg
Sweden
Telephone: + 46 (0)31-772 1000

Cover: Example design of a three-buoy array configuration.

Printed by Chalmers Reproservice

Göteborg, Sweden 2018

Efficient point absorbing wave energy converter configurations: influence of environment and array design
Master's Thesis in the International Master's Programme in Naval Architecture and Ocean Engineering
CHARLENE VANCE
Department of Mechanics and Maritime Sciences
Division of Marine Technology
Chalmers University of Technology

Abstract

Waves are a sustainable energy resource that have significant potential for utilization. Point absorbing wave energy converters (WECs) use the heave motion of the waves to generate electricity. Configurations include the WEC buoy, mooring system, and electricity collection system. This thesis studies key parameters that affect the performance of the point absorbing WEC configuration through analyzing the power absorption of the WEC and fatigue life of the mooring lines. Waves4Power's WaveEL 3.0 device, installed in Runde, Norway, is used as a baseline model for hydrodynamic and structural response simulations. Two versions of the WaveEL buoy are considered with different shaft lengths. The environmental conditions at various locations are studied. Basic arrays of three (TriBuoy) and four (SquareBuoy) are then designed. Single buoy configurations are simulated with the conditions found at various studied locations, while array configurations are simulated applying the environmental conditions found at Runde. Simulations are run through SESAM software. The results are then post-processed in MATLAB. Fatigue life and power absorption are studied varying environmental parameters, mooring system, and WEC buoy version. Select configurations are further analyzed through an analysis of LCOE and LCA. The results show that optimal mooring line geometry depends on the depth at the location, and that optimal WEC buoy shaft length depends on the average sea conditions at the location. The best location in terms of power absorption for the WaveEL device is Garðskagi, Iceland. The array simulations at Runde show that small WEC separating distances will limit the mooring line length, which will result in lower power absorption and lower fatigue lives in the mooring lines. The LCOE shows that the SquareBuoy configuration is the most profitable, and that assuming a different sea state affects the calculated LCOE significantly. The LCA shows that the main process contribution to climate change is the manufacturing of the WEC buoy itself, and that the buoy with the longer shaft has a higher environmental impact per MWh produced. The final recommendations are to further explore the Garðskagi site for WEC farm potential, to use a mooring line geometry that is optimized depending on the water depth, to choose a large enough separating distance between WECs where the optimal mooring line geometry can be applied, and to focus on decreasing the costs and CO_2 emissions associated with the manufacturing of the WEC buoy. It is also recommended to simulate for more sea states and run more analyses in further stages when more details are obtained about the sites and properties of the WEC system.

Keywords: fatigue, LCOE, LCA, point absorber, wave energy, WEC array, WEC mooring system

Table of Contents

Preface

This thesis is part of the requirements for the master's degree at Chalmers University of Technology, Göteborg, and has been carried out at the Division of Marine Technology, Department of Mechanics and Maritime Sciences, Chalmers University of Technology between January and June of 2018. It is also part of the requirements for the Nordic 5 Tech Joint Nordic Master's degree program in Innovative Sustainable Energy Engineering – Heat and Power Engineering track between Chalmers University of Technology and the University of Iceland.

I would like to thank my supervisor and examiner Professor Jonas Ringsberg at the Department of Mechanics and Maritime Sciences, Chalmers University of Technology for his knowledge, feedback and encouragement throughout this work. I would also like to thank my co-supervisor Hafþór Sigurjónsson at the School of Engineering and Natural Sciences, University of Iceland for his contribution to this work. I would like to thank Adjunct Professor Erland Johnson at the Department of Mechanics and Maritime Sciences for his valuable comments and Xiao Lang at the Department of Mechanics and Maritime Sciences for his generous help.

I would like to give special thanks to Shun-Han Yang in the Department of Mechanics and Maritime Sciences, Chalmers University of Technology for her knowledge and feedback throughout these months and particularly for her unwavering guidance in the modelling and simulations done in this work.

I would also like to thank Waves4Power AB for providing information and motivation for the models and simulations performed in this thesis work, and Vegagerðin and SMHI for their cooperation in obtaining relevant data.

Finally, I would like to thank my family and friends for their endless support and love. Thank you for encouraging me to chase my dreams, wherever and whatever they bring me.

Göteborg, June 2018

Charlene Vance

Nomenclature

List of acronyms

ELCD	European Life Cycle Database
ILCD	International reference Life Cycle Database system
LCA	Life Cycle Assessment
LCI	Life Cycle Inventory
LCIA	Life Cycle Impact Assessment
LCOE	Levelized Cost Of Energy
LCS	Life-cycle Cost System
PTO	Power Take-Off
WACC	Weighted Average Cost of Capital
WEC	Wave Energy Converter

List of unit abbreviations

deg	degrees
kg	kilograms
kW	kilowatt
kWh	kilowatt-hours/year
m	meters
N	newtons
s	seconds

Variables

WEC power absorption		*Unit*
$\bar{P}$	average power absorption	kW
T	total time	S
B_{33}^{PTO}	linear PTO damping coefficient	Ns/m
$\xi(t)$	WEC motion in the heave direction	M

Fatigue life		*Unit*
FD	accumulated fatigue damage	-
n_i	number of axial stress cycles at the stress range	-
S_i	stress range	N/m^2
S_C	characteristic strength	N/m^2
R_i	ratio between S_i and S_C	-
S_{MBS}	minimum breaking strength	N/m^2
m	material parameter, dependent on material	-
α	material parameter, dependent on material	-

Environment		*Unit*
H_s	significant wave height	m
T_p	wave period	S
dir_{wave}	dominant wave direction	deg
V_{wind}	wind speed	m/s
dir_{wind}	dominant wind direction	deg
V_{curr}	current speed	m/s
dir_{curr}	dominant current direction	deg

LCOE		*Unit*
E	total electricity produced by the offshore energy farm	kWh/year
$E_{1DEVICE}$	energy produced by one device	kWh/year
NA	number of devices	-
$\eta_{availability}$	percentage of availability	-
$\eta_{transmission}$	transmission efficiency	-
N_{farm}	lifetime of the offshore energy farm	years
n	period of life cycle from year 0 to year N_{farm}	year
r	discount rate	-

1 Introduction

1.1 Background and Motivation of Study

Climate change will cause considerable damage to humans and the environment if immediate action is not taken. The European Environment Agency (2017) warns that with land and sea temperatures increasing, sea levels rising, and precipitation patterns changing, significant effects on biodiversity and human lives can be expected. Extreme weather can cause massive destruction, ecosystems can fail, large industries such as forestry, fishery and agriculture can be severely affected, and the communities hit hardest with climate change impacts can be faced with economic and resource costs that they are unable to meet.

To reduce the severe impacts of climate change, the Paris Agreement aims to limit the global average temperature increase to 1.5 degrees above pre-industrial levels (United Nations, 2015a). For this an immediate response is needed that rapidly reduces greenhouse gas emissions; however, the United Nations (2015a) also stress that mitigation measures must not hinder socioeconomic growth, food security, or the needs of developing countries.

The concept of sustainability is essential to meet these goals. Most famously defined by Bruntland and the World Commission on Environment and Development in the report "Our Common Future" (1987, p. 41), sustainable development is "development that meets the needs of the present without compromising the ability of future generations to meet their own needs". For a product or service to be truly sustainable, it is important that the three key dimensions of sustainable development: economical, ecological, and social development, must all be fulfilled.

In this context, renewable energy can contribute to sustainable development in a number of ways. Increasing the share of renewables can diversify local and global energy supplies, increasing energy security and accessibility, create jobs in a rapidly growing market, and reduce the carbon footprint of the heat and power generation sector by replacing the burning of fossil fuels, which can then contribute to a better ecological environment and better air quality, water quality, and human health. Consequently, the renewable energy market is growing. The share of modern renewables such as geothermal, solar, wind, and ocean energies in the world primary energy supply increased from 0.1% in 1973 to 1.5% in 2014 (IEA, 2017). In terms of world electricity generation, the share of renewables increased from 0.6% in 1973 to 7.1% in 2015[1] (IEA, 2017).

One renewable energy source of increasing interest for electricity generation is marine or ocean energy. Ocean energy is not only a non-polluting energy source but has massive potential for energy generation. In their Ocean Energy Forum (2016), the European Commission finds that by 2050, 100 GW of ocean energy could be deployed in Europe and that ocean energy could potentially represent 10% of the European Union's power supply. This explosion in ocean energy capacity could be a huge benefit to the European industry and economy, with an annual market of up to €53 billion by 2050 (Ocean Energy Forum, 2016). The benefits of this proportion further extend to the environment. By 2050, power generated by the ocean energy sector could avoid the equivalent of 276 tons of CO_2 emissions annually (Ocean Energy Forum, 2016). Through these benefits, the development of ocean energy technologies directly contributes to the development of affordable and clean energy, climate action, and sustainable

[1] Including non-renewable wastes, not including hydropower.

economic growth. These represent three of the United Nations 17 Sustainable Development Goals for ending poverty, protecting the environment and ensuring prosperity for all (United Nations, 2015b). However, as can be seen in Figure 1.2, through contributing to these three goals, the development of ocean energy technologies then could indirectly contribute to all other goals. Thus, in all aspects ocean energy contributes to sustainable development.

Figure 1.1: The United Nation's 17 Sustainable Development Goals (United Nations, 2015b).

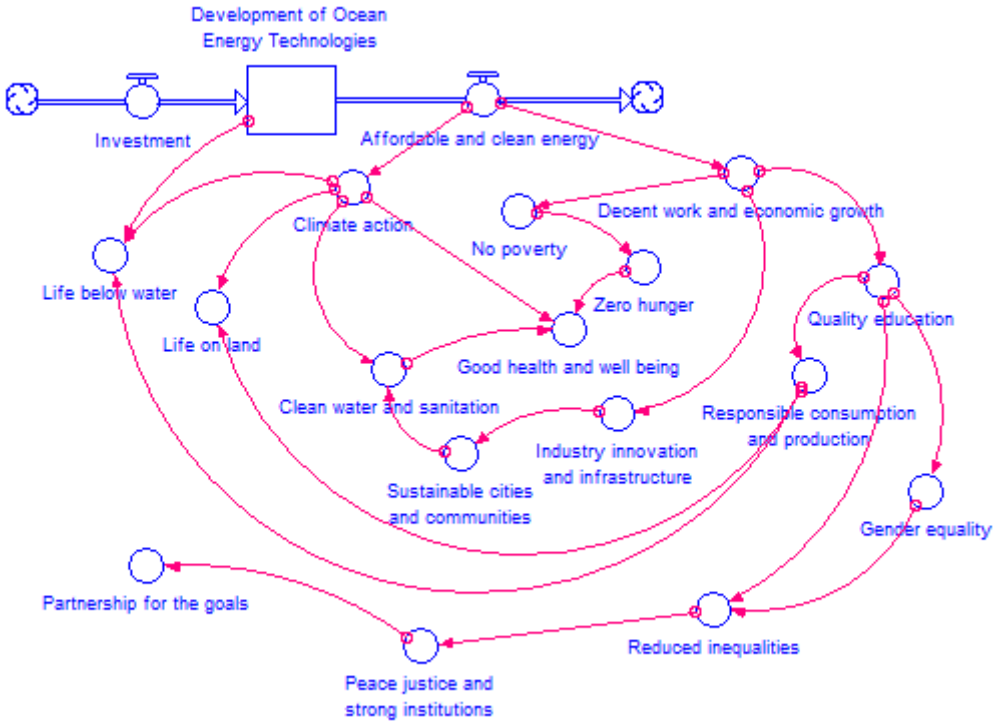

Figure 1.2: Causal loop diagram relating all of the 17 sustainable development goals [created with STELLA (isee systems, 2013)].

The main ocean energy technologies currently in development and deployment take advantage of the waves, currents, tides, thermal properties and salinity gradients found in various sea waters (Ocean Energy Forum, 2016). Tidal range technology, the furthest developed technology, is similar to hydropower, using differences in water levels between the high and low tides to produce electricity. Tidal stream turbines utilize the flow of currents to produce electricity, and wave energy converters (WECs) use the movement of waves. Ocean Thermal Energy Conversion (OTEC) uses the temperature gradient between oceans' cold deep waters and warm surface waters to produce electricity, and salinity gradient power generation uses osmosis or reverse electro dialysis (RED) to produce electricity from differences in salt content between freshwater and saltwater.

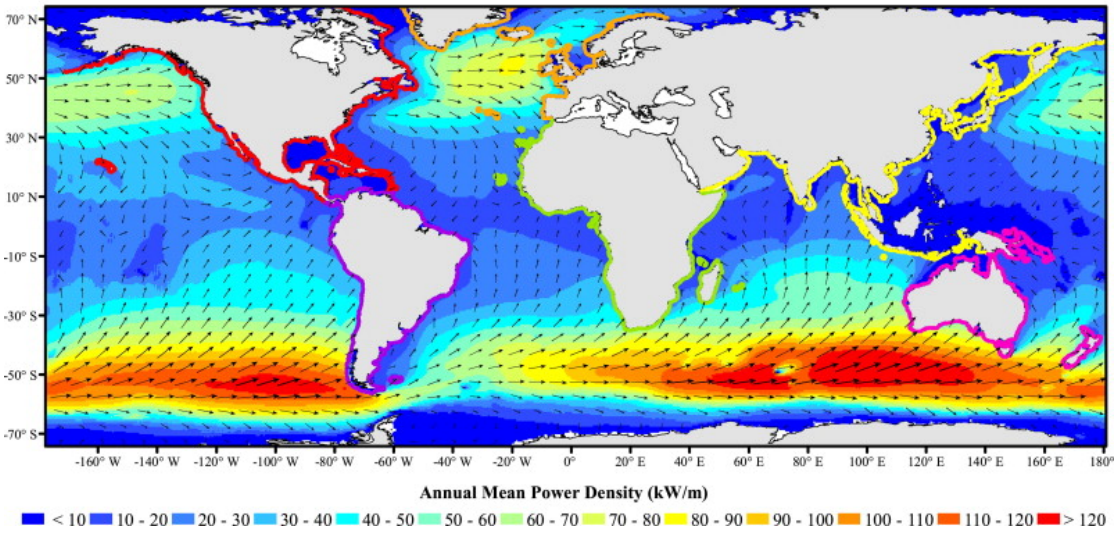

Figure 1.3: Global distribution of annual wave power potential (Gunn & Stock-Williams, 2012).

Wave energy is particularly interesting for many investors due to its massive potential. According to the World Energy Council (2016), the total theoretical potential of wave energy alone is 32 PWh/year; by contrast, the world electricity generation in 2015 was 24 PWh (IEA, 2017). As seen in Figure 1.3, the southern oceans have significant wave power potential, with the highest mean power found in the area southwest of Australia. In the northern oceans, the regions southwest of Alaska and to the west of the European continent have the highest potentials.

The innovation of design in wave energy conversion technologies is also impressive. Some of the main types of wave energy converters (WECs) are oscillating water columns, overtopping devices, attenuators and point absorbers. Oscillating water columns (OWCs) use the oscillation of water level induced by a wave as a piston to compress air and drive a turbine (World Energy Council, 2016). Overtopping devices collect breaking waves into a reservoir as potential energy and generate energy through a low-head hydraulic turbine. Attenuators are offshore devices either surface floating or fully submerged which use wave power to create oscillations between adjacent components (World Energy Council, 2016). Finally, point absorbers use the relative motion between a floating oscillating body and a fixed component to generate energy (Vicente et al., 2009). They are nearshore devices which are relatively small in comparison to the wavelengths from which they extract energy.

The Swedish company Waves4Power has developed just one example of a successful WEC design. Their WaveEL buoy is a point absorber with a long vertical acceleration tube encompassing a water piston that acts like "a gigantic pump" (Waves4Power, 2017a). Point absorbers are well known for their survivability in the ocean environment, as they ride the movements of the ocean instead of fighting against them. Thus, an important aspect of the WaveEL device is that it includes a mooring system that secures the WEC while allowing free vertical movement (Waves4Power, 2017a). It also includes a dynamic cable connecting the buoy to the electricity collection hub. In 2016 Waves4Power installed a full-scale prototype, the WaveEL 3.0, including the buoy, mooring system, cable and hub at a demonstrate site off the coast of Runde, Norway (Waves4Power, 2017b). In 2017 the system began delivering electricity to the local power grid through a subsea cable. The purpose of the installation is to demonstrate the reliability of the energy production and survivability of the WaveEL system to investors and to the world (Waves4Power, 2017b).

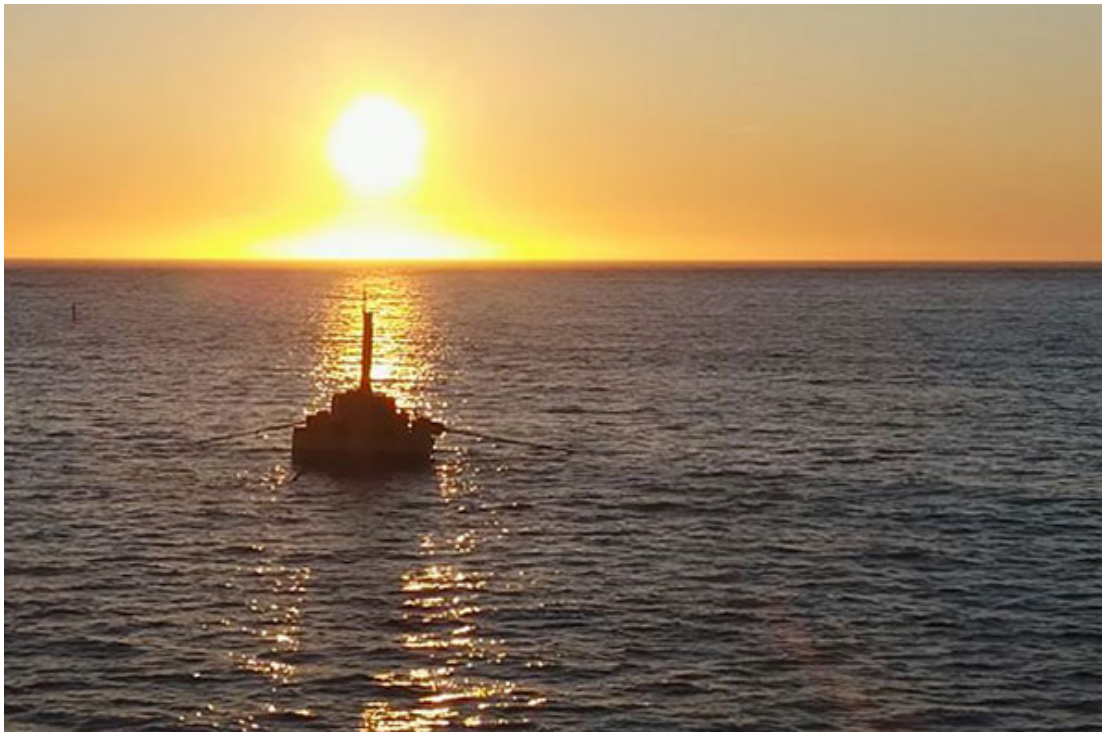

Figure 1.4: Waves4Power's installed prototype WaveEL 3.0 Buoy (Waves4Power, 2017a).

Despite positive developments, ocean energy is still by far one of the smallest contributors to electricity generation, and wave energy a small fraction of that. The total renewable power capacity (excluding hydropower) was 921 GW in 2016; by contrast, there was only approximately 536 MW of operating capacity for all ocean energies combined by the end of 2016, with tidal range contributing to 90% of the ocean energy operating capacity (Ren21, 2017). As of mid-2016, a mere 12 MW of wave energy had been deployed in the European Union (Ocean Energy Forum, 2016). This is mainly due to the continuing economic challenges of relatively high risk and high upfront costs, as wave energy is still mostly in the pre-commercial development stage (Ren21, 2017). Furthermore, along with other ocean energies, wave energy engineering includes the difficulties of marine spatial planning and permitting, where jurisdiction is often unclear and licensing and consenting processes are inefficient (Ren21, 2017). In the ecological dimension, the impacts of ocean energy technologies are still

very much unknown. Effects currently investigated are potential interactions with marine animals, impacts of sound propagation and effects of electromagnetic fields generated from cables underwater (Ren21, 2017).

To demonstrate that the benefits of ocean energy technologies such as wave energy converters can outweigh the challenges, it is important to use various analyses to provide a comparison to other energy types as well as a comparison of different design alternatives. A common way to compare the economic attractiveness of renewable energy projects is through the calculation of levelized cost of energy (LCOE), which weighs the total cost of a project from conception to decommission over the total energy generation of the project in its lifetime (Castro-Santos et al., 2016). To quantify and compare the environmental and social impact of different project alternatives, a Life Cycle Assessment (LCA) can be used. An LCA considers the defined lifetime of a product and determines the inputs and outputs associated with a functional unit (Uihlein, 2016). Outputs in the form of emissions can be assessed to find the biggest process contributions to impact categories such as climate change, human toxicity and land use.

With approximately €1 billion invested by the ocean energy industry to develop and deploy ocean energy technologies, growth is imminent (Ocean Energy Forum, 2016). For wave energy technologies, the next step in commercialization is to consider the design of large farms of devices (Göteman et al., 2014). Research must be focused on improving the feasibility of wave farm projects by increasing their efficiency, decreasing costs, and quantitatively assessing their contributions to sustainable development.

1.2 Objective and Goals

The objective of this thesis is to further the commercial development of wave energy technologies by studying the key factors that affect the efficiency of point absorbing WECs. By studying the effects of these factors in the form of a comprehensive parametric analysis, developers can distinguish which parameters have a significant effect on the performance of the system and which do not.

The first goal is to identify the desired outputs, then identify the key factors and variable parameters affecting those outputs. This can be done through a literature review. The parametric analyses will be done through running hydrodynamic and structural response simulations: thus the next goal is to have a realistic model of the WEC configuration and realistic inputs to the simulation, including environmental conditions that are reasonable for representing a specified location. The final goal is to analyze the output data using reliable methods that produce comparable numerical results. These goals will make it possible to make significant conclusions and recommendations, which developers can use to determine preferable installation sites, make appropriate design choices for a WEC array and mooring configuration at a given site, and calculate the economic, environmental and social impact of their project.

1.3 Delimitations

In this thesis, only point absorbing type WECs are discussed. Specifically, in the simulations and analyses performed, the WaveEL device designed by Waves4Power will be used as a baseline model. This thesis will consider two predetermined versions of the WaveEL buoy with different geometries, called V1 and V2. As will be described in further detail in section 4.1, the only difference between the versions is the length of the acceleration tube.

Variations of mooring system properties such as mooring line material, mooring line cross-section, floater type and anchor type are not considered. Only variations of the mooring line lengths and the presence of floater units will be considered.

The electricity collection system including cable and hub is considered minimally in this thesis work. As will be explained further in section 6, the modelling of the cable and hub is neglected in array simulations due to incompatibility with some of the designed arrays. No investigation is performed on the responses of the cable to parameter variations and its effects on the efficiency of the WEC system. The effects of biofouling on all components will be neglected.

Many additional assumptions and simplifications are made to limit the number of parameters analyzed, the number of simulations performed, and the simulation time. These will be described in further detail in the upcoming sections.

1.4 Outline of Thesis Work

The following outline of the thesis work gives the number and name of each chapter, relevant page numbers and a brief summary of the contents.

Chapter	Title	Pages	Description
2	Literature Review	9-12	State-of-the-art research is studied to understand how to calculate the power absorption and lifetime of a WEC system, explore the factors that affect the success of WEC system and identify the key parameters that contribute to that success.
3	Methodology	13-19	The workflow of the thesis is described, as well as the software used, simulation procedure, post-processing methods, LCOE, LCA, and basic assumptions.
4	Baseline Configuration	21-25	Details can be found regarding the baseline configuration used in the simulation processes. This includes descriptions and simplified schematics of the two versions of the WEC buoy, initial mooring configuration, and initial electricity collection system.
5	Location Study	27-39	This section describes the geographical location, water depth and wave, wind, and current conditions from the following locations: Runde, Norway (section 5.1, pp. 27-29), San Juan, Puerto Rico (section 5.2, pp. 30-32), Väderöarna and Läsö Ost, Sweden (section 5.3, pp. 33-37), and Garðskagi and Grimseyjarsund, Iceland (section 5.4, pp. 37-39).
6	Array Design Selection	41-45	The array designs TriBuoy and SquareBuoy are introduced, and the motivation for how and why they were chosen is described.
7	Results and Discussion	47-87	This section is divided into 4 large subsections. Single buoy simulations (section 7.1, pp. 47-66): compares single buoy simulations including a base case with a variation in environmental location, mooring configuration, WEC buoy type and sea state.

			Array simulations (section 7.2, pp. 67-80): compares simulations of array configurations with a variation in mooring configuration, WEC buoy type and sea state. LCOE (section 7.3, pp. 80-83): select array configurations are compared through their LCOE. LCA (section 7.4, pp. 83-87): select array configurations are compared through their environmental and social impact.
8	Conclusions	89-90	This section summarizes and concludes the main findings of the results section.
9	Recommendations	91-92	Possible applications of the thesis work and prospective future topics of research are explored.

2 Literature Review

The purpose of the literature review is to gain insight into the most influential factors in WEC efficiency and sustainability. This is done by reviewing state-of-the-art technology and research in point absorbing wave energy converters, WEC arrays, and WEC mooring systems. It is also important to identify which challenges are known in this topic, and what solutions have been proposed or can be explored in the work done in this thesis.

2.1 Theory

The purpose of a wave energy converter is quite simply to generate electricity. The most important indicators to judge the effectiveness of a WEC are consequently its power absorption and the lifetime that the WEC system will be in operation. In a point absorbing wave energy converter, the vertical translational motion, known as heave, and vertical rotational motion, known as pitch, are the important motions for the energy conversion (World Energy Council, 2016). In some point absorbing WECs such as the WaveEL device, the power absorption is only a function of the heave motion, and can be represented through equation 1 (Yang et al., 2017):

$$\bar{P} = \frac{1}{T}\int_0^T B_{33}^{PTO}\,[\dot{\xi}(t)]^2 dt \tag{1}$$

By damping the relative vertical movement of the WEC, energy is captured by the system (Waves4Power, 2017a). In the simplified power absorption equation above, a constant linear power take-off (PTO) damping coefficient is assumed. However, in a smart WEC device, PTO damping should be automatically adjusted to optimize power absorption at the incident wave conditions (Waves4Power, 2017a).

The lifetime of a WEC device includes not only the lifetime of the WEC buoy but also the lifetime of the mooring system, power cable and electricity hub. Slender elements such as the mooring lines are a particularly important consideration in the lifetime of the system (Yang et al., 2017). Mooring lines connect the fixed anchors to the floating WEC buoy. They must keep the WEC device from floating away while giving it freedom to follow the wave movements and are constantly subject to line tensions induced by environmental loads (DNV GL, 2015). The lifetime of a mooring line can be assumed to be its fatigue life, which is calculated from the accumulated fatigue damage due to cyclic loads acting on the line elements. For inelastic materials, fatigue damage can be calculated through equation 2 and the S-N diagram (Yang et al., 2017). The number of stress cycles for irregular loading can be counted using analytical software through a method called rainflow counting (WAFO-group, 2017).

$$FD = \sum_i \frac{n_i {S_i}^m}{\alpha} \tag{2}$$

If elastic materials are used, the R-N relationship is applied. The fatigue damage can be calculated through equation 3:

$$FD = \sum_i \frac{n_i {R_i}^m}{\alpha} \tag{3}$$

The characteristic strength is used to calculate the R ratio and is represented by equation 4:

$$S_C = 0.95 * S_{MBS} \tag{4}$$

2.2 Parameter Selection

It is important to consider all of the factors that influence the power absorption and lifetime of individual WEC configurations and particularly arrays of WECs in the steps towards commercialization. There are two types of influencing factors discussed: internal factors, which are affected by the design and thus controllable, and external factors, such as future weather conditions that are uncontrollable. Parameters refer to the variables that can be numerically and systematically varied to study these factors.

For an individual WEC, internal factors include WEC type, WEC size, mooring system and electricity collection system. In this thesis, only a point absorber modelled after the Waves4Power WaveEL device is considered so variation of the WEC type will not be included. A redesign of the electricity collection system is also not considered. In an array of WECs, the forces on the WECs and their components are complicated by interaction effects between WECs. Waves are radiated and diffracted by each WEC, causing either constructive or destructive interference with the other WECs (Borganino et al., 2012). Constructive interference corresponds to an addition of wave amplitudes while destructive interference corresponds to a subtraction of wave amplitudes (de Andres et al., 2014). These interactive effects will influence the performance and lifetime of individual WECs as well as the total power production and variance, and are affected by the WEC separation, array configuration, array orientation, and array size. Thus, in this literature review the factors studied are the WEC size, mooring line material, mooring line configuration, WEC separation distance, array configuration, array orientation, and array size.

A WEC's size can be measured through multiple parameters: volume, mass, surface area, or its specific dimensions. Generally, the larger the WEC area, the more energy can be captured, and thus the higher the power absorption (Göteman et al., 2014). However, in larger sizes the cost of materials and cost of deployment also increases, which leads to many smaller WECs being more economical than few larger WECs (Göteman, 2017). Furthermore, larger WECs will lead to larger forces on the mooring system, which will require stronger lines and potentially higher costs. These are important considerations for commercialization and particularly in the design of WEC farms where there will be large-scale production of WEC devices.

One way of representing the efficiency of a WEC size is by its power-to-mass ratio, with higher power-to-mass ratios corresponding to higher efficiencies. Increasing the power-to-mass ratio indicates that for the same amount of power output, less mass is needed; thus, less materials need to be purchased and costs decrease per unit of power produced (Göteman, 2017). In his research Göteman (2017) suggests that in order to increase the total power-to-mass ratio in arrays, the array should include devices of different sizes and dimensions. Göteman et al. (2014) also find that increasing buoy size along the wave direction increases the total power output of the array.

The power absorption of a point absorbing WEC is maximized when the WEC's resonance frequency corresponds to the frequency of the incoming waves (Yang et al., 2016). However, each WEC has a limited resonant frequency bandwidth, which will limit the energy extraction in irregular wave climates with many different frequencies (Kim et al., 2015). The research of Kim et al. (2015) suggests that employing buoys of different resonant frequency bandwidths in a system can increase energy absorption by creating a wider frequency bandwidth. WEC

buoys with different shaft lengths can be used to investigate the effect of different resonant frequencies.

In the mooring lines, elastic materials with more compliant behavior are preferred (Yang et al., 2017). This is because though they are often used in the oil and gas industry, metallic materials such as chains or wire mooring are not an efficient way to moor point absorbing WECs. Metals are heavy and have high damping levels, which can increase the material costs and reduce the conversion efficiency (Paredes et al., 2016). Furthermore, metal corrosion is accelerated in marine applications. Thus, the use of synthetic materials such as polyester is suggested for WEC mooring systems.

The length of the mooring line as well as the horizontal distance from the WEC to the anchor has significant effects on both the power absorption and lifetime of the system. In the research of Yang et al. (2017) it is found that shorter mooring lines not only limit the movement of the WEC unit, but also have a significantly reduced fatigue life. However, if the system is faced with severe wave conditions, a shorter mooring line length will reduce the possibility of a slack line in severe wave conditions. Furthermore, as anchors can be placed closer together, shorter mooring lines will result in a mooring system that takes up less space. This could be a significant benefit for minimizing the size of wave energy parks (Paredes et al., 2016).

The mooring system should have the capability of withstanding the failure of one of its mooring lines, so having more lines reduces the risk of the WEC detaching and floating away (DNV GL, 2015). However, to minimize costs the number of mooring lines should be limited to three or four per WEC. Three line configurations are preferred as they give more freedom to the WEC's movement and thus result in higher power absorption than four line configurations (Yang et al., 2017). Furthermore, with less mooring lines WEC devices in arrays can be placed closer together and anchors can be shared by the mooring lines of different devices (Paredes et al., 2016). For very densely packed arrays, Vicente et al. (2009) suggest an interbody mooring connection, where a triangular array of WECs are drawn close to each other through a floater connection between them.

Buoy separation is found to be a key factor in the efficiency of a WEC array configuration. At small separating distances, the interaction effects between WECs is larger, and thus amplify both constructive and destructive effects (Borgarino et al., 2012). Conversely, at distances of over 2000m, interaction effects between buoys are negligible. In the research of de Andres et al. (2014), optimal buoy separation is found to be half the wavelength at the natural resonance period of the WEC. However, this research does not consider the mooring system layout, which may have a large influence on optimum WEC separation distance.

In design, the power absorption of point absorbers does not depend on wave incidence angle (Kim et al, 2015). However, with the inclusion of radiation and diffraction effects from interactions between the mooring system, electricity collection system, and other buoys in an array, wave incidence angle becomes more important. To achieve constructive interference between the WECs in the array, the incidence angle of the waves on the array has a large impact. Wave directionality in the considered location is thus important in deciding on the orientation of the array. For triangular arrays, the optimal angle of incidence is 30 degrees and for rectangular arrays, the optimal angle of incidence is 45 degrees (de Andres et al., 2014). Here triangular arrays refer to configurations of three equidistant WECs, and square arrays refer to configurations of four equidistant WECs. The study by de Andres et al. (2014) also

highlights the importance of variability of wave directionality on the chosen array layout. Generally, for unidirectional climates square configurations are more favorable; however, for multidirectional climates triangular configurations are more efficient (de Andres et al., 2014).

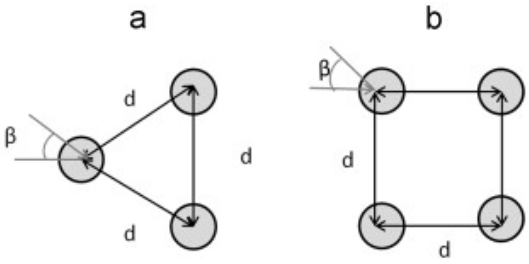

Figure 2.1: Triangular configuration (a) and square configuration (b) considered in the research of de Andres et al. (2014). β represents the angle of incidence and d represents the WEC separation distance.

The size of the array can also be influential on the overall effectiveness. Research finds that regarding point absorbers, larger arrays of smaller devices are more efficient than smaller arrays of larger devices (Göteman, 2017). Furthermore, as the number of WECs increases, the cost per device will decrease through the principle of economies of scale. In terms of power fluctuation, larger arrays can be successful in normalizing the power output (Göteman et al., 2014). In their research, Borgarino et al. (2012) find that the most significant interactions occur in the first three rows and that constructive effects generally cannot be maintained after more than three rows due to masking effects. However, as the positive and negative interactions cancel each other out, there is then more freedom in the separation distance of the WECs.

The external factors affecting the power absorption and fatigue life of WECs are the sea and environmental conditions. The environmental forces acting on the WEC configuration include the wave, wind, current and tides (DNV GL, 2017a). The parameters that are important in quantifying these loads are significant wave height, wave period, wave spectrum, wave direction, wind speed, wind direction, current speed as a function of water depth, and current direction (DNV GL, 2015). Biofouling, which refers to the growth of marine organisms on the components, is also a significant external factor. Research suggests that biofouling can reduce the power absorption of a WEC by up to 10% and decrease the fatigue life of its mooring system by 20% (Yang et al., 2017). Thus, the external factors should be a constant consideration for the design of WECs and WEC arrays.

3 Method

Figure 3.1 displays a flow chart describing the methodology used in this thesis:

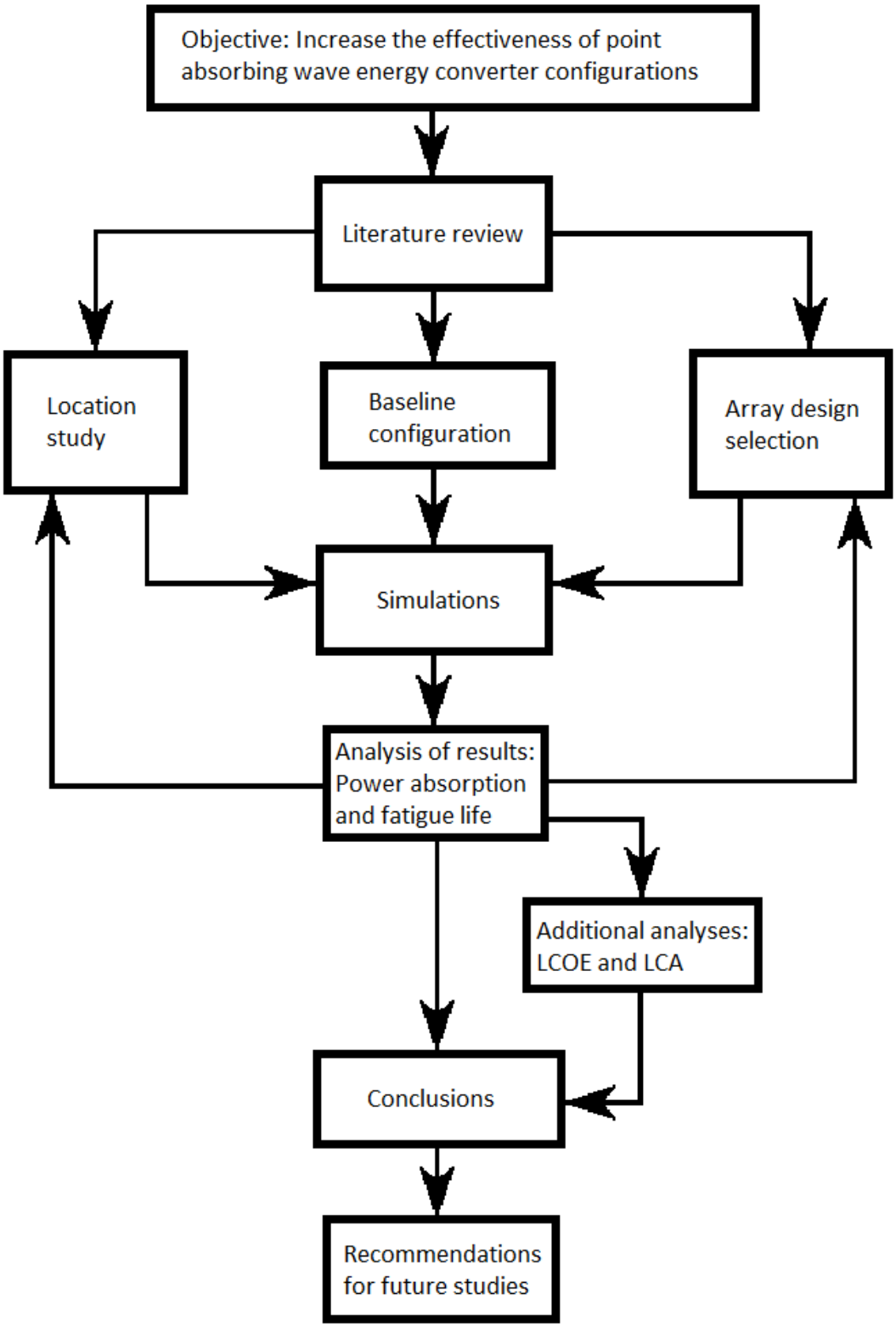

Figure 3.1: Flow chart describing the methodology applied in this thesis work.

The methodology of the thesis work is organized to produce multiple stages of results in the limited timeframe. It begins by assessing the objective of the thesis, which is to study the parameters that affect the efficiency of point absorbing wave energy converter configurations. The literature review provides the foundations for the parameters to be considered and the theory used in the analysis. The baseline configuration in the simulation model based on the WaveEL device is then defined. The configurations are modelled and simulated using DNV GL's SESAM software (DNV GL, 2018a). The numerical results obtained from each simulation are post-processed to find the average WEC power absorption and estimated fatigue life. For select configurations the results are used in an LCOE analysis and LCA. From all results, conclusions are drawn and discussed. Finally, recommendations are made for future studies.

This thesis considers two topics particularly important to the development of commercialized wave energy: prospective locations and their environments, and the design of WEC array configurations. The exploration of each takes time and is independently represented in the methodology. As simulation results are processed and analyzed, it may become clear what parameters relating to different locations or array designs are more interesting than the others. Thus, a return to the location study and design selection processes occurs after the analysis of the previous round of simulation results.

In the simulations, the results of the location study i.e. the environmental conditions of different sites are applied only to single WEC buoy configurations. For the simulations of the array configurations, the location of the current installed WaveEL device off the coast of Runde, Norway is assumed. As Runde is the only site which has been actively explored by Waves4Power in terms of full-scale demonstration, the information for this site is considered as the most abundant and reliable. In the other sites, more exploration is needed before the design of an array can be considered. Nonetheless, the simulation results can indicate which of the sites have the highest potential and provide motivation for exploring array designs in those locations in future studies.

3.1 Modelling and Simulation

3.1.1 Software

For the hydrodynamic and structural response simulations, DNV GL's SESAM software is used. SESAM software tools can be used for both fixed and floating offshore structures as well as moorings and subsea umbilicals, which makes it a suitable software package for the purposes of this thesis (DNV GL, 2018a). Specifically, in this thesis the interfaces HydroD (DNV GL, 2017b) and SIMA (DNV GL, 2017c) are used to obtain the hydrodynamic and structural responses of the design.

The geometries of the WECs, which in this thesis are the geometries of buoys V1 and V2, have been previously modelled from GeniE software. GeniE is a tool used to create conceptual models of offshore structures with a finite element mesh (DNV GL, 2018d). These geometries are imported into HydroD, which is the interface used to provide the hydrodynamic responses between WECs in an array for a set of environmental loading conditions (DNV GL, 2018b). As will be proven later, it is important to first simulate for the WEC array in HydroD and then export these results for use in SIMA. This is because the wave interaction effects between the WECs must be obtained through the frequency domain hydrodynamic analysis program WADAM, a solver used by HydroD (DNV GL, 2018e).

Mooring lines and power cables are WEC components which comprise the slender system. Modelling and simulation of the slender system is included in SIMA but not in HydroD; thus, to account for any slender elements in the WEC configuration, it is also important that SIMA is used. SIMA provides an interface with which a coupled analysis of the motions and forces acting on the WEC components can be obtained (DNV GL, 2018c). As described in the research of Yang et al. (2016), coupled simulations in the time domain solve for the motions of the WEC body and slender elements simultaneously, as opposed to de-coupled simulations which first solve for the motions of the WEC and then calculate for the motions of the slender system. Coupled simulations thus have the advantage of identifying interactive effects between the WEC and mooring system. This is important to accurately predict the stress response of the mooring lines and identify mooring configurations that contribute to efficient WEC movement (Yang et al., 2016). To analyze the structural responses in the slender system, SIMA uses the solver RIFLEX (DNV GL, 2018f). To analyze the hydrodynamic loads and motions of the WEC buoy, the solver SIMO is used (DNV GL, 2018f). The output of the simulations yields the motions and forces acting on the WEC bodies and the slender system for the time range simulated.

3.1.2 Procedure

Simulation procedure requires the definition of many parameters. Thus, many assumptions are necessary to model and run simulations, make calculations and obtain comparable results. These assumptions are briefly explained in the following section.

The loading sequence of the static calculation parameters defines in which order the hydrostatic forces will be solved, with how many steps and iterations, and the degree of accuracy (DNV GL, 2017c). The dynamic calculation parameters include details about the time domain analysis and storage of the force responses of the slender components. Details regarding the static and dynamic calculation parameters are displayed in Appendix 11.4. The base case simulation is run for a simulation time of 3 hours, which is assumed to be the minimum time to represent a steady sea state in irregular sea state simulations (DNV GL, 2017a).

In the simulations, the hub and anchors are modelled as fixed points. The floaters are also modelled as points, but their locations, along with the locations of the mooring line segments, are solved for in the static analysis by using the hub and anchor locations as boundary conditions. The hub and anchor locations are then used again in solving the slender system configuration in the dynamic analysis.

The force responses are only stored for elements of the mooring lines defined in the dynamic calculation parameters. The mooring line elements correspond to a segment and element number, where each element is one meter long and thus the number of elements corresponds to the length of the mooring line segment, as seen in Figure 3.2. While storing the force responses for all the elements would give the most complete results, simulation time increases as more force responses are stored. The stored elements are therefore carefully chosen depending on the mooring line segment lengths and will differ for different simulations.

In Figure 3.2 an example mooring line with two segments of 26 m and 39 m is shown. There is a total of 65 possible elements for which force responses could be stored. The 24 elements in red are chosen for force response storage. From initial simulations performed, the highest axial forces are in most cases found at the end of segments; thus, more elements are chosen at the ends of segments. The elements chosen for the base case is displayed in Appendix 11.4.

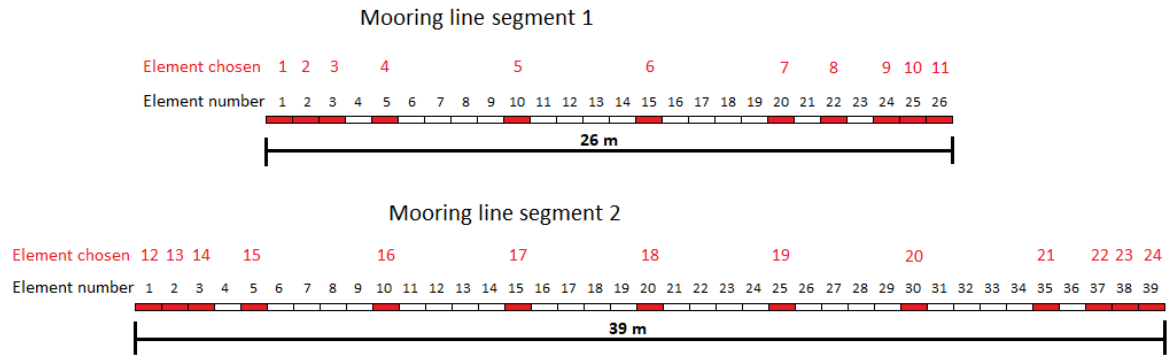

Figure 3.2: Example schematic of mooring line segment elements and elements chosen for storage.

3.2 Post-processing

The hydrodynamic simulations output various numerical data including the position of the WEC in six degrees of freedom and the axial forces acting in the mooring lines. In their research, Paredes et al. (2016) define maximum tension forces in the most loaded mooring line as a critical factor in indicating the survivability of a mooring configuration. Thus, in some simulation results the maximum tension forces will be used to quickly compare the forces on the mooring lines. To obtain the WEC power absorption and fatigue life estimates in the mooring lines, the results must be post-processed in another application. In this case the data is input into MATLAB (MathWorks Inc., 2016), where the equations mentioned in section 2.1 can then be used.

To obtain the power absorption, the derivative of the WEC´s position the z direction is taken to obtain the heave velocity. Using equation 1, instantaneous power is first obtained by squaring the heave velocity and multiplying by the PTO damping coefficient. Then, cumulative energy is calculated from integrating over the total simulation time. Finally, time-averaged power can be obtained by dividing the cumulative energy by the total simulation time.

To obtain the fatigue life of the lines, the axial stress should be calculated for each element of a mooring line for each time step. In the simulations run in this thesis, the storage time step from the coupled time domain simulations is one second. Axial stress is calculated by dividing the axial force by the cross-sectional area of the element. The Wave Analysis for Fatigue and Oceanography (WAFO) toolbox in MATLAB is used to count the rainflow cycles from the axial forces recorded per second (WAFO-group, 2017). Then, using equations 2 and 3, the accumulated fatigue damage can be calculated for each element of each mooring line. The fatigue life of each mooring line will be calculated from the element that sustains the most accumulated fatigue damage. This is represented as the number of years until failure.

Because PTO damping is assumed linear and constant, and only one sea state of many possible sea states is represented in each simulation, the values calculated should not be expected to represent precise estimates for the actual power production and fatigue life values. These simplified estimates are used relatively to compare the different designs.

3.3 LCOE

The LCOE is used to quantify the economic effectiveness of the array designs. The method described in Castro-Santos et al. (2016) is used to calculate the LCOE.

In the research of Castro-Santos et al. (2016), the life cycle of a floating offshore renewable energy farm is defined as including the following six phases: concept definition, design and development, manufacturing, installation, exploitation and dismantling. The associated total Life-cycle Cost System (LCS) is represented by equation 5:

$$LCS = C1 + C2 + C3 + C4 + C5 + C6 \quad (5)$$

C1 through C6 represent the costs associated with the six phases. Each phase of costs is divided into sub-costs, which can be seen in Figure 3.3.

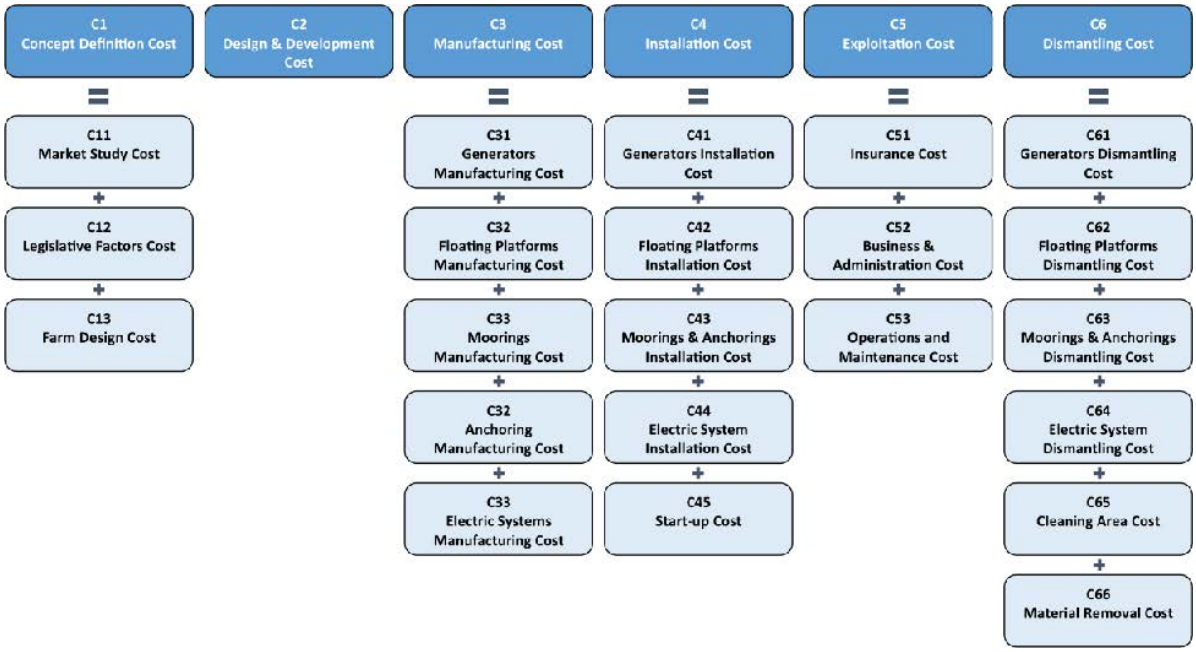

Figure 3.3: Costs and sub-costs of the LCS (Castro-Santos et al., 2016).

The concept development cost and design and development cost are a small fraction of the overall cost and their influence on the overall cost decreases as the size of the wave farm increases (Castro-Santos et al., 2016). All costs are expected to decrease significantly as the technology matures.

To calculate the annual energy produced from an offshore energy farm, Casto-Santos et al. (2016) use equation 7. In the case of a farm of wave energy devices, equation 6 is used to calculate the energy produced per WEC device. The power absorption of a wave energy device depends on the sea conditions, so to measure the energy produced in its lifetime, the power produced at each possible sea state should be weighed by the probability of that sea state occurring (Castro-Santos et al., 2016). This however does not account for interaction effects changing the power absorption of individual devices.

$$E_{1DEVICE} = Power\ matrix_{device} * Sea\ state\ matrix_{location} \quad (6)$$

$$E = NA * E_{1DEVICE} * \eta_{availability} * \eta_{transmission} \quad (7)$$

Finally, the levelized cost of energy is calculated through equation 8:

$$\text{LCOE} = \frac{\sum_{n=0}^{n=N} \frac{LCS_n}{(1+r)^n}}{\sum_{n=0}^{n=N} \frac{E}{(1+r)^n}} \tag{8}$$

When companies are financing new projects, Weighted Average Cost of Capital (WACC) is often used in place of discount rate as a better reflection of project risk and return (Myhr et al., 2014). Thus, it can be beneficial to consider WACC values in the LCOE calculations.

3.4 LCA

A life cycle assessment (LCA) quantifies the environmental impact of a product or service through its entire life cycle. This analysis is particularly important in renewable energy conversion technologies, because while the energy sources themselves produce no emissions, there are still environmental impacts due to the manufacturing, operation, and decommissioning of the associated equipment (Thomson et al., 2011). Environmental impacts can also be extended to pollutants with impacts on human health: thus, the LCA will be used to assess both the environmental and social sustainability of the product.

To conduct an LCA, the framework must first be defined, which includes the goal and scope definition, life cycle inventory (LCI) analysis, the life cycle impact assessment (LCIA) and interpretation (Thomson et al., 2011). The functional unit and system boundaries must also be defined. In the LCA of wave energy converters, the assessment should include not only the device itself but also mooring system as well as the subsea connecting power cable (Uihlein, 2016). Downstream electrical components need not be included (Thomson et al., 2011).

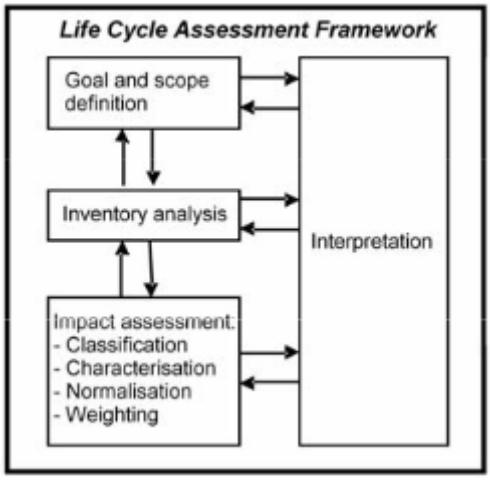

Figure 3.4: LCA framework (Thomson et al., 2011).

The goal and scope is to compare the environmental impact of different WEC array designs and to identify the most critical life cycle stages in terms of environmental impacts. The assumed lifetime of the WEC system is 25 years. The research conducted by Uilhlein (2016) on the LCA of ocean energy technologies considers the system's boundaries as from 'cradle-to-grave' and the functional unit as one kWh of electricity generated. 'Cradle-to-grave' refers to all life cycle steps until the end of the system's life, including component manufacturing, device assembly, installation, exploitation and decommissioning (Thomson et al., 2011). The

LCI then details the inputs and outputs to each process within the life cycle. Process inputs can include resource uses and energy while process outputs can include product, waste flows or emissions to the air or water (Thomson et al., 2011).

In this thesis the software OpenLCA (GreenDelta, 2016) is used to model the lifecycle process, flows and product systems of the compared array designs. Databases can be downloaded from the OpenLCA website which contain input elementary flow data for general processes and flows. Specifically, data from the European Life Cycle Database (ELCD) created by the European Commission's Joint Research Center is used to input processes and flows related to material production and transport.

The LCIA weighs the emissions and resource consumption data from the LCI in terms of various environmental impact categories. Many methods can be used to assess impact, and should be chosen depending on the project. The impact assessment method used in the research of Uihlein (2016) which will also be used in this thesis is the ILCD midpoint method. ILCD is the International Reference Life Cycle Data System also created by the Joint Research Center to analyze several LCIA methodologies (Acero et al., 2015). The method used depends on the environmental impact category. The impact potentials are calculated from the elementary flows and include categories such as climate change, human toxicity, acidification, ecotoxicity, land use and more (European Commission, 2017). Contributing to both human health and natural environment, the climate change impact category measures the kilograms of CO_2 equivalent per functional unit and is included in nearly all LCIA methods (Acero et al., 2015).

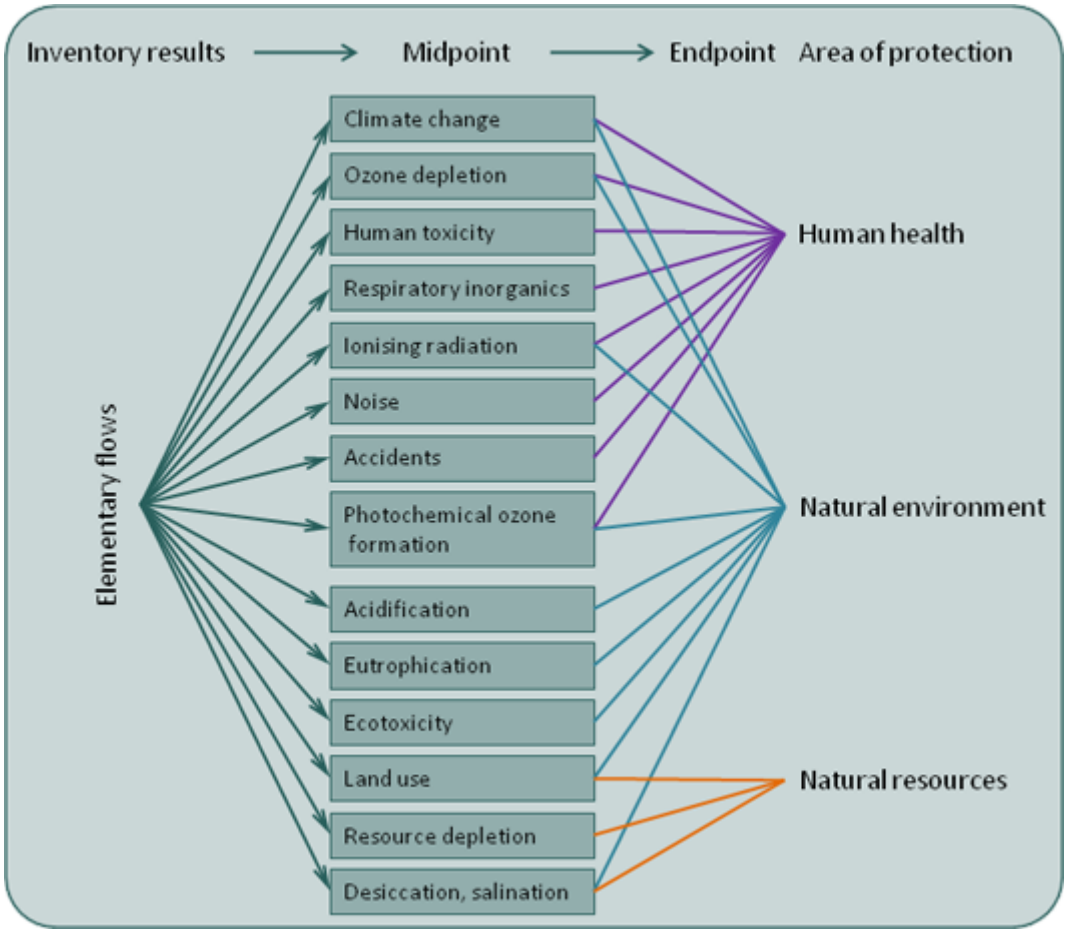

Figure 3.5: Life cycle impact categories (European Commission, 2017).

4 Baseline Configuration

This thesis uses the WaveEL device designed by Waves4Power as a baseline for the WEC design. The WaveEL device consists of three main components: the WaveEL buoy, the mooring system, and the electricity collection system, which includes the power cable and the electricity hub. The WEC simulation model is based on previous work done by Yang et al. (2016; 2017). The locations and directions in the model are defined through both rectangular coordinates and polar coordinates, seen in Figure 4.2. In the baseline model, the WEC is located at the origin of the coordinate system [0,0,0]. The z-axis, not pictured, is the vertical axis, where the sea surface is at z = 0 and the sea floor is located in the negative z-direction. Wave, wind and current direction are initially set to 0 degrees, which corresponds to the eastward direction. For the sake of symmetry, the mooring lines of the baseline configuration are modelled at exactly 120 degrees from each other, with the power cable and hub placed in between mooring lines 2 and 3 and directly opposite from mooring line 1. A schematic for the top view of the baseline configuration can be seen in Figure 4.1.

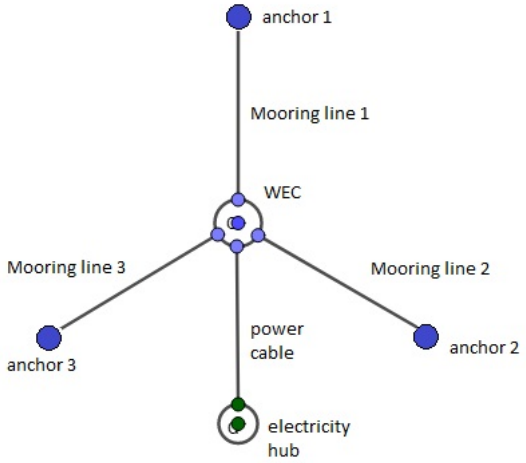

Figure 4.1: Top view of baseline configuration based on the WaveEL device. The size of the WEC, electricity hub, and anchors are not to scale.

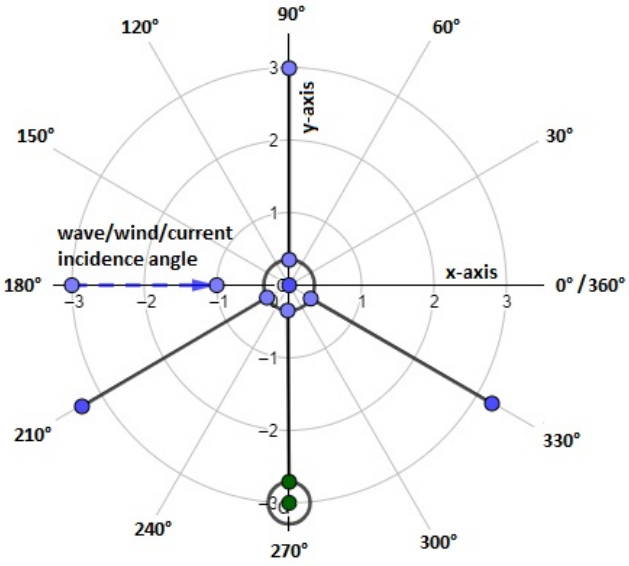

Figure 4.2: Top view of baseline configuration, showing the coordinate system.

4.1 WaveEL Buoy

Two versions of the WaveEL buoy with different shaft lengths have been considered by Waves4Power, called V1 and V2. The first version, V1, had a 27.8 m draft, referring to the vertical distance between the water surface and the bottom of the submerged device. In the second version V2, which was the version installed in the prototype WaveEL 3.0 device, the tube was shortened to a 14.5 m draft (Waves4Power, personal communications, 4 May 2018). Simplified schematics of the V1 and V2 buoys can be seen in Figure 4.3.

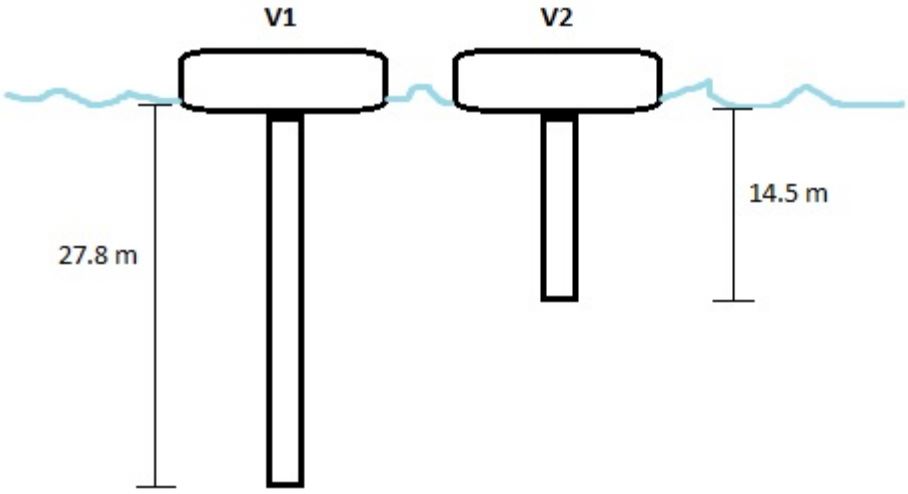

Figure 4.3: Simplified side view schematic of the WaveEL buoy versions V1 and V2, showing the difference in draft.

In the plans for the WaveEL 4.0 Next Generation buoy, the geometry is based on the original V1 design. The longer acceleration tube is preferred by the company as it can reach below the movement of the waves, which will result in a still standing water pillar inside the tube that acts as a counterweight against the buoy movement (Waves4Power, personal communications, 4 May 2018). Furthermore, the different dimensions of V1 and V2 lead to different resonance frequencies for the buoys. As described in section 2.2, this may result in the buoys being more or less successful depending on the wave frequency of the sea state. Thus, WEC models based on both designs V1 and V2 are explored through the simulations. The properties of the V1 and V2 models used in the simulations can be seen in Table 4.1.

Table 4.1: Properties of the WEC buoys V1 and V2.

	V1 buoy	V2 buoy
Draft (m)	27.8	14.5
Mass (kg)	452898	268416
Center of gravity [x,y,z] (m)	[0, 0, -14.1]	[0, 0, -5.25]
Radius of gyration [x,y,z] (m)	[17.69, 17.69, 0.69]	[7.45, 7.45, 1.67]
PTO damping in heave direction (Ns/m)	36400	42850

4.2 Mooring System

As seen in Figure 4.1, the WaveEL mooring system consists of 3 equidistant mooring lines. Each mooring line includes two segments connected by a floater, as seen in the schematic in

Figure 4.4. The first segment refers to the segment connecting the WEC and the floater, and the second segment refers to the segment connecting the floater and the gravity anchor.

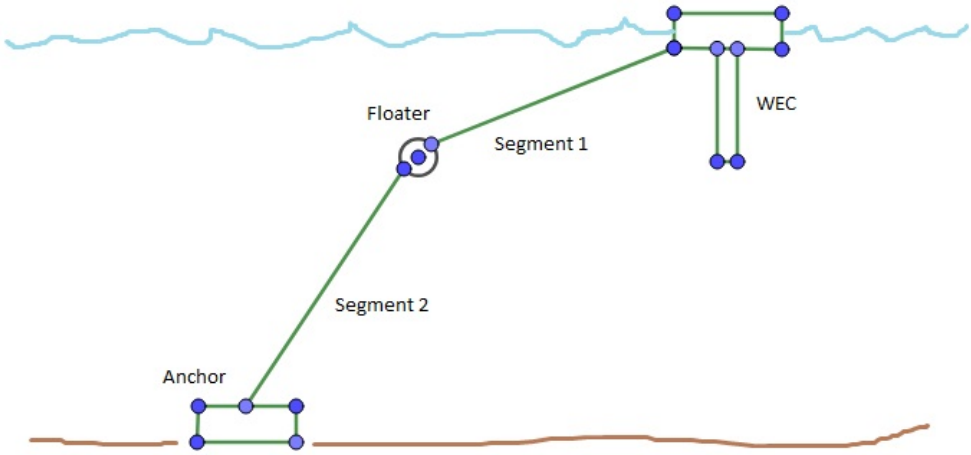

Figure 4.4: Side view schematic of the WaveEL mooring line configuration showing a single mooring line and anchor. The size of the WEC, floater and anchor are not to scale.

Due to varying water depth, the WaveEL 3.0 device installed at Runde has anchors lying at 3 different water depths (Jansson & Örgård, 2017). Thus, in the baseline configuration, the length of each segment of the mooring line and the anchor radius also differs for each mooring line. The anchor radius refers to the horizontal distance from the center of the WEC to the center of a mooring line anchor. Table 4.2 displays the mooring line number, anchor depth, anchor radius, and lengths of mooring line segments 1 and 2.

Table 4.2: Mooring line specifications for baseline configuration.

Mooring line number	Anchor depth (m)	Anchor radius (m)	Mooring line segment 1 length (m)	Mooring line segment 2 length (m)
1	-86.6	127.3	96	76.6
2	-54.1	132.1	113	44
3	-66.6	122.5	98	56.5

Two mooring line types are considered in this thesis. The first type is the same as in the current WaveEL 3.0 device and can be seen in Figure 4.4. The second type considered is a single segment mooring line. This mooring line type does not include the use of the floater and instead attaches the WEC directly to the anchor. The removal of the floater could reduce costs but may affect the axial forces in the mooring lines and the cable and the movements of the WEC device. The dimensions and properties of the mooring lines are displayed in Table 4.3 and Table 4.4.

Table 4.3: Dimensions and properties of the mooring lines.

Mass per unit length (kg/m)	Cross-sectional area (m^2)	α	m
8.55	0.0036	0.26	13.46

Table 4.4: Tension-elongation relationship in the mooring lines. For each relative elongation from the original length shown in the left column, the axial force increases by the value shown in the right column.

Relative elongation	Axial force (N)
0	0
0.025	1.19E+05
0.050	2.38E+05
0.068	3.57E+05
0.082	4.76E+05
0.094	5.95E+05

4.3 Electricity Collection System

In the WaveEL 3.0 device, the WEC buoy is attached to the electricity hub with a dynamic power cable situated between two mooring lines, as seen in Figure 4.5. The cable including bending stiffener is 135 m long but the horizontal distance between the WEC and the hub is only 100 m, resulting in a free floating slack cable as can be seen in Figure 4.5. This reduces the risk of creating tensile stresses from the movement of the WEC buoy, which results in a long lifetime for the cable. The electricity is then transferred from the hub to the shore through a subsea cable. The dimensions and properties of the cable can be seen in Table 4.5.

Table 4.5: Dimensions and properties of cable and mooring lines.

Axial stiffness (N)	Bending stiffness (Nm^2)	Torsional stiffness (Nm^2/rad)	Cross-sectional area (m^2)	α	m
4.7E+06	5.0	3.0	0.0011	6.10E+19	6.24

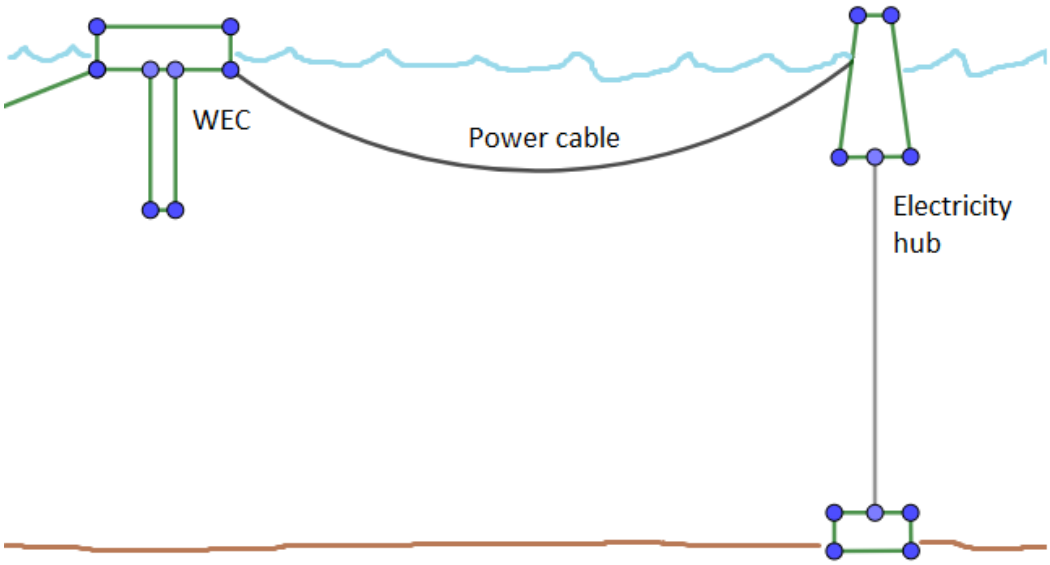

Figure 4.5: Simplified side view schematic of the WaveEL cable and hub configuration. Subsea cable not pictured.

5 Location Study

The purpose of the location study is to assess different locations for their suitability for a point absorbing WEC installation and particularly for the performance of the WaveEL device. The first location is the location of the installed WaveEL 3.0 device off the coast of Runde. The remaining locations are chosen due to accessibility to data on the wave, wind and current climate through open access resources. As mentioned in the literature study, the wave energy resource and weather conditions at the proposed location have a huge impact on the feasibility of the wave energy project. Thus, it will be a goal of this location study to find as much reliable information as possible about the environmental conditions at a site. These environmental parameters are as follows:

- Significant wave height
- Wave period
- Wave spectrum
- Wave direction
- Wind speed
- Wind profile exponent
- Wind direction
- Current speed
- Current direction

The wave spectrum used in the simulations is the JONSWAP 3 parameter spectrum (Jansson & Örgård, 2017). The wave spectrum parameters describe the behavior of the waves in certain sea conditions, with peakedness parameter describing the distribution of wave energy as a function of wave frequency. In this thesis, aside from significant wave height and wave period, the parameters displayed in Table 5.1 will be assumed the same in all simulated environments. The wind spectrum used in the simulations is the NPD spectrum. This assumes that wind speed varies randomly over time, deviating from an average velocity defined by the environment (DNV GL, 2017a). The wind profile exponent is assumed as 0.12 in all simulations.

Table 5.1: Parameters set for all simulations describing the wave spectrum.

Spreading type	Spreading exponent	Number of directions	Peakedness parameter
Unidirectional	1	1	3.3

5.1 Runde, Norway

The first location considered is the installation site of the first prototype WaveEL 3.0 designed by Waves4Power near Runde, Norway. Figure 5.1 displays the geographical location of the WaveEL buoy. At the installation location of the WaveEL 3.0 device, the depth of the seabed is between 54.1 and 86.6 m (Jansson & Örgärd, 2017). The typical wave characteristics are represented by the density plot of wave significant height and wave period occurrences in Figure 5.2. Here and throughout the report the unique combination of H_s and T_p values is referred to as a sea state. The data compiled in previous research indicates that the maximum current speed at the surface of the water is about 0.5 m/s (Yang et al., 2017).

Figure 5.1: Geographical location of Runde on the Norwegian west coast.

Not much is known about the dominating directions of wave, wind and current. The wind speed and direction can be estimated from the historical data from nearby weather stations (Windfinder, 2018). From this data a realistic wind speed for the region is found to be 9 m/s. Figure 5.3 shows the wind rose for the nearest weather station in Fosnavåg. As can be seen from the wind rose, the wind direction is fairly multidirectional, with every direction yielding an annual distribution between 4-10%. Thus, it will be assumed that the wave direction will have a similar variability. This is supported by the research of de Andres et al. (2014), which suggested that the wave climate of the North Atlantic in Europe is very multidirectional. To confirm the direction of the current, the forecasts from February 28 to April 5 of 2018 provided by the Norwegian Meteorological Institute and Norwegian Broadcasting Corporation (2018) are used to deduce the range of current speeds and directions that can be expected. From this information, one can notice that the current forces mainly act in two opposing directions. These directions are assumed to be 60 degrees and 240 degrees, if eastward is considered to be 0 degrees.

mean significant wave height Hs (m)	wave period Tp (s)													
	2.5	3.5	4.5	5.5	6.5	7.5	8.5	9.5	10.5	11.5	12.5	13.5	14.5	15.5
12.5	0	0	0	0	0	0	0	0.01	0.02	0.03	0	0	0	0
11.5	0	0	0	0	0	0	0	0.02	0.07	0	0	0	0	0
10.5	0	0	0	0	0	0	0	0.11	0.1	0	0	0	0	0
9.5	0	0	0	0	0	0	0.06	0.42	0.1	0	0	0	0	0
8.5	0	0	0	0	0	0.02	0.29	0.87	0.02	0	0	0	0	0
7.5	0	0	0	0	0	0.14	1.07	1.03	0.02	0	0	0	0	0
6.5	0	0	0	0	0	0.44	2.67	0.33	0.05	0.01	0	0	0	0
5.5	0	0	0	0	0.07	1.66	3.37	0.37	0.07	0.02	0	0.01	0	0
4.5	0	0	0	0	0.43	5.58	1.36	0.32	0.14	0.05	0.01	0.01	0	0
3.5	0	0	0	0.01	3.71	5.63	1.23	0.48	0.19	0.06	0.02	0.01	0	0
2.5	0	0	0.04	1.79	8.77	3.03	1.3	0.71	0.33	0.16	0.07	0.02	0	0
1.5	0	0	2.21	10.1	5.01	2.2	1.46	1.1	0.66	0.36	0.16	0.03	0.01	0
0.5	6.44	3.67	6.84	2.48	1.07	1.42	1.62	1.92	1.17	0.64	0.19	0.22	0.03	0.04

Figure 5.2: Density plot for Runde, Norway, where the value in each cell is the probability of occurrence of a specified sea state out of 100.

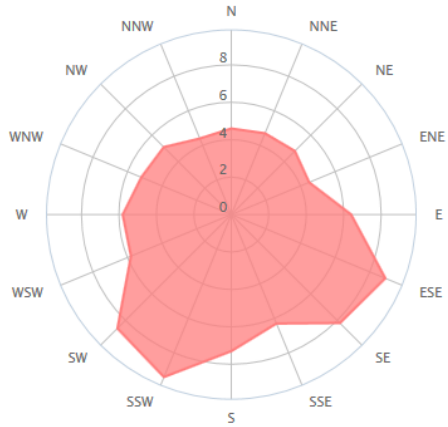

Figure 5.3: Wind rose of wind direction distribution in Fosnavåg (Windfinder, 2018).

Table 5.2 summarizes the environmental conditions found at Runde that will be used in most simulations. The significant wave height and wave period represent the most common sea state found from the scatter diagram. No dominant wave or wind direction can be deduced from the location study, so no value is input in those categories.

Table 5.2: Environmental conditions assumed at the Runde location.

H_s (m)	T_p (s)	dir_{wave} (°)	V_{wind} (m/s)	dir_{wind} (°)	V_{curr} (m/s)	dir_{curr} (°)
1.5	5.5	-	9.0	-	0.5	60 || 240

5.2 San Juan, Puerto Rico

As an island with high electricity prices and heavy reliance on oil imports, Puerto Rico is a prime example of a location that could benefit greatly from the development of wave energy. An incredibly thorough resource for marine data found on the National Buoy Data Center (NOAA, 2018) is the historical data for a measurement buoy located near San Juan, Puerto Rico (see Figure 5.4). This measurement buoy, owned and maintained by the Caribbean Integrated Coastal Ocean Observing System, contains hourly data from 2010 to 2016, as well as real time data. The parameters measured include average wind speed and direction, maximum wind speed (gusts), current speed and direction, wave mean significant height, wave period, and wave direction. Data for wave direction is collected hourly, data for wind direction is collected and averaged every 10 minutes, and data for current direction is collected every 30 minutes. The water depth is stated to be 32 meters.

Figure 5.4: Location of measurement buoy in San Juan, Puerto Rico.

Using the historical data from 2012-2015, a data analysis is performed to obtain the average environmental conditions. A density plot of the frequency of observed sea states is seen in Figure 5.5. The frequency of dominating wave directions is displayed in Figure 5.6. The frequency of dominating wind and current directions observed are displayed in Appendix 11.1. Finally, a summary of average environmental conditions is displayed in Table 5.3, with H_s and T_p representing the most common sea state found from the density plot.

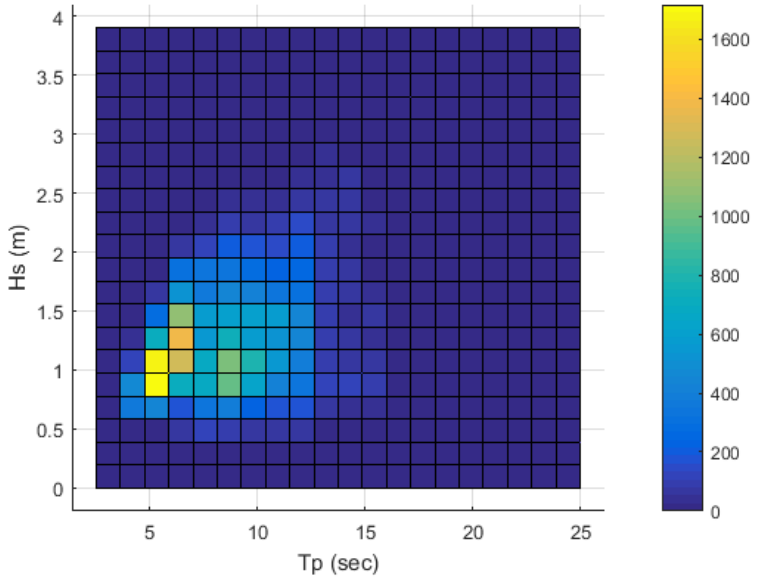

Figure 5.5: Sea state density plot for the San Juan location, where the color bar represents the frequency of sea state occurrences out of the complete data set analyzed.

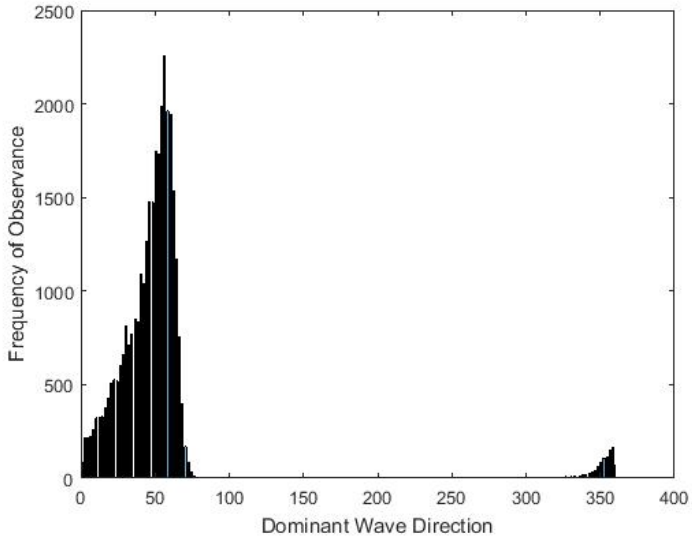

Figure 5.6: Frequency of dominant wave direction observances at San Juan site.

Table 5.3: Environmental conditions assumed at the San Juan location.

H_s (m)	T_p (s)	dir_{wave} (°)	V_{wind} (m/s)	dir_{wind} (°)	V_{curr} (m/s)	dir_{curr} (°)
1.0	5.5	57	5.3	81	0.24	175 || 355

An interesting environmental condition worth studying is the effect of hurricanes. Along with many other Caribbean islands, Puerto Rico is prone to strong winds and waves during certain periods of the year when hurricanes are abundant. In September 2017, Puerto Rico was rattled by Hurricane Maria, where the island reportedly experienced 103 km/h winds with up to 182 km/h gusts (NBC, 2017). Using the same National Buoy Data Center (NOAA, 2018), the wind, wave and current data for September 2017 was obtained and analyzed. The density plot of observed sea states from September 2017 is displayed in Figure 5.7. The observed frequencies of different wave, wind and current directions are displayed in Appendix 11.1. Finally, Table 5.4 summarizes the extreme environmental conditions taken from the data for September 2017. Maximum values from the data set were taken for wave height, wave period, wind speed and current speed.

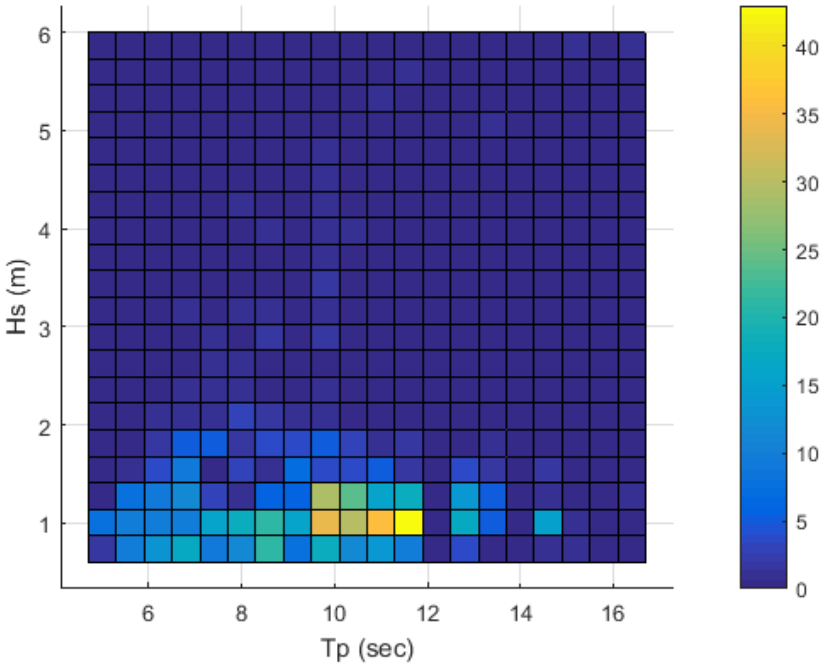

Figure 5.7: Sea state density plot at the San Juan location in September 2017, where the color bar represents the frequency of sea state occurrences out of the complete data set analyzed.

Table 5.4: Extreme environmental conditions assumed at the San Juan location.

H_s (m)	T_p (s)	dir_{wave} (°)	V_{wind} (m/s)	dir_{wind} (°)	V_{curr} (m/s)	dir_{curr} (°)
6.0	16.7	51	33.9	146	1.12	279 || 355

5.3 The Swedish West Coast

The Swedish Meteorological and Hydrological Institute [SMHI] provides open access to all of its historical data for both meteorological and oceanographic observations (SMHI, 2018a; SMHI, 2018b). The wave and current data obtained from two buoys located off the west coast of Sweden are considered, shown in Figure 5.8 (SMHI, 2018a). The first, which will be referred to as the Väderöarna buoy, is located northwest of Gothenburg, near the Norwegian border. The second, referred to as the Läsö Ost buoy, is located southwest of Gothenburg, closer to Varberg. Developing WEC farms near Gothenburg could provide offshore electricity beneficial to the shipping industry, as Gothenburg is the largest port in Scandinavia.

Figure 5.8: Locations of the two measurement buoys used for prospective WEC farm installation sites.

The water depth at these locations is found using the Swedish Oceanographic Stations map (Swedish Maritime Administration, 2018). Väderöarna buoy is located at a sea depth of 73 m. Läsö Ost buoy is located at a sea depth of 70 m. To find the wind speed and direction, the historical data from the meteorological observation locations closest to the Väderöarna and Läsö Ost buoys are used (SMHI, 2018b). These can be seen in Figure 5.9. It should be noted that in this case, the wind, wave and current data are not from the same range of years. The Väderöarna buoy data includes wave measurements from 2005 to 2018, while measurements for current do not begin until 2013. The wind data used for the Väderöarna location, on the other hand, is measured from 1966 up to 2017. The Läsö Ost buoy measurements for wave and current are taken from 2001 to 2009, while the wind data used is measured from 2004 to 2008.

Figure 5.9: Location of the wind measurement sites compared to the location of the wave and current measurement sites. The wind measurement sites are located by the red pointers.

With this data an analysis is again done. Figure 5.10 displays the sea state density plot for the Väderöarna location. Figure 5.11 displays the same for the Läsö Ost location. The dominant wave, wind and current directions for Väderöarna and Läsö Ost are displayed in Appendix 11.1. It is found that the location at Läsö Ost has a more multidirectional climate in terms of wave, wind, and current, while Väderöarna has a more unidirectional climate. A summary of the environmental conditions at the two sites are displayed in Tables 5.5 and 5.6, where H_s and T_p represent the most common sea state found from the density plot.

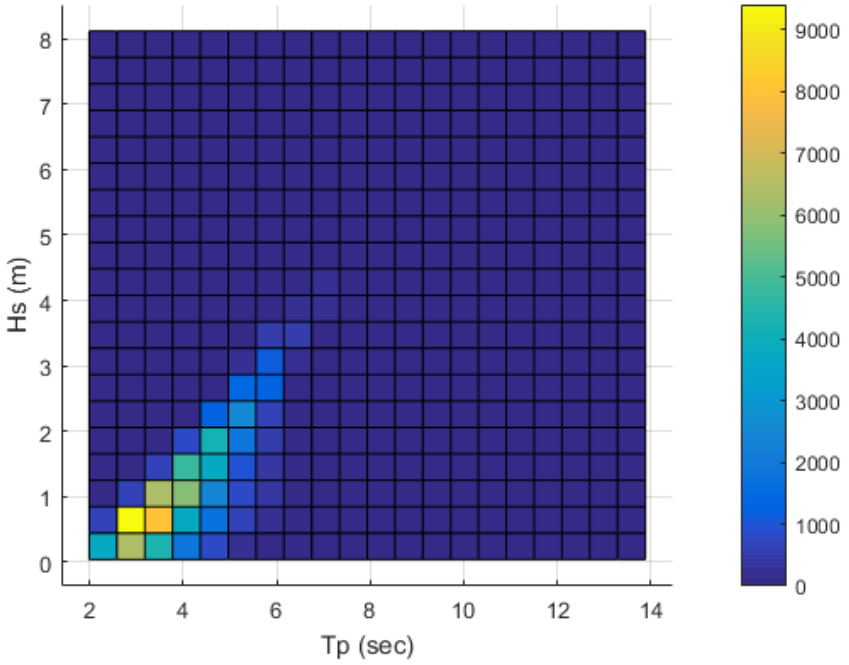

Figure 5.10: Sea state density plot for the Väderöarna location, where the color bar represents the frequency of sea state occurrences out of the complete data set analyzed.

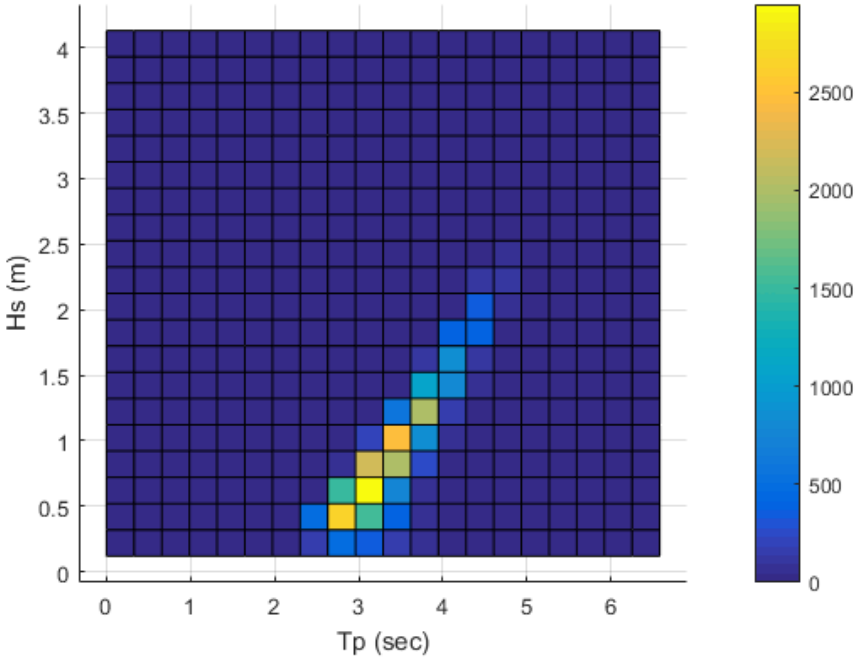

Figure 5.11: Sea state density plot for Läsö Ost location, where the color bar represents the frequency of sea state occurrences out of the complete data set analyzed.

Table 5.5: Environmental conditions assumed at the Väderöarna location.

H_s (m)	T_p (s)	dir_{wave} (°)	V_{wind} (m/s)	dir_{wind} (°)	V_{curr} (m/s)	dir_{curr} (°)
0.75	3.0	237	7.9	231	0.41	336 || 156

Table 5.6: Environmental conditions assumed at the Läsö Ost location.

H_s (m)	T_p (s)	dir_{wave} (°)	V_{wind} (m/s)	dir_{wind} (°)	V_{curr} (m/s)	dir_{curr} (°)
0.75	3.7	195	6.5	263	0.22	300 || 120

The ocean current data found for both sites includes measurements for current speed for different levels of water depth. Thus, the data can be analyzed per water depth level. As can be seen in Figure 5.12 and Figure 5.13, the average current speed generally decreases as water depth increases.

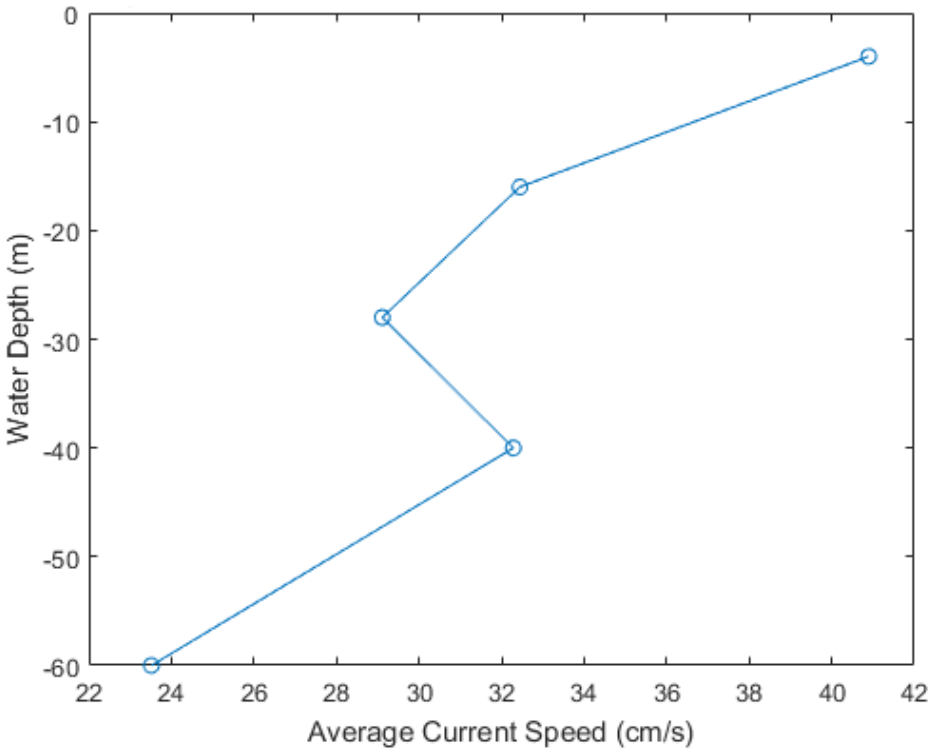

Figure 5.12: Average current speed as a function of water depth in Väderöarna location.

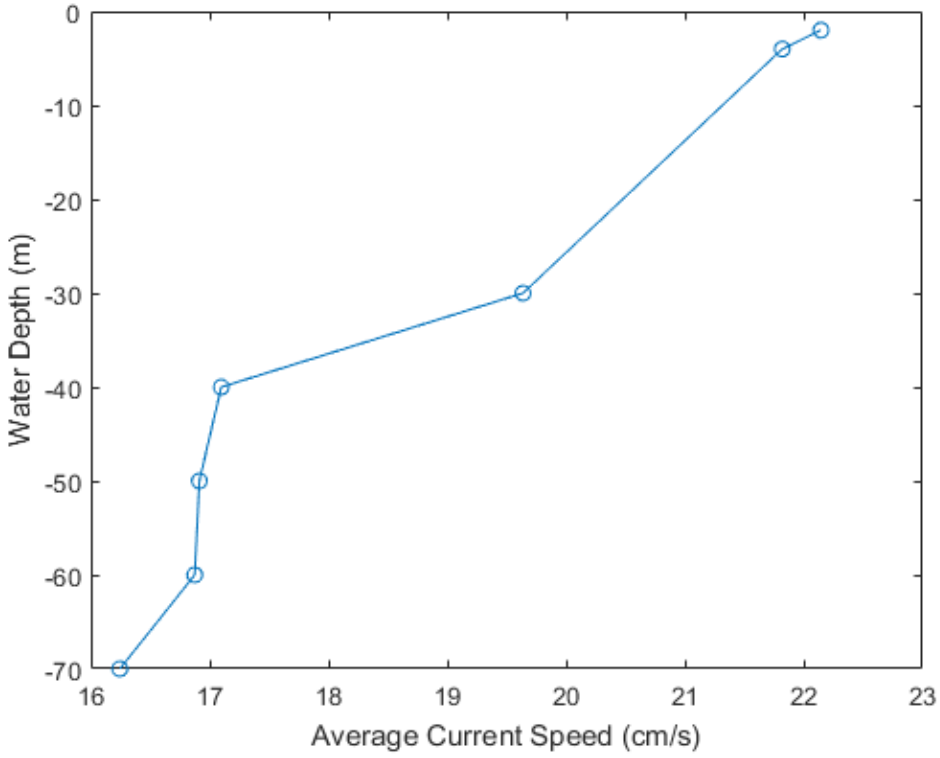

Figure 5.13: Average current speed as a function of water depth in Läsö Ost location.

5.4 Iceland

The final two sites explored are off the coast of Iceland. Iceland has a large fishing industry, and if electrified it could create significant incentive for the development of offshore electricity outposts using wave energy converters. The data for the wave, wind and current data is provided by Vegagerðin, the Icelandic Road and Coastal Administration. The two sites considered are Garðskagi, which lies off the southwest coast of Iceland near Reykjavik, and Grimseyjarsund, which lies off the north coast of Iceland closer to Akureyri. The water depth at Garðskagi is reported as 60 m and the water level at Grimseyjarsund is reported to be 96 m (Vegagerðin, 2018c).

Figure 5.14: Location of Garðskagi (Vegagerðin, 2018d).

Figure 5.15: Location of Grimseyjarsund (Vegagerðin, 2018e).

Data for the significant wave height and wave period for Garðskagi and Grimseyjarsund between the years of 1990-2018 is given directly from the Icelandic Road and Coastal Administration. The corresponding sea state density plots are displayed in Figures 5.16 and 5.17. To obtain the average wind speed and direction, a week of data for each month from April 2017 to March 2018 is recorded and analyzed (Vegagerðin, 2018b). To obtain the average current speed and direction, the forecast is used for 10 days of each month from April 2017 to March 2018 (Vegagerðin, 2018a).

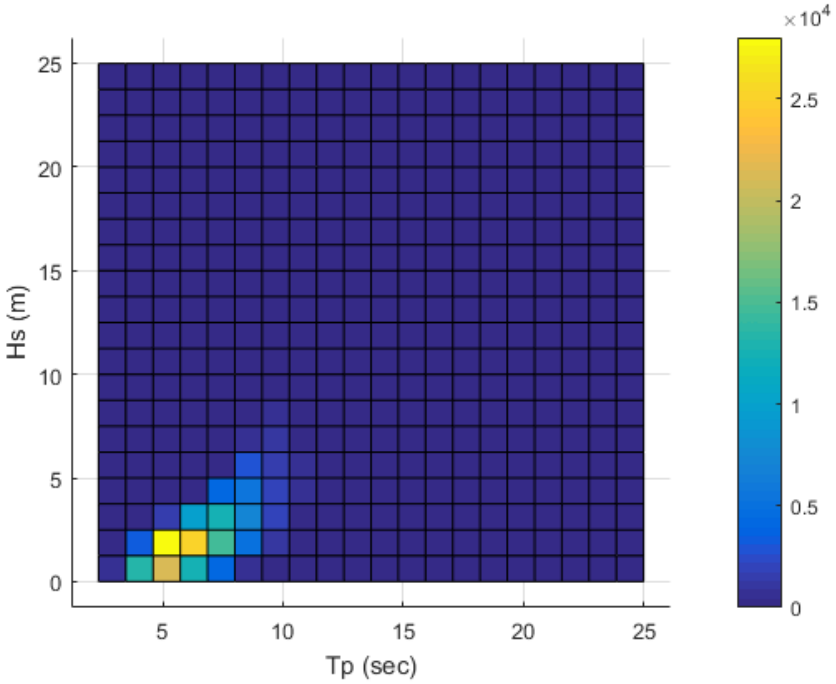

Figure 5.16: Sea state density plot for Garðskagi location, where the color bar represents the frequency of sea state occurrences out of the complete data set analyzed.

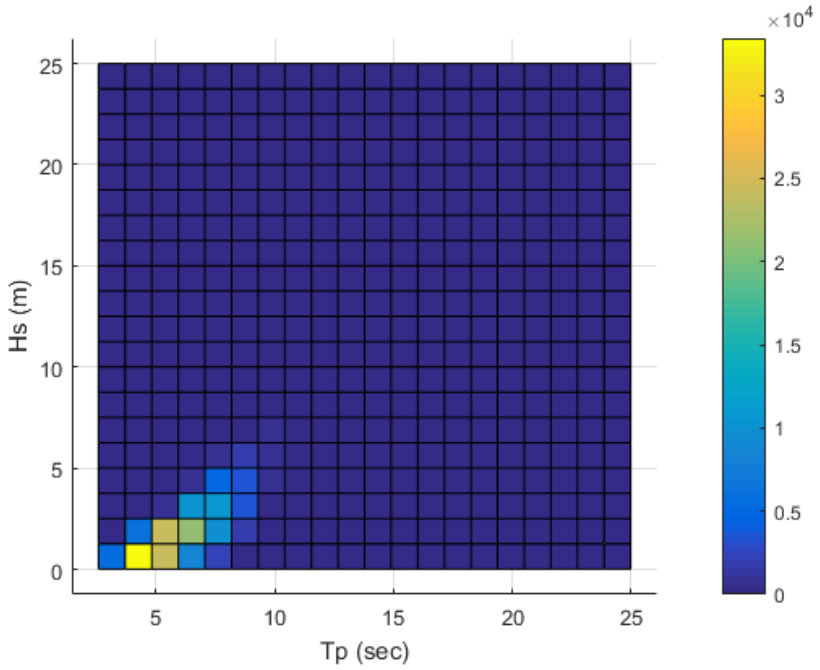

Figure 5.17: Sea state density plot for Grimseyjarsund location, where the color bar represents the frequency of sea state occurrences out of the complete data set analyzed.

Tables 5.7 and 5.8 display environmental conditions found for the Garðskagi and Grimseyjarsund locations. Again, the wave height and wave period are taken from the most common sea state found using the density plots. In both sites the wind direction is found to be very multidirectional, and no information is available for wave direction. Thus, no estimates for dominant wind and wave directions are included.

Table 5.7: Environmental conditions assumed at the Garðskagi location.

H_s (m)	T_p (s)	dir_{wave} (°)	V_{wind} (m/s)	dir_{wind} (°)	V_{curr} (m/s)	dir_{curr} (°)
2.0	5.0	-	8.6	-	0.1	340 || 160

Table 5.8: Environmental conditions assumed at the Grimseyjarsund location.

H_s (m)	T_p (s)	dir_{wave} (°)	V_{wind} (m/s)	dir_{wind} (°)	V_{curr} (m/s)	dir_{curr} (°)
1.0	4.5	-	6.7	-	0.1	306 || 126

6 Array Design Selection

The designs considered are chosen with simplicity in mind. From the knowledge gained from the literature study, a great deal of design concepts can be ruled out. The two array configurations chosen for simulations are the triangular configuration and the square configurations, as from de Andres et al. (2014). These two array configurations are simple enough to model in the simulation software, and geometries can be easily combined to create larger arrays.

A large constraint in the mooring system design is the electricity collection system. In the WaveEL 3.0 device, the WEC buoy is attached to a floating hub by a free-floating cable, as shown in the schematic in section 4.3. This means that in array design the WECs must not be placed too far from the proposed location of the electricity hub, and that space must be left unobstructed for the free-floating location of the cable. As more WECs are added to the array, cable length will need to be increased and there may be an overcrowding of cables. This increases the risk of cables colliding as well as risk for maintenance boats attempting to enter the farm location.

If a new electricity collection system is designed and implemented, there are many additional configurations that can be considered. However, the design of the electricity collection system is not in the scope of this thesis. Thus, two types of designs are discussed. The first type assumes that the cable and hub design used in the WaveEL 3.0 device would also be used in the array. The second type does not consider the restrictions of that design. Thus, to maintain comparability for all array designs, the cable and hub will not be modelled in the array simulations.

6.1 TriBuoy

6.1.1. Original collection system

In the TriBuoy simulations, three equidistant WECs are placed at a defined separation distance. The first separation distance is chosen assuming that the cable and hub design will not be changed; thus, the 100 m horizontal distance between WEC and hub is applied to all WECs. This leads to a WEC separation distance of 173 m. Separation distances of 260 m and 130 m are later considered to study the effects on the WEC array system. For the 260 m and 130 m separating distances, the horizontal distances from hub to WEC are 150 m and 75 m, respectively. The incidence wave, wind and current angles are all assumed to be coming at a 0 degree angle relative to the grid orientation defined in the baseline configuration. WEC 1 is placed at the origin point of the grid.

When assuming the continued use of the WaveEL 3.0 cable and hub design, the TriBuoy mooring configuration design includes three equidistant mooring lines with the first mooring line facing in the opposite direction of the center of the array as seen in Figure 6.1. The angle between each of the mooring lines is 120 degrees. The mooring line total lengths and relative segment lengths can be varied. If mooring line total lengths are maximized, the lines of different WECs share anchors. Figure 6.1 displays a schematic of a TriBuoy configuration with a WEC separating distance of 173 m and shared anchors. The configuration is denoted Tri.V2.173.1, according to the naming system defined in Appendix 11.3.

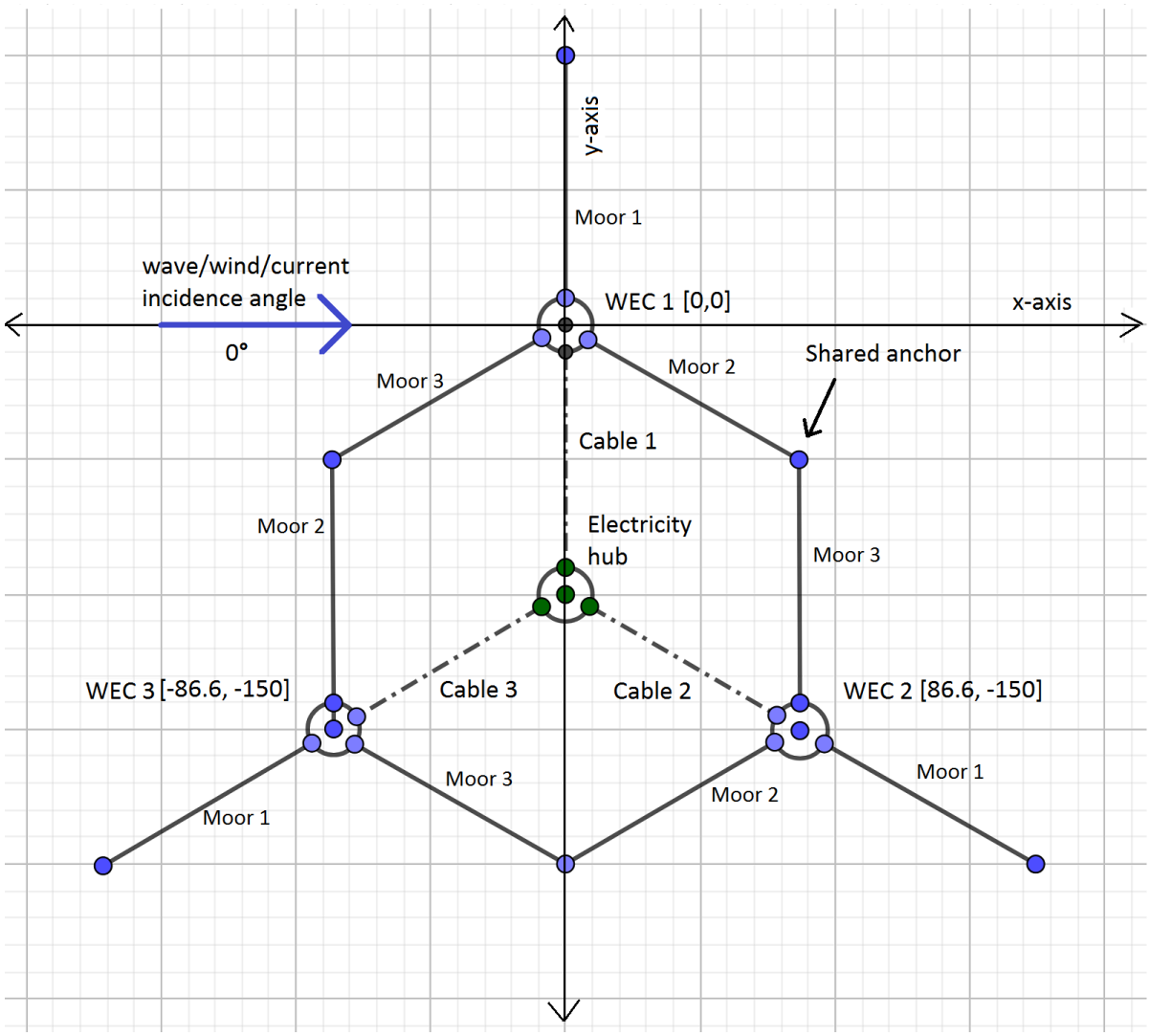

Figure 6.1: Conceptual schematic of TriBuoy configuration Tri.V2.173.1 considering the original electricity collection system.

It is important to mention the differences between the conceptual design of the array and the simulation models. As seen in Figure 6.2a and in all array configuration models, the cable and hub are not present: only the WECs and mooring system are included. The origin point, where WEC 1 is located, is indicated by a large circle with a red arrow in the x-direction and green arrow in the y-direction. From the top view of the simulation models, it is also difficult to tell the lengths of the mooring lines, ratio between the lengths of the mooring line segments, and the WEC separating distance. Thus, this information will be included through the naming system and table of specifications defined in Appendix 11.3. Finally, the model of Tri.V2.173.1 displayed in Figure 6.2a seems to have intersecting mooring lines. This is due to the difference in defined anchor location before and after the static analysis, as seen by comparing to Figure 6.2b.

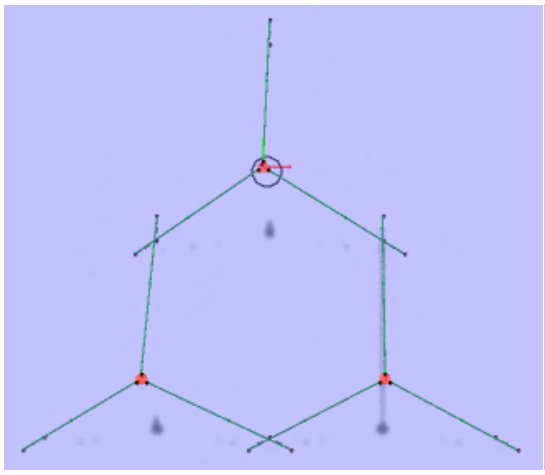

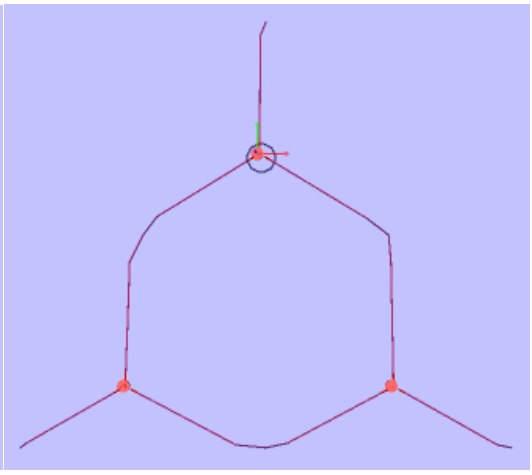

Figure 6.2a: Modelled Tri.V2.173.1. *Figure 6.2b: Static Tri.V2.173.1.*
Figure 6.2a-b: Top view of the simulation model of Tri.V2.173.1, before performing the static analysis (a) and after (b). After the static analysis, the buoyancy of the floater will alter the position of the mooring lines, and the anchor points join together.

6.1.2. Modified collection system

With a modified collection system a second mooring configuration for the TriBuoy array is considered. The separation distances considered are again 173 m, 260 m and 130 m. Here the mooring lines are still spaced 120 degrees apart, but one mooring line of each WEC extends towards the center of the array. If the mooring line lengths are maximized, this leads to the sharing of an anchor by the three central mooring lines, as can be seen in Figure 6.3b.

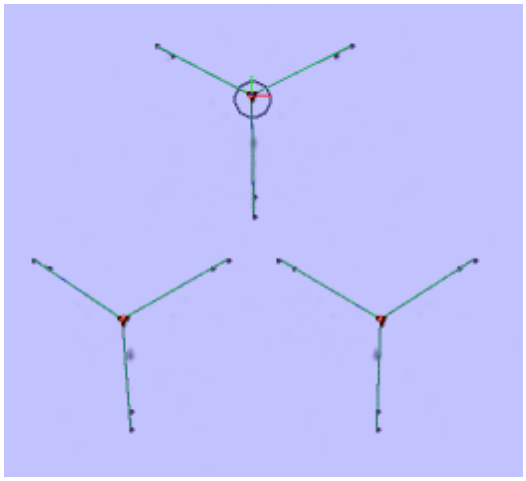

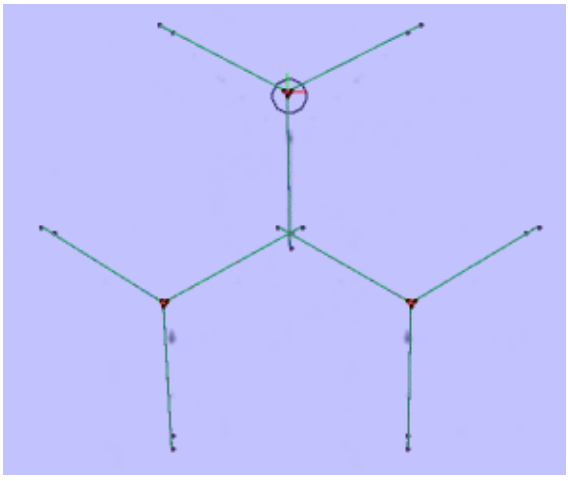

Figure 6.3a: Modelled Tri.V2.260.6. *Figure 6.3b: Modelled Tri.V2.260.8.*
Figures 6.3a-b: TriBuoy configurations Tri.V2.260.6 and Tri.V2.260.8. Tri.V2.260.8 maximizes mooring line length to share an anchor between the three central mooring lines.

6.2 SquareBuoy

6.2.1. Original collection system

In the SquareBuoy simulations, four equidistant WECs are placed at a defined separation distance. Assuming that the cable and hub design will not be changed and that the horizontal distance between all WECs and the hub should be 100 m, the WEC separation distance is found to be 141 m. A separation distance of 282 m is later considered, corresponding to a horizontal distance from WECs to hub of 200 m. In the SquareBuoy configurations, the incidence wave, wind and current angles are all assumed to be coming at a 60 degree angle relative to the simulation grid orientation. Again, WEC 1 is placed at the origin of the grid.

Considering the original cable and hub configuration of the WaveEL 3.0 device, the SquareBuoy configuration designed also contains 3 mooring lines per WEC with one mooring line of each WEC extending out in the direction opposing the center of the configuration. In this design the other two mooring lines are placed 135 degrees clockwise and counterclockwise from that line. Thus, as can be seen in Figure 6.4, the second and third mooring lines of each WEC form a square shape and can share anchors if the mooring line lengths are maximized.

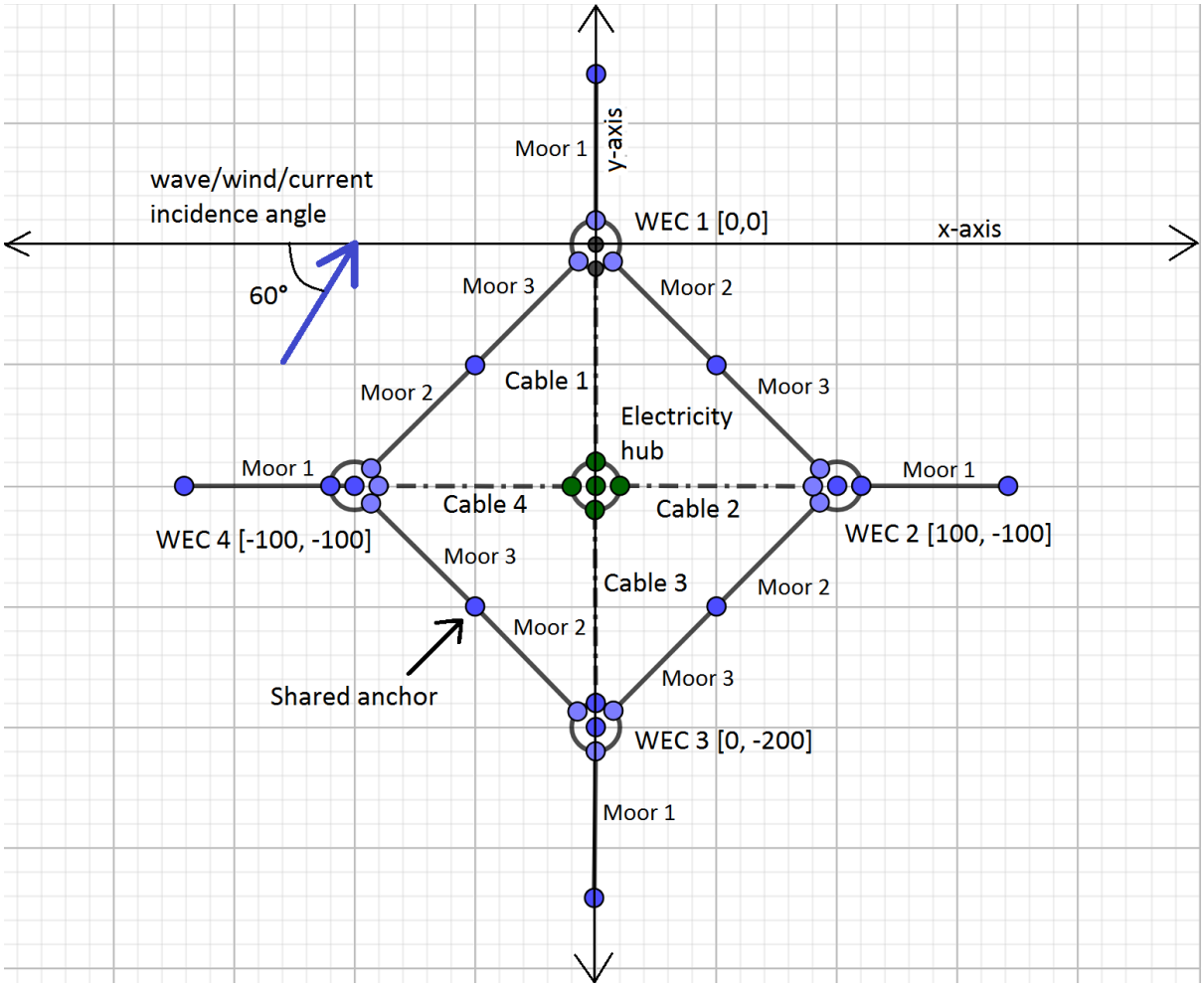

Figure 6.4: SquareBuoy configuration considering the original electricity collection system. In this configuration the WEC separating distance is 141 m, and anchors are shared between mooring lines 2 and 3 of adjacent WECs.

6.2.2. Modified collection system

Many new mooring line configurations can be considered for the SquareBuoy array with a modified collection system. Figures 6.5a-d display some of the configurations designed and modelled. In the configurations displayed in Figures 6.5b and 6.5c, a mooring line of WEC 2 and a mooring line of WEC 4 share an anchor. In the configuration displayed in Figure 6.5d, 4 mooring lines share an anchor in the center of the array.

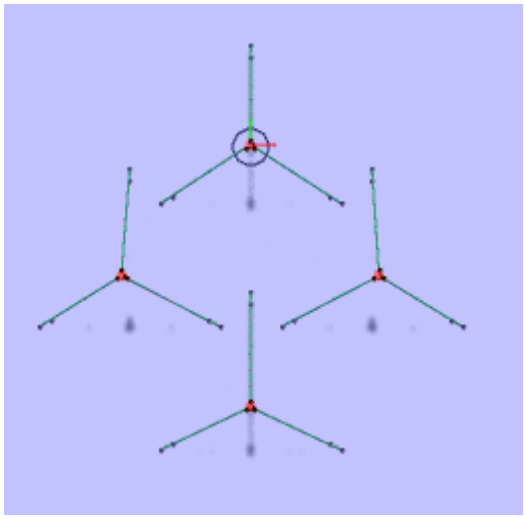

Figure 6.5a: Modelled Sq.V2.141.2.

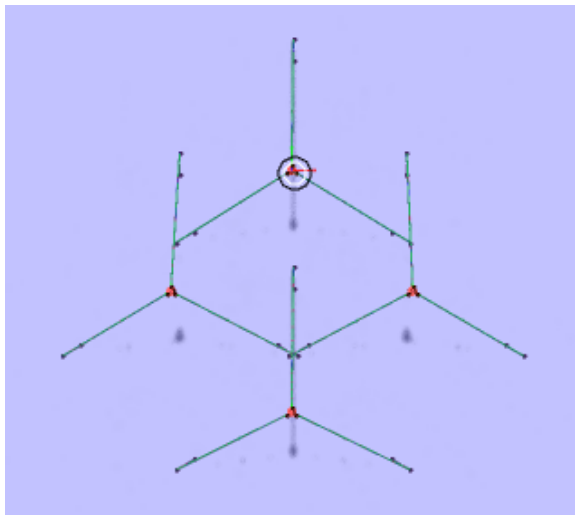

Figure 6.5b: Modelled Sq.V2.141.3.

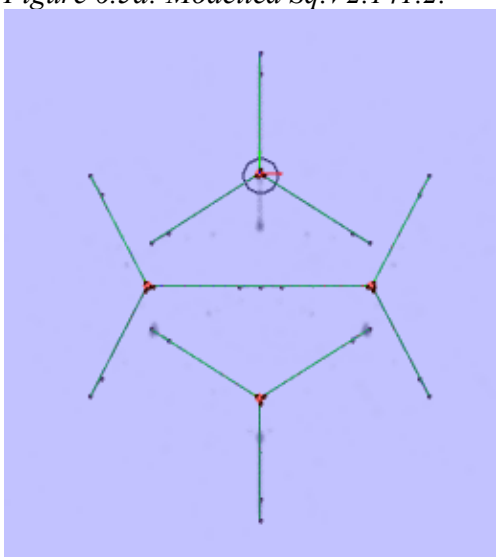

Figure 6.5c: Modelled Sq.V2.141.5

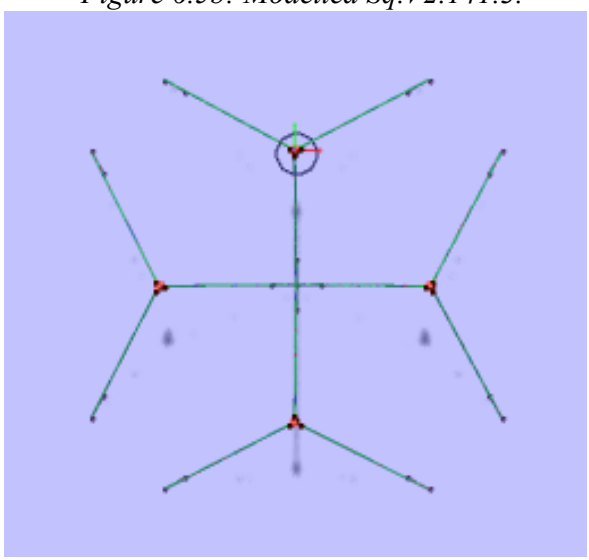

Figure 6.5d: Modelled Sq.V2.141.4.

Figures 6.5a-d: Different mooring configuration designs for the SquareBuoy array.

Top views of all modelled array configurations can be found in Appendix 11.3.

7 Results and Discussion

The results include the post-processed results for single buoy simulations, followed by post-processing results for the simulated array configurations. The post-processed information includes the calculated power absorption, maximum axial forces and/or fatigue life. Finally, for select configurations, results are presented for LCOE and LCA.

7.1 Single Buoy Simulations

In the single buoy simulations, an analysis will be performed on parameters to investigate their relevance at different locations. The order in which the results are presented is not necessarily the original order in which the studies were performed but are categorized according to the conclusions that can be drawn from each step.

The base case for the initial simulations is the model of the current prototype WaveEL 3.0 device, with buoy design V2, off the coast of Runde, Norway. The input environmental conditions are those defined in section 5.1 and displayed in Table 5.2. The wave, wind and current incidence angles are assumed to be 0 degrees. The data is obtained for 10800 seconds of simulation time (3 hours). The first study in the initial simulations examines the effects of varying simulation time. This is followed by the study of simulations assuming a uniform water depth, with a low, medium and high scenario.

To compare the power absorption potential for different sites, a single buoy configuration using the V2 buoy design is then modelled at each location, starting with Runde, followed by San Juan, Väderöarna, Läsö Ost, Garðskagi and Grimseyjarsund. Sensitivity analyses on various environmental factors will then be performed. First, the effect of including wind and current forces in the simulation is studied using the Runde environmental conditions. Then, the variation of wave, wind and current incidence angle is studied using the environmental conditions at Runde followed by San Juan. The next study applies extreme loads to the simulation of the WaveEL buoy, representative of a hurricane in San Juan. The final environmental study simulates current speed as a function of depth and compares it to the constant current speed assumption, using the conditions at Väderöarna and Läsö Ost. Next, a study varying the mooring line geometry for single V2 buoy configurations is conducted for the Runde, San Juan, and Garðskagi sites. Then, the buoy design V1 is introduced and simulated at the Runde, Garðskagi and Grimseyjarsund locations and compared to the V2 design. Finally, a second sea state is modeled for the Runde, Garðskagi, and Grimseyjarsund locations, representing the second most likely sea state conditions. The results are compared to the results of simulations using the first sea state conditions. A final discussion of the key results from the single buoy simulations is included in 7.1.7.

Table 7.1.1: Outline of the presentation of single buoy simulation results.

7.1.1. Initial simulations
a. Base case
b. Simulation time variation
c. Uniform water depth assumption
7.1.2. Comparison of sites
a. Runde, Norway
b. San Juan, Puerto Rico
c. Väderöarna, Sweden
d. Läsö Ost, Sweden

e. Garðskagi, Iceland
f. Grimseyjarsund, Iceland

7.1.3. Environmental factors
a. Effect of wind and current forces
i. Runde, Norway
b. Wave incidence angle
i. Runde, Norway
ii. San Juan, Puerto Rico
c. Extreme conditions
i. San Juan, Puerto Rico
d. Current loading as a function of depth
i. Väderöarna, Sweden
ii. Läsö Ost, Sweden

7.1.4. Mooring line geometry variation
a. Runde, Norway
b. San Juan, Puerto Rico
c. Garðskagi, Iceland

7.1.5. Introduction of alternative buoy dimensions: V1
a. Runde, Norway
b. Garðskagi, Iceland
c. Grimseyjarsund, Iceland

7.1.6. Simulation of a second sea state
a. Runde, Norway
b. Garðskagi, Iceland
c. Grimseyjarsund, Iceland

7.1.7. Discussion

7.1.1 Base Case Simulations

a) Base Case

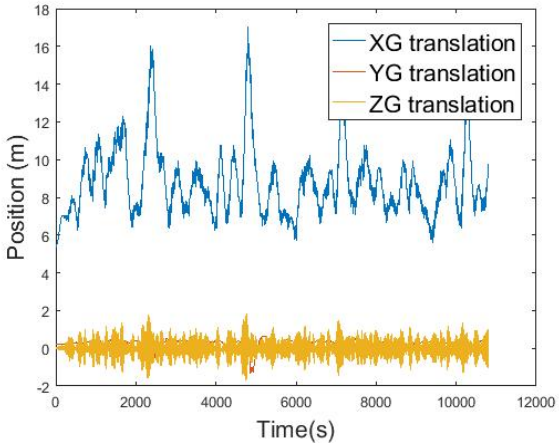

Figure 7.1.1: WEC motion in x,y,z directions.

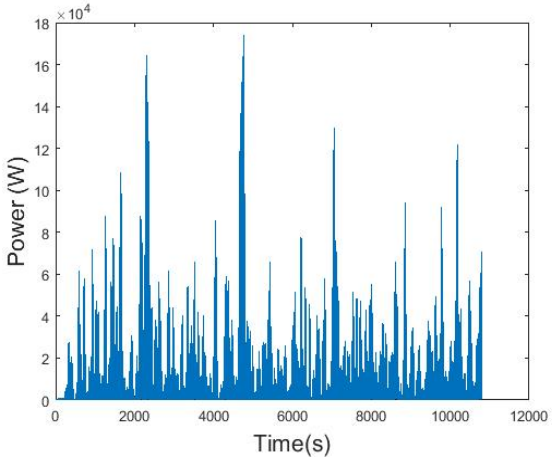

Figure 7.1.2: Instantaneous WEC power.

In Figure 7.1.1, the x, y and z translational motion of the WEC in the base case scenario are displayed as a function of time. It can be seen that the WEC's motion in the x direction is a

degree larger than the WEC's motions in the y and z directions. However, translational motion in the z direction, or the heave motion, is most important for power generation in the design of the WaveEl buoy. Figure 7.1.2 displays the instantaneous power per second, found by taking the derivative of the heave motion. Using equation 1, time-averaged power can be then obtained. The results for the base case simulation can be found in Table 7.1.2. Power rating refers to the maximum instantaneous power absorption achieved in the simulation time, and time averaged power refers to the average power absorption over the course of the simulation.

Table 7.1.2: The power rating and time-averaged power calculated from the base case simulation.

Power rating (kW)	Time averaged power (kW)
173.85	12.81

The maximum axial forces observed per element and per second of the base case simulation are displayed in Appendix 11.5. As displayed in Table 7.1.3, the maximum axial forces occur in the 13th data element of mooring line 1, the 14th data element of mooring line 2, and the 16th data element of mooring line 3. This corresponds to the first element of segment 2 in mooring lines 1 and 2, and the 18th element of segment 2 in mooring line 3 (see Appendix 11.4).

Table 7.1.3: the maximum axial force recorded in each mooring line, and where and when it is found.

Mooring line	Maximum axial force (kN)	Element	Time (seconds)
1	74.46	13	10223
2	72.92	14	9535
3	177.19	16	10224

In Table 7.1.4 the number of years until failure is shown, using the post-processing procedure described in the methods section. It is important to note that because only the most common sea state found from the scatter diagram is simulated, the estimated lifetime is not a precise reflection of the actual fatigue life but is simply used for comparison between the simulations. Thus, the shortest fatigue life calculated of 27.46 million years is obviously unrealistic but is a good indication of the security of the mooring line configuration in the base case.

Table 7.1.4: Years to failure (fatigue life) of mooring lines in base case.

Fatigue life: Mooring line 1 (years)	Fatigue life: Mooring line 2 (years)	Fatigue life: Mooring line 3 (years)
1.03E+14	1.07E+13	2.75E+07

b) Simulation time variation

For the simulation of 10800 seconds, the run time is significant. Thus, for the initial numerical simulations a shorter simulation time is desired that still accurately captures the motions of the WEC and forces acting on the cable and mooring lines. A few simulation times will be tested: 5 minutes, 15 minutes, and 1 hour. Simulations using the base model with new simulation times of 5 minutes, 15 minutes, and 1 hour are run, post-processed and analyzed. Then, the output from these simulations are scaled to more accurately reflect the steady sea state. The modified results will be post-processed and discussed.

Table 7.1.5: Comparison of power, maximum axial forces and fatigue lives using simulation times of 3 hours (10800 seconds), 1 hour (3600 seconds), 15 minutes (900 seconds) and 5 minutes (300 seconds).

Simulation	Base case	1	2	3
Simulation time (seconds)	10800	300	900	3600
Power rating (kW)	173.85	16.09	43.01	109
Time averaged power (kW)	12.81	1.09	5.26	10.34
Maximum axial force: Mooring line 1 (kN)	74.46	69.12	70.12	71.40
Element number	13	13	13	13
Maximum axial force: Mooring line 2 (kN)	72.92	69.98	69.11	70.74
Element number	14	14	14	14
Maximum axial force: Mooring line 3 (kN)	177.19	99.05	124.76	133.21
Element number	16	13	16	16
Fatigue life: Mooring line 1 (years)	1.03E+14	3.40E+18	4.80E+17	2.21E+17
Fatigue life: Mooring line 2 (years)	1.07E+13	8.62E+13	5.35E+13	2.80E+13
Fatigue life: Mooring line 3 (years)	2.75E+07	1.68E+10	9.97E+08	4.93E+08

The 5 minute, 15 minute and 1 hour simulations do not produce similar results compared to the 3 hour steady state simulation. WEC time absorbed power reduces by 19%, 59%, and 91% for the 1 hour, 15 minute and 5 minute simulations, respectively, and the maximum axial force observed reduces by 25%, 30%, and 44%. The estimated fatigue life in the weakest mooring line is longer in the 1 hour, 15 minute and 5 minute simulations by a factor of 16.96, 35.3 and 609 compared to the 3 hour simulation. In the 5 minute simulation, the representation of steady sea state is far from achieved. This can be seen in Figures 7.1.3a and 7.1.3b, where the maximum axial forces and the instantaneous power produced is growing throughout the 5 minute simulation. Conversely, the graphs of the maximum axial force in mooring line 3 and the power produced per second in the 15 minute and 1 hour simulations look similar to the base case 3 hour simulation (see Appendix 11.6).

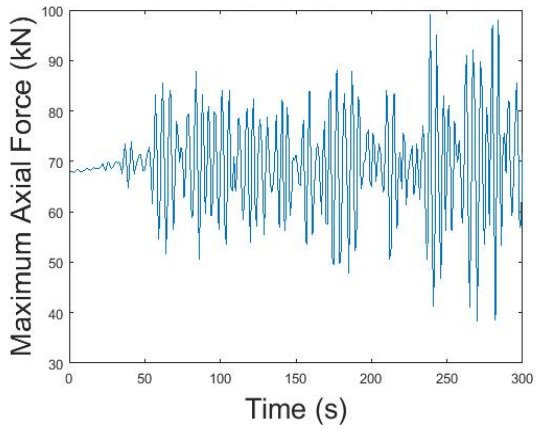

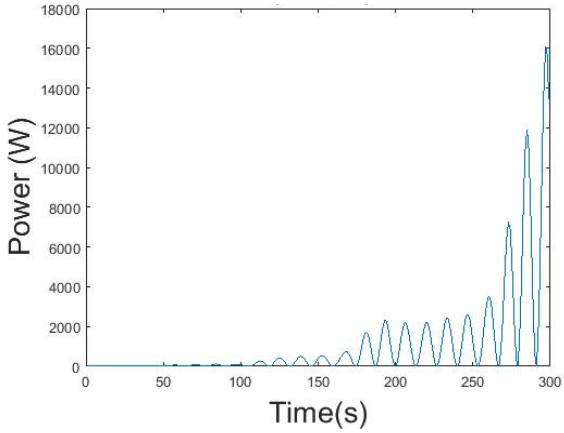

Figure 7.1.3a: Maximum axial force vs time. *Figure 7.1.3b: Power vs time.*
Figures 7.1.3a-b: Maximum axial force in mooring line 3 as a function of time (a) and power produced by WEC as a function of time (b) in the 5 minute simulation.

To use shorter simulations with comparable values to the base case 3 hour simulation, the results must be modified. The relationships found can be used later in the more complex simulations of the arrays. If the axial forces for the 5 minute, 15 minute and 1 hour simulations are multiplied by 1.79, 1.42 and 1.33, respectively, the maximum axial force observed in the most stressed mooring line is then equal to the maximum axial force observed in the 3 hour simulation. Using these alternative values for axial force, the fatigue life calculations will change. Table 7.1.6 displays the new estimated fatigue life in the weakest mooring line if the axial forces are increased to compare to the 3 hour simulation. It also displays the WEC power absorption if the 1 hour, 15 minute and 5 minute simulations are multiplied by 1.24, 2.43 and 11.75 respectively. With this method, the estimated fatigue life in the 5 minute, 15 minute and 1 hour simulations reduce significantly. Compared to the 3 hour simulation, fatigue life in the weakest mooring line is about a quarter of the length with the modified 5 minute simulation, about a third of the length with the modified 15 minute simulation, and 4/10 of the length with the modified 1 hour simulation. Nonetheless, these fatigue life values are significantly closer to the fatigue life expected for a steady sea state simulation than the original values, with the 1 hour simulation producing the most comparable results.

Table 7.1.6: Modified power absorption, maximum axial force, and fatigue life calculations using shorter simulation times to reflect a steady sea state.

	WEC power absorption (kW)	Maximum axial force (kN)	Estimated fatigue life (years)
3 hour simulation	12.81	177.19	2.75E+07
	Modified WEC power absorption (kW)	Modified maximum axial force (kN)	Modified estimated fatigue life (years)
5 minute simulation	12.81	177.29	6.62E+06
15 simulation	12.79	177.15	8.89E+06
1 hour simulation	12.82	177.16	1.06E+07

Thus, it is assumed that the 1 hour simulation is sufficient for comparing simulation results throughout the parametric variation, and that the 1 hour simulation with modified axial force and power absorption values is sufficient for representing a steady sea state in the array

simulations. However, using the modified values for the 1 hour simulation will shorten the fatigue life to less than half that obtained from a 3 hour simulation. Thus, the modified fatigue life calculated will be considered as a conservative estimate.

c) Uniform water depth assumption

As was mentioned earlier, in the design of the arrays, because the exact bathymetry of the sites is not known, a uniform water depth must be assumed. This estimate may be much lower or higher than the actual average. Thus the purpose of this sensitivity analysis is to find the effect of the uniform water depth assumption on the power absorption and maximum axial forces in the mooring lines. In all simulations the mooring lines are anchored at the same depth and identical.

In the first simulation, the water depth is assumed to be 86.6 m for all anchors. Because this is the actual water depth of the anchor of mooring line 1 in the installed prototype WaveEL configuration, the mooring line geometry of WaveEL's mooring line 1 will be used for all mooring lines. Thus, the horizontal distance between the WEC and the anchor, also known as anchor radius, is set as 127.3 m for all 3 mooring lines, and the lengths of mooring line segments 1 and 2 are set to 96 m and 76.6 m. The second and third simulation represent a low and high estimate for water depth, set to 54.1 m and 150 m, respectively. In order to produce comparable results to the base case, the relative geometries of the mooring configurations are proportional to the base case. Specifically, in all cases, the ratio between mooring line segments 1 and 2 is between 1.24 and 1.27, and the anchor radius is greater than the water depth by a factor of 1.6.

Table 7.1.7: Results of low, medium and high estimate for uniform water depth at Runde.

	Base estimate	Shallow estimate	Deep estimate
Water depth (m)	86.6	54.1	150
Anchor radius (m)	127.3	80	220.5
Mooring line segment 1 length (m)	96	58	162
Mooring line segment 2 length (m)	76.6	46	130
Segment 1:2 length ratio	1.25	1.26	1.25
WEC power absorption (kW)	10.06	9.82	10.84
Maximum axial force: Mooring line 1 (kN)	72.08	80.85	72.41
Maximum axial force: Mooring line 2 (kN)	80.11	86.51	77.04
Maximum axial force: Mooring line 3 (kN)	130.69	154.29	135.34

As can be seen in Table 7.1.7, the shallow estimate of water depth yields 18% higher maximum axial forces in the most stressed mooring line and 2% lower power absorption compared to the

base estimate. The deep estimate yields 4% higher maximum axial forces in the most stressed mooring line but 8% higher power absorption compared to the base estimate.

7.1.2 Comparison of sites

In Figure 7.1.4, the WEC power absorption is compared for each of the locations from the location study using a one hour simulation and a defined mooring line configuration. The purpose of this comparison is to show that certain sites are better suited for producing electricity from wave energy with the WaveEL device. The simulations each use the most common sea state from that location and the assumed water depth of that location, with the depth at Runde being 86.6 m. It should be noted that with each location, water depth differs, so the mooring line configuration is different in each case. The details of the mooring line configurations used can be found in Appendix 11.2 and correspond to moor configuration number 1 in all sites. Thus, the results represent one option in a range of mooring line configuration options for that site.

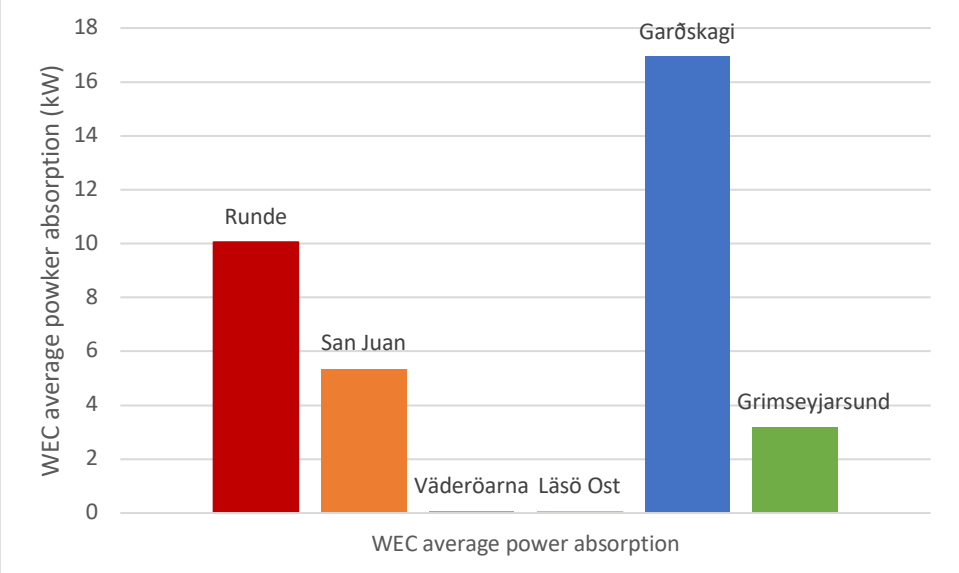

Figure 7.1.4: Comparison of WEC power absorption at various locations.

It is clear that Garðskagi is the site which potentially produces the most power, followed by Runde, San Juan and Grimseyjarsund. Both Swedish sites of Läsö Ost and Väderöarna produce negligible amounts of power. This is due to the low average significant wave heights and periods at both sites.

7.1.3 Environmental factors

a) Effect of wind and current load

The effect of including the wind and current forces in the simulation will be studied using the environmental conditions at Runde. To find the effect of the wind and current load on the single buoy configuration, 3 simulations are compared. The first is the one hour simulation of the base case configuration. The second is the same configuration without the presence of wind. The third is again the base case configuration, this time without the presence of current loading.

Table 7.1.8: Effect of removing wind and current forces from simulation at Runde site.

	Simulation 1: Complete load	Simulation 2: No wind	Simulation 3: No current
Maximum axial force: Mooring line 1 (kN)	71.40	71.43	72.84
Maximum axial force: Mooring line 2 (kN)	70.74	70.90	81.09
Maximum axial force: Mooring line 3 (kN)	133.21	132.48	112.90
WEC time-averaged power absorption (kW)	10.34	10.34	10.98

Table 7.1.8 displays the maximum forces found in mooring lines 1, 2, and 3, and the WEC power absorption for each simulation case. As can be seen, the results of simulation 2 does not differ much from simulation 1, while the results of simulation 3 with no current loading changes the results significantly. This shows that the current has a significant impact on the forces on the mooring lines as well as the WEC motion.

b) Wave, wind and current incidence angle

i. Runde, Norway

Without tangible historical data for the dominant wave direction at the Runde site, the best conclusion that can be made is that the wave climate is multidirectional, with equal probability of each incidence angle with the WEC device. The same conclusion is made for the wind direction. The current direction, however, is found to be bidirectional. Thus, the current incidence angle is varied between 0 and 90 degrees, with the wave and current direction arbitrarily set to the same incidence angle. The results are displayed in Table 7.1.9. A current incidence angle of 0 degrees produces the highest power absorption, followed by 60 degrees, 90 degrees and then 30 degrees. The maximum axial forces are lowest at a current incidence angle of 90 degrees and highest at an incidence angle of 30 degrees.

Table 7.1.9: Effects of varying current incidence angle on power absorption and maximum axial force at the Runde site.

Simulation	1	2	3	4
Current incidence angle (deg)	0	30	60	90
Wave incidence angle (deg)	0	30	60	90
Wind incidence angle (deg)	0	30	60	90
WEC time averaged power absorption (kW)	10.06	9.91	10.05	9.92

Maximum axial force: Mooring line 1 (kN)	72.08	73.74	80.73	83.85
Maximum axial force: Mooring line 2 (kN)	80.11	73.25	71.92	106.38
Maximum axial force: Mooring line 3 (kN)	130.69	142.82	132.33	106.95

ii. San Juan, Puerto Rico

The location study of San Juan indicates that the wave, wind and current directions are generally unidirectional. Thus, simulations for this environment differ from environments such as Runde because the wave incidence angle corresponds to a specific range of wind and current incidence angles. 6 simulations are run varying the wave incidence angle using the environmental conditions at San Juan. The corresponding wind and current incidence angles are displayed in Table 7.1.10. The results indicate that wave incidence angles of 0 or 60 degrees are optimal for WEC power absorption, increasing power absorption by 6% compared to the worst incidence angle of 90 degrees. However, it should be noted that the wave incidence angles of 0 and 60 degrees also correspond with the highest maximum axial forces.

Table 7.1.10: Effects of varying wave incidence angle on power absorption and maximum axial force at the San Juan site.

Simulation	1	2	3	4	5	6
Wave incidence angle (deg)	0	30	60	90	150	330
Wind incidence angle (deg)	25	55	85	115	175	355
Current incidence angle (deg)	120	150	180	210	270	90
WEC time averaged power absorption (kW)	5.44	5.31	5.43	5.12	5.32	5.12
Maximum axial force: Mooring line 1 (kN)	104.62	106.71	104.93	109.66	108.26	106.24
Maximum axial force: Mooring line 2 (kN)	106.30	108.09	108.79	106.37	117.14	109.69
Maximum axial force: Mooring line 3 (kN)	121.13	117.01	120.33	106.56	106.59	106.30

c) Extreme conditions

A one hour simulation is used to compare the forces acting on the single buoy configuration at the San Juan site in average environmental conditions and the extreme environmental conditions found during hurricane season. The mooring line system has the configuration described in Table 7.1.11.

Table 7.1.11: Properties of mooring line configuration used for simulation of extreme conditions at San Juan site.

Anchor radius (m)	Length of segment 1 (m)	Length of segment 2 (m)	Total length (m)	Segment 1/2 length ratio
70	55	25	80	2.2

Table 7.1.12 shows the results comparing the simulations. The hurricane conditions result in a significant decrease in the fatigue life of the mooring lines. However, also notable is that the average power absorption increases by nearly four times.

Table 7.1.12: Effect of assuming average conditions or hurricane conditions on power absorption, maximum axial force and fatigue life calculations in the San Juan site.

	Average conditions	Hurricane conditions
Average power absorption (kW)	5.26	20.07
Maximum axial force: Mooring line 1 (kN)	76.68	121.63
Maximum axial force: Mooring line 2 (kN)	87.61	125.78
Maximum axial force: Mooring line 3 (kN)	97.79	89.90
Fatigue life: Mooring line 1 (years)	1.22E+19	1.30E+11
Fatigue life: Mooring line 2 (years)	1.29E+13	1.84E+10
Fatigue life: Mooring line 3 (years)	1.31E+11	4.27E+10

d) Current loading as a function of depth

In previous simulations, current speed has been assumed constant as a function of depth. However, the current data provided for the Väderöarna and Läsö Ost locations indicates that current speed decreases as water depth increases. The comparison of including this relationship in the simulations is displayed in Tables 7.1.13 and 7.1.14.

Table 7.1.13: Effects of including the current gradient at the Väderöarna location.

	Without current gradient	With current gradient
Average power absorption (W)	69.38	69.47
Maximum axial force: Mooring line 1 (kN)	75.58	74.63
Maximum axial force: Mooring line 2 (kN)	86.51	86.71
Maximum axial force: Mooring line 3 (kN)	87.86	87.97

Table 7.1.14: Effects of including the current gradient at the Läsö Ost location.

	Without current gradient	With current gradient
Average power absorption (W)	80.87	80.92
Maximum axial force: Mooring line 1 (kN)	82.23	81.96
Maximum axial force: Mooring line 2 (kN)	87.76	87.83
Maximum axial force: Mooring line 3 (kN)	94.63	94.67

The inclusion of the current gradient slightly increases the calculated power absorption and has a small effect on the maximum axial forces observed. This indicates that assuming a constant current speed as a function of depth is justified in that the effect is so small.

7.1.4 Mooring Line Geometry Variation

The next study is to vary the mooring line segment lengths and horizontal distance from the anchor to the WEC (referred to as the anchor radius) at different sites. At each site, the simulations will use the same WEC buoy, same cable and hub design, and the same environmental conditions. It must be noted that in the environmental conditions only the most common sea state found from the location study is used in the analysis of optimal mooring line configuration. The results may differ if another sea state had been applied.

Using the results of each simulation, the optimal geometry can be found that maximizes WEC heave motion and thus WEC power absorption yet still has a realistic fatigue life. The specifications for each different mooring line configuration simulated are displayed in Appendix 11.2.

a) Runde, Norway

Figure 7.1.5 displays a graph made using the results from 16 one-hour simulations at Runde, Norway. A uniform water depth of 86.6 m is assumed. It can be seen that larger anchor radii correspond to a higher power absorption, and that the power absorption increases as the ratio between segment 1 and 2 decreases. Figure 7.1.6 displays the maximum stress observed in any mooring line in the configuration during the 1 hour simulation. There does not seem to be any significant relationship between mooring line segment ratio, anchor radius, and the estimated fatigue life. Thus, maximizing anchor radius and minimizing the ratio between segments 1 and 2 could be the priority of two segment mooring line configurations at the Runde site.

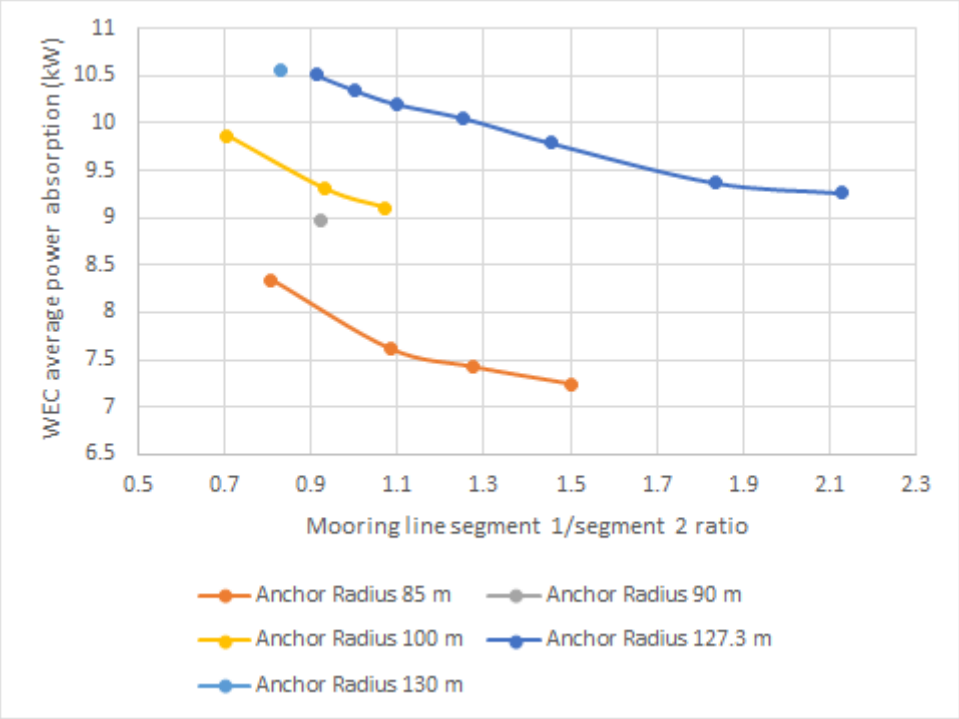

Figure 7.1.5: Relationship between WEC power, mooring line segment ratio, and anchor radius for a single V2 buoy configuration in Runde.

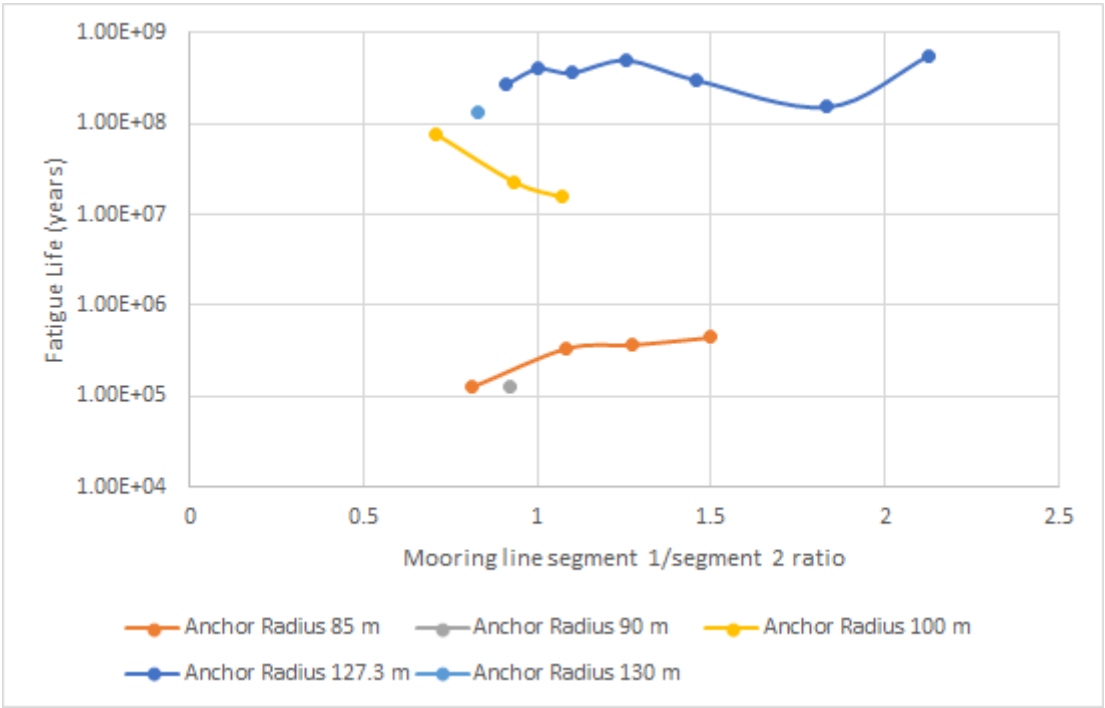

Figure 7.1.6: Relationship between estimated fatigue life, mooring line segment ratio, and anchor radius for a single V2 buoy in Runde.

Figure 7.1.7 displays a graph made using the results from four one-hour simulations with only 1 mooring line segment. Without the use of a floater, the pre-tension force in the mooring lines is assumed to be zero. In these simulations the anchor radius is constrained by the length of the mooring line and vice versa. As can been seen, the geometry that obtains the highest power

absorption is the largest anchor radius of 194 m. However, this mooring geometry also has a significantly lower estimated fatigue life than the other geometries. Thus, it can be concluded that for single segment lines in a water depth of 86.6 m, an anchor radius between 120 and 150 m is optimal. When comparing to two segment mooring line configurations with anchor radii of 127.3, the estimated power absorption is within the same range, while the fatigue life in the weakest line is found to be significantly lower.

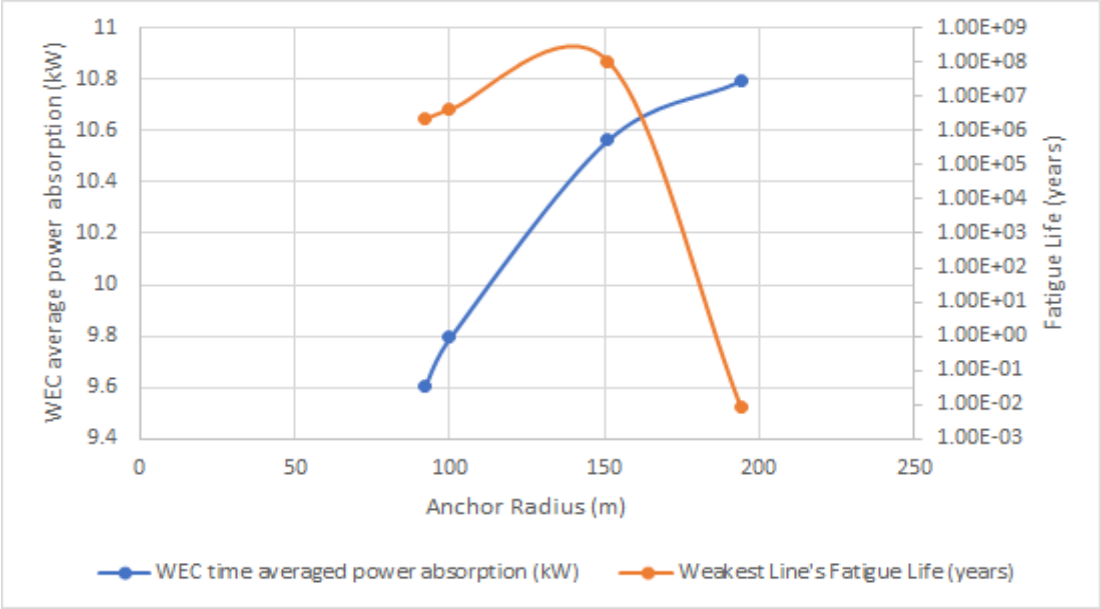

Figure 7.1.7: Relationship between WEC power, estimated fatigue life and anchor radius for a single V2 buoy in Runde with a 1 segment mooring line configuration.

b) San Juan

Fourteen one-hour simulations are run varying mooring line geometry in two segment mooring lines for the location at San Juan. As can be seen from Figure 7.1.8, the maximum WEC power absorption is achieved when the mooring line segment ratio is between about 1.2 and 1.5, and the best simulated anchor radius is the lowest simulated at 70 m. Figure 7.1.9 shows that at an anchor radius of 70 m, the longest estimated fatigue life is achieved with a mooring line segment ratio of about 2. However, all simulations estimate a long fatigue life, so the mooring line segment ratio suggested for San Juan will still be between 1.2 and 1.5 for maximum power absorption.

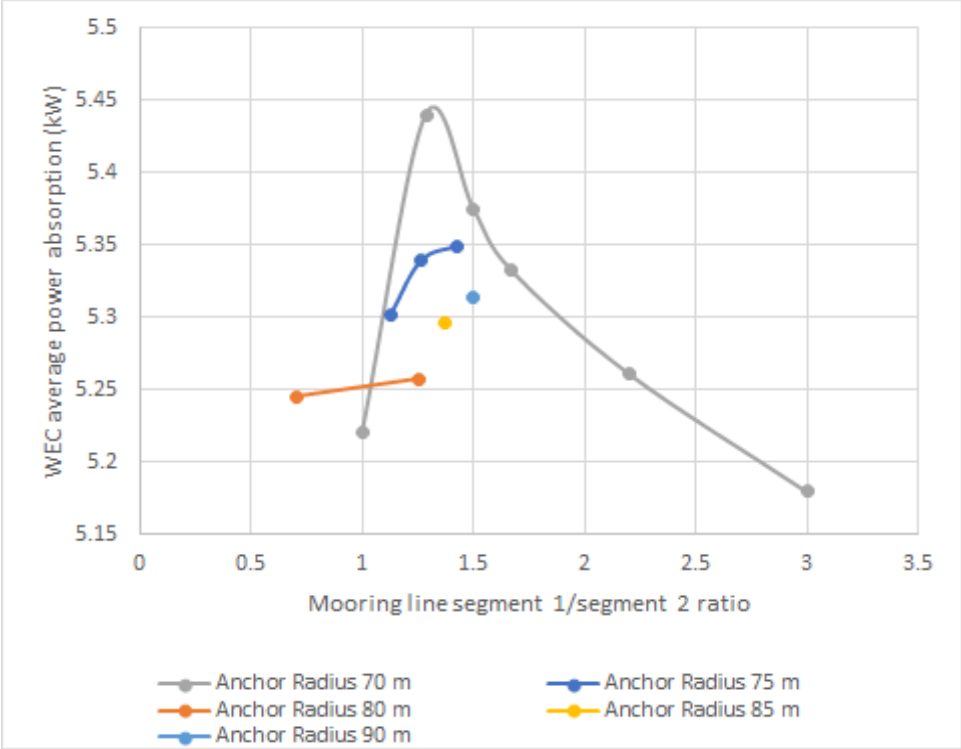

Figure 7.1.8: Relationship between WEC power, mooring line segment ratio, and anchor radius for a single V2 buoy configuration in San Juan.

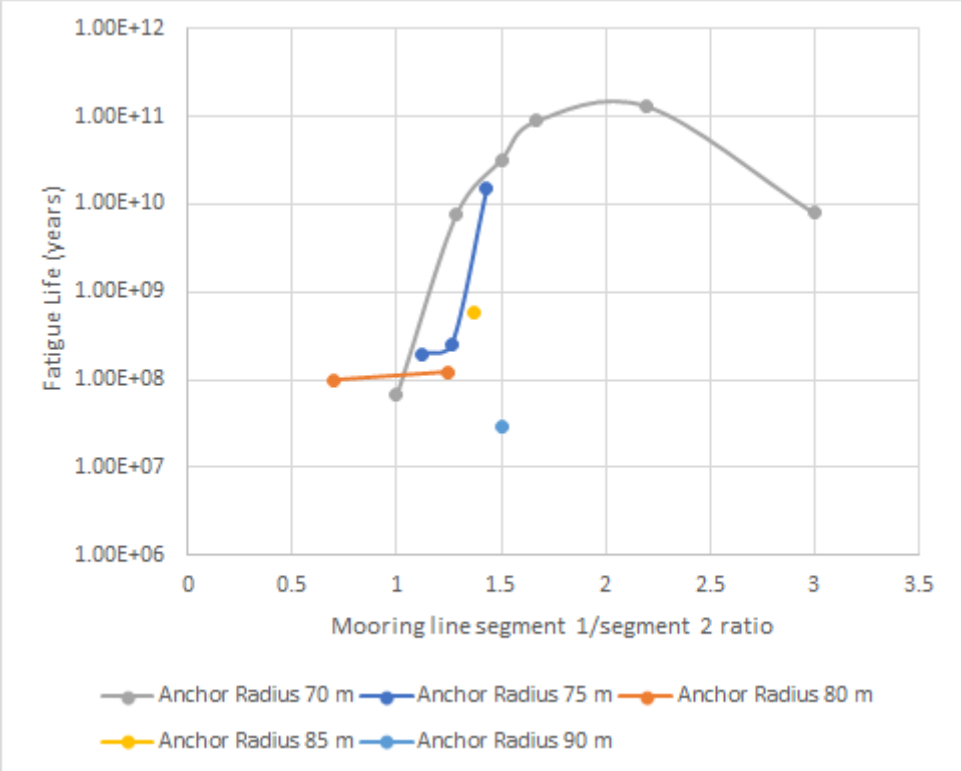

Figure 7.1.9: Relationship between estimated fatigue life, mooring line segment ratio, and anchor radius for a single V2 buoy in San Juan.

Three one-hour simulations are conducted for one segment mooring lines at the San Juan location. The results displayed in Figure 7.1.10 show that again, the optimal anchor radius is 70 m. This anchor radius maximizes both power absorption and the estimated fatigue life in the weakest line. However, it should also be noted that for the same anchor radius, the power absorption is significantly less than the power absorption with two segment mooring lines, while the fatigue life is significantly higher than at of the two segment mooring line.

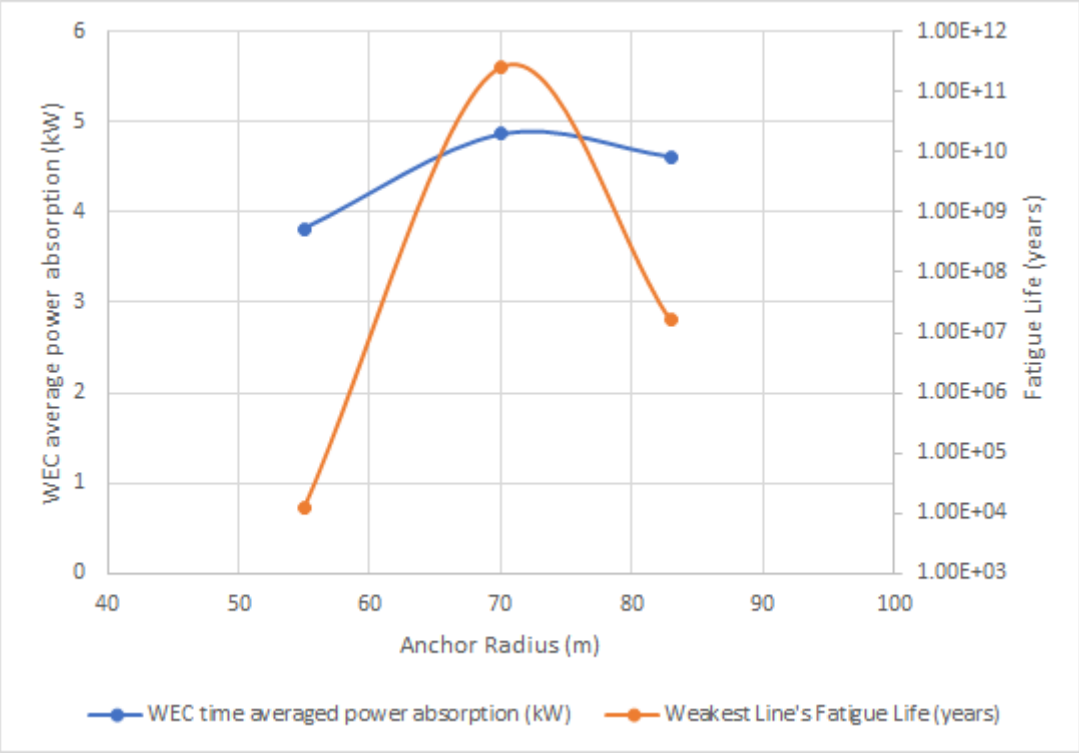

Figure 7.1.10: Relationship between WEC power, estimated fatigue life and anchor radius for a single V2 buoy in San Juan with a 1 segment mooring line configuration

c) Garðskagi, Iceland

Ten one-hour simulations are run for two segment mooring line configurations at the Garðskagi site. Figure 7.1.11 displays the average power absorption calculated from the simulations. The highest power absorption is obtained from the highest anchor radius simulated of 120 m, and between the mooring line segment ratios of 1.1 and 1.2. In Figure 7.1.12, the estimated fatigue life in the weakest line generally increases as mooring line segment ratio increases and as anchor radius increases. Thus, the anchor radius of 120 m is suggested, with a mooring line segment ratio of about 1.2.

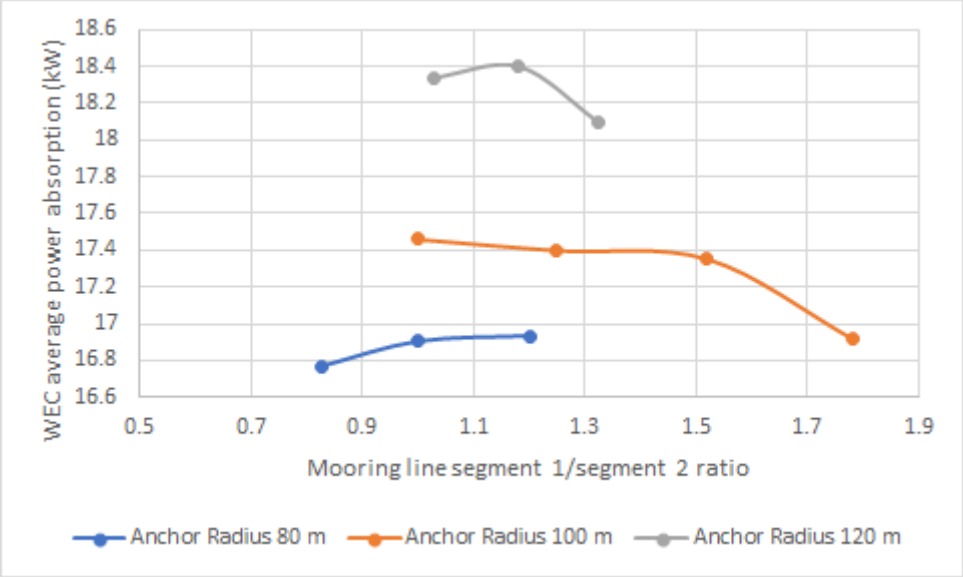

Figure 7.1.11: Relationship between WEC power, mooring line segment ratio, and anchor radius for a single V2 buoy configuration in Garðskagi.

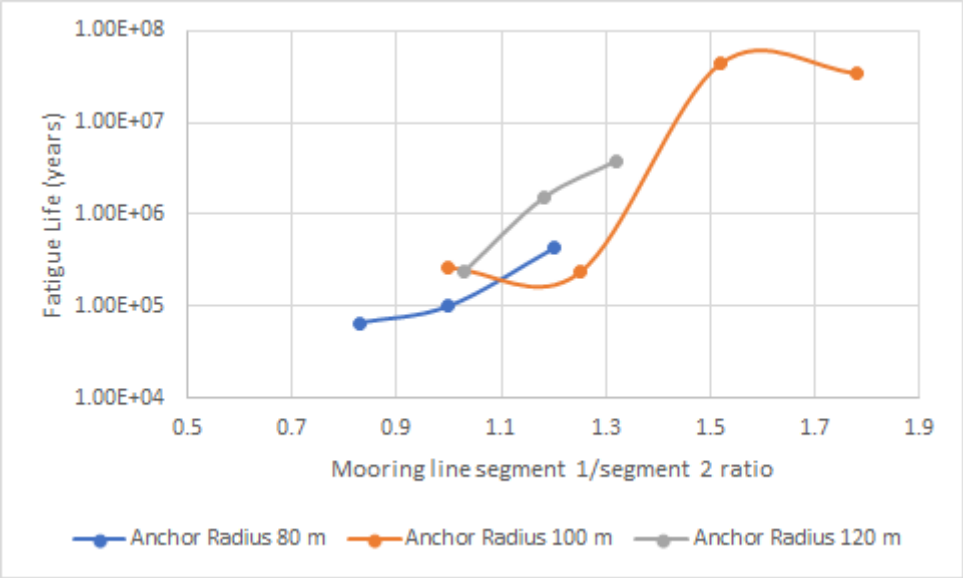

Figure 7.1.12: Relationship between estimated fatigue life, mooring line segment ratio, and anchor radius for a single V2 buoy in Garðskagi.

7.1.5 Introduction of Different Buoy Dimensions: V1 Buoy

As mentioned in section 4.1, V1 buoy has a longer shaft and thus a different resonant frequency than the V2 buoy. Thus, it is possible that the V1 buoy will be more successful in certain locations depending on the range of wave frequencies found. In Figure 7.1.13, simulations of the V1 buoy are compared to simulations of the V2 buoy in the Runde, Garðskagi and Grimseyjarsund locations. The mooring line geometries at each site are the same for both buoys to ensure a reliable comparison; details can be found in Appendix 11.2. For the V2 buoys, the mooring configuration numbers are 15 for Runde, 8 for Garðskagi and 1 for Grimseyjarsund. For the V1 buoys, the mooring configuration numbers are 5 for Runde, 1 for Garðskagi and 1

for Grimseyjarsund. The results show that in all three locations the V2 buoy performs better than the V1 buoy.

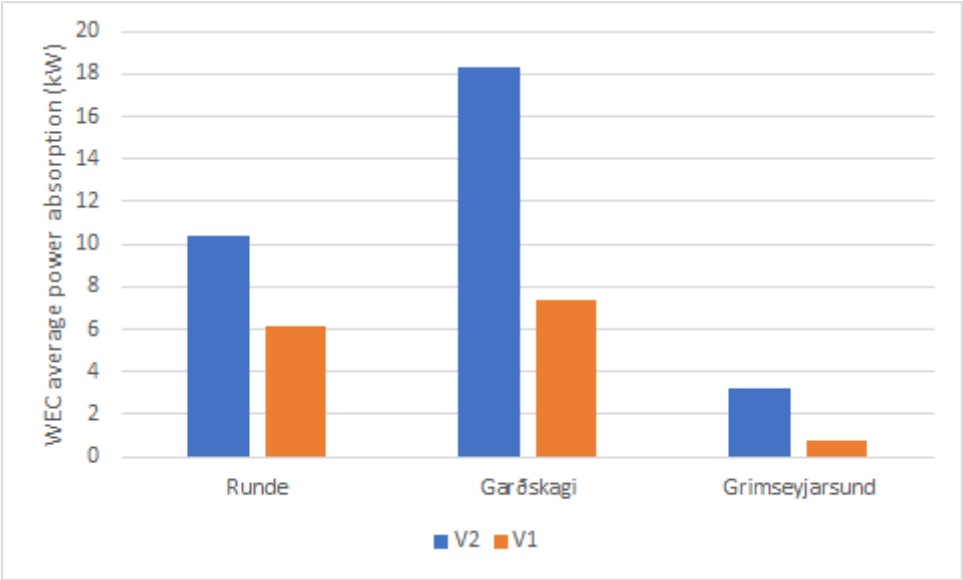

Figure 7.1.13: Comparison of power absorption of V2 and V1 buoys in Runde, Garðskagi and Grimseyjarsund.

7.1.6 Simulation of a Second Sea State

In all previous simulations, the input H_s and T_p have been limited to the most common sea state observed at a given location, found from the scatter diagrams in section 4. However, simulating for just one sea state is not a realistic representation of the environment. Thus, in the Runde, Garðskagi and Grimseyjarsund locations simulations are also run using the second most common sea state as input. Table 7.1.15 displays the difference between the H_s and T_p of the first and second most common sea states, called sea state 1 and sea state 2. Both V2 and V1 buoys are simulated with the second sea state to see if this will affect their productivity.

Table 7.1.15: H_s and T_p values for sea states 1 and 2 in the Runde, Garðskagi and Grimseyjarsund locations.

	Sea state 1		Sea state 2	
Site	H_s (m)	T_p (s)	H_s (m)	T_p (s)
Runde	1.5	5.5	2.5	6.5
Garðskagi	2.0	5.0	2.0	6.5
Grimsey	1.0	4.5	2.0	5.5

a) Runde, Norway

As can be seen in Figure 7.1.14, simulating for the second most common sea state in Runde results in an increase in power for both V1 and V2 buoys. It is also noticeable that the simulation of the second sea state is much more favorable for the V1 buoy. Comparing the two designs, the V2 buoy design produces more power in the most common sea state conditions, while the V1 buoy design produces more power in the second most common sea state conditions. This suggests that the resonance frequencies of the buoys are quite different.

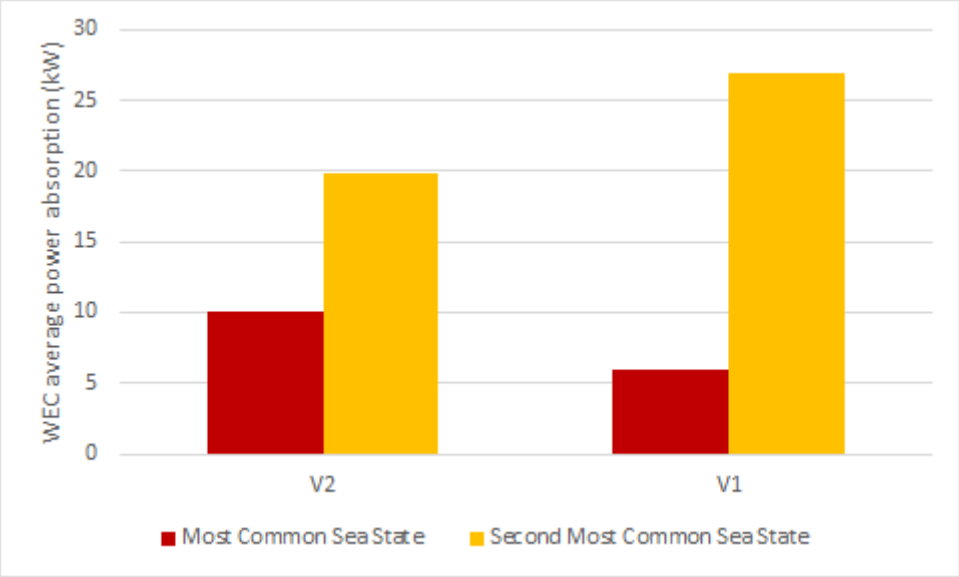

Figure 7.1.14: Comparison of the WEC power absorption calculated from simulating the most common sea state and the second most common sea state for V2 and V1 buoys in Runde.

Another consideration is the effect of simulating a second sea state on the fatigue life. In Runde the second most common sea state has a higher mean significant wave height and wave period than the most common, which will increase the forces on the mooring lines and thus decrease their fatigue life. An example of this is displayed in Figure 7.1.15, showing the fatigue lives of 3 models of the V1 buoy with different mooring line geometries. It is obvious that in all models, the second most common sea state reduces the fatigue life of the weakest mooring line drastically. It can also be seen that by increasing the mooring line segment length ratio, the fatigue life can be slightly improved.

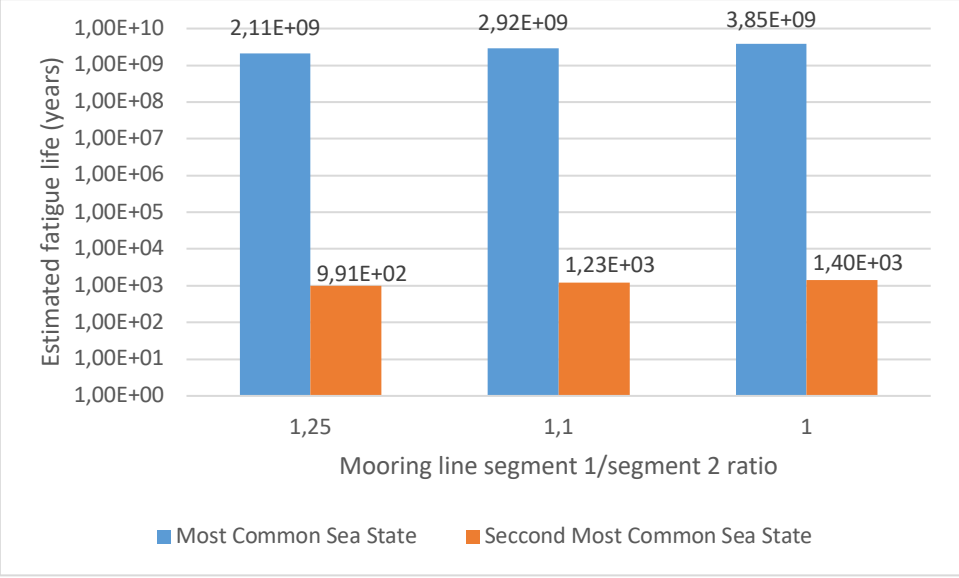

Figure 7.1.15: Effects of mooring line segment ratio and simulating sea states 1 and 2 on the fatigue life calculations.

b) Garðskagi, Iceland

Like Runde, simulating the second most common sea state is clearly more favorable for the V1 buoy. However, as seen in Figure 7.1.16, the second most common sea state conditions at Garðskagi reduces the average power absorption of the V2 buoy compared to the most common sea state conditions. The V2 buoy design produces more power in the most common sea state conditions, while the V1 buoy design produces more power in the second most common sea state conditions.

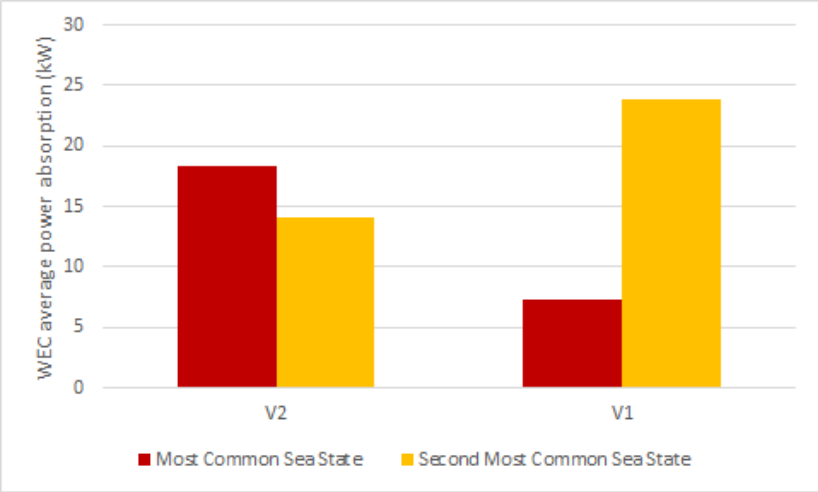

Figure 7.1.16: Comparison of the WEC power absorption calculated from simulating the most common sea state and the second most common sea state for V2 and V1 buoys in Garðskagi.

c) Grimseyjarsund, Iceland

At the Grimseyjarsund site, the second most common sea state leads to a much higher power absorption for the V2 buoy and for the V1 buoy. In both simulations of the most common sea state and the second most common sea state the V2 buoy is preferable. This indicates that neither of the resonance frequencies of the buoys are optimized in wave periods lower than 4.5 seconds.

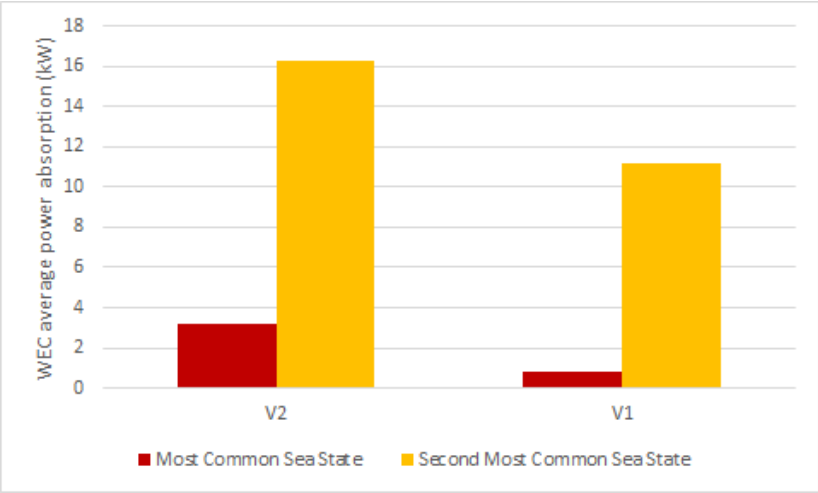

Figure 7.1.17: Comparison of the WEC power absorption calculated from simulating the most common sea state and the second most common sea state for V2 and V1 buoys in Grimseyjarsund.

7.1.7 Discussion

The base case simulations show that simulation times shorter than 3 hours do not produce results that can be compared to that of a steady sea state, but for comparison between simulations while performing the parametric variations, a 15 minute or one-hour simulation is sufficient. For use in LCOE or LCA calculations where more accurate values of power absorption and fatigue life is desired, the results of shorter simulations can be modified. Assuming a uniform water depth that is shallower than the actual average will result in lower power absorption calculations, and vice versa for deeper water depth assumptions.

In terms of environmental conditions, the WEC configuration is most sensitive to changes in wave and current conditions. Particularly, the mean significant wave height and wave period which make up a sea state have a large effect on the efficiency and survivability of a WEC configuration. Wave periods which are closer to the resonance frequency of the WEC result in higher power absorption, while higher wave heights result in higher power absorption and lower fatigue lives. For this reason Garðskagi is the best site in terms of power absorption for the WaveEL device. Due to the difference in their resonant frequencies, the V1 and V2 perform better or worse depending on the wave period assumed. The angle of incidence does not have a significant effect on the system in multidirectional climates but could be optimized in unidirectional climates. Assuming current speed as constant for all water depths rather than as a gradient does not have a significant effect on the results of the simulations.

Optimal mooring line geometry depends on the water depth. By optimizing mooring line geometry appropriately, the power absorption of the WEC can be increased significantly. However, the optimal mooring line geometry for maximizing power absorption may not necessarily be the optimal mooring line geometry for maximizing fatigue life. Single segment mooring lines generally do not perform as well as two segment mooring lines of the same anchor radius, sacrificing either power absorption or fatigue life. Thus, only two segment mooring lines are considered in the array configurations.

7.2 Array Simulations

The purpose of the array simulations is to justify that WECs in an array configuration are more efficient than individual WECs, and to find the optimal parameters for a small WEC array. All array simulations use the environmental conditions found at the Runde site.

First, interaction effects are studied using two buoy arrays. An array is simulated with two buoys of the V2 design, followed by simulations with two buoys of the V1 design. The effect of including WEC interactions in simulations will be studied using these models, as well as the effects of varying separation distance and the array orientation with respect to the wave incidence angle.

The two array patterns described in the array design selection, TriBuoy and SquareBuoy, will be modelled with a variation in mooring system design. Using the V2 buoy design in the TriBuoy configuration, 3 mooring designs are created for a separating distance of 173 m, 8 mooring designs for a separating distance of 260 m, and 3 mooring designs for a separating distance of 130 m. Then, a mooring design for each of the separating distances of 173 m and 260 m is created for TriBuoy configurations using the V1 buoy design. For the SquareBuoy configuration, only the V2 buoy design is considered. 5 mooring designs are created for a separating distance of 141 m and 6 mooring designs for a separating distance of 282 m.

Appendix 11.3 displays the naming system, design names and specifications of each design, as well as top views of the models.

Finally, for select configurations the second sea state defined in section 7.1.6 is simulated. The effects on the model, power absorption and estimated fatigue life are discussed.

For each design, a one-hour simulation is run. This is again due to computing time constraints, which due to the complexity of even a simple array model, grows significantly as the simulation time is increased. To conduct the LCOE and LCA, it is more important to have values for power absorption and fatigue life that more accurately reflect that of a steady sea state. Thus, for select configurations the results from the one-hour simulations will be scaled using the relationship found in the initial simulation 7.1.1.b). These modified results are displayed in section 7.2.6, as well as a discussion of the key results from the array simulations.

Table 7.2.1: Outline of the presentation of array simulation results.

7.2.1. Two Buoy Interaction
a. V2
b. V1
7.2.2. TriBuoy, V2
a. Separation distance 173 m
b. Separation distance 260 m
c. Separation distance 130 m
7.2.3. TriBuoy, V1
a. Separation distance 173 m
b. Separation distance 260 m
c. Separation distance 130 m
7.2.4. SquareBuoy, V2
a. Separation distance 141 m
b. Separation distance 282 m
7.2.5. Second Sea State
a. Tri.V2.173.2
b. Tri.V2.260.3
c. Tri.V1.260.1
d. Sq.V2.141.3
7.2.6. Modified Results and Discussion

7.2.1 Two Buoy Interaction

In the following studies, the base case represents two individual buoy configurations separated by an infinite distance and thus independent and unaffected by the other. Thus, the power absorption in the base case is assumed to be equal to twice that of an individual buoy. Two cases are studied for a separating distance of 100 m and for a separating distance of 200 m. In the first case, two individual models of the buoy are imported into SIMA. In the second case, the two buoy array is first modeled in HydroD, then a Wadam analysis is run, and finally the Wadam result file is imported to SIMA. The result file includes the interaction effects between the two buoys. Thus, the purpose of this study is to see how the inclusion of the WEC interaction effects captured by this result file will affect the calculated power absorption of the array. In all cases the water depth is 86.6 m, the location is Runde, and the mooring system is modelled after mooring configuration number 1 seen in Appendix 11.2. Simulations are run

for different wave incidence angles to show how array orientation affects power absorption in the cases.

a) V2

Figure 7.2.1 displays the average power absorption of a two V2 buoy array configuration. As can be seen, without the inclusion of the result file from the Wadam analysis, the power absorptions of the two buoy arrays at both separating distances of 100 m and 200 m are very similar to the power absorption of the base case. The best wave incidence angles for greater power absorption are 0 deg and 60 deg. When interaction effects are included, the power absorption is maximized at a wave incidence angle of 90 degrees at a separating distance of 100 m and at 60 degrees at a separating distance of 200 m. For the array with a WEC separating distance of 100 m, a wave incidence angle of 0 degrees yields about 200 W less power absorption than the base case, while a wave incidence angle of 90 degrees yields 500 W more power absorption than the base case. For the array with a WEC separating distance of 200 m, all wave incidence angles yield a higher power absorption than the base case as well as the array with the 100 m WEC separating distance.

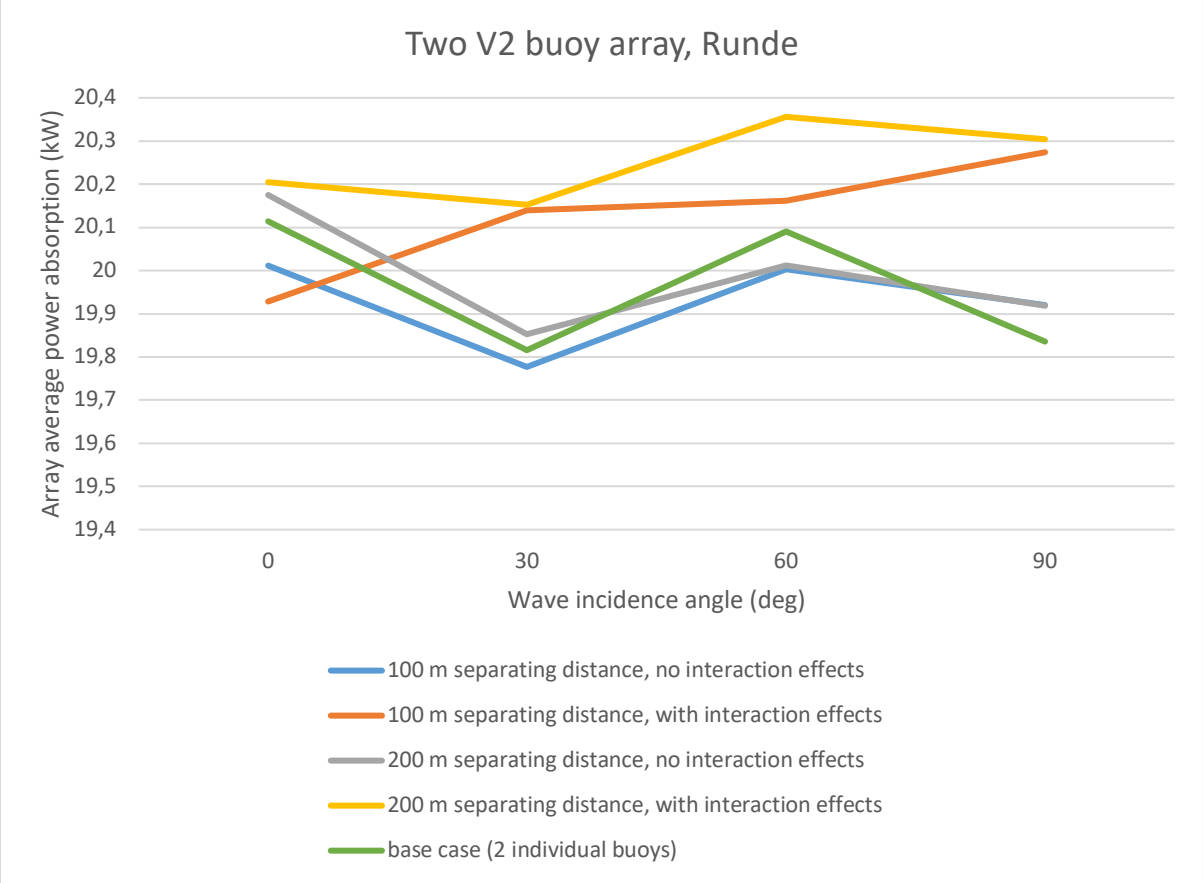

Figure 7.2.1: Relationship between array power absorption, wave incidence angle, separating distance, and the calculation of interaction effects in a two buoy array of V2 buoys in Runde.

b) V1

Figure 7.2.2 displays the average power absorption of a two buoy array configuration where both buoys are of the V1 design. In this case, the power absorptions of the two buoy arrays at both separating distances of 100 m and 200 m not considering interaction effects are most

comparable to each other than to the power absorption of the base case. Except for the base case, the best wave incidence angles in all cases for larger power absorption is 30 deg. When interaction effects are included, the power absorption compared to the cases with no interaction effects decreases at a separating distance of 100 m and increases at a separating distance of 200 m. The array with a WEC separating distance of 200 m again yields a higher power absorption at all wave incidence angles than the base case as well as the array with the 100 m WEC separating distance.

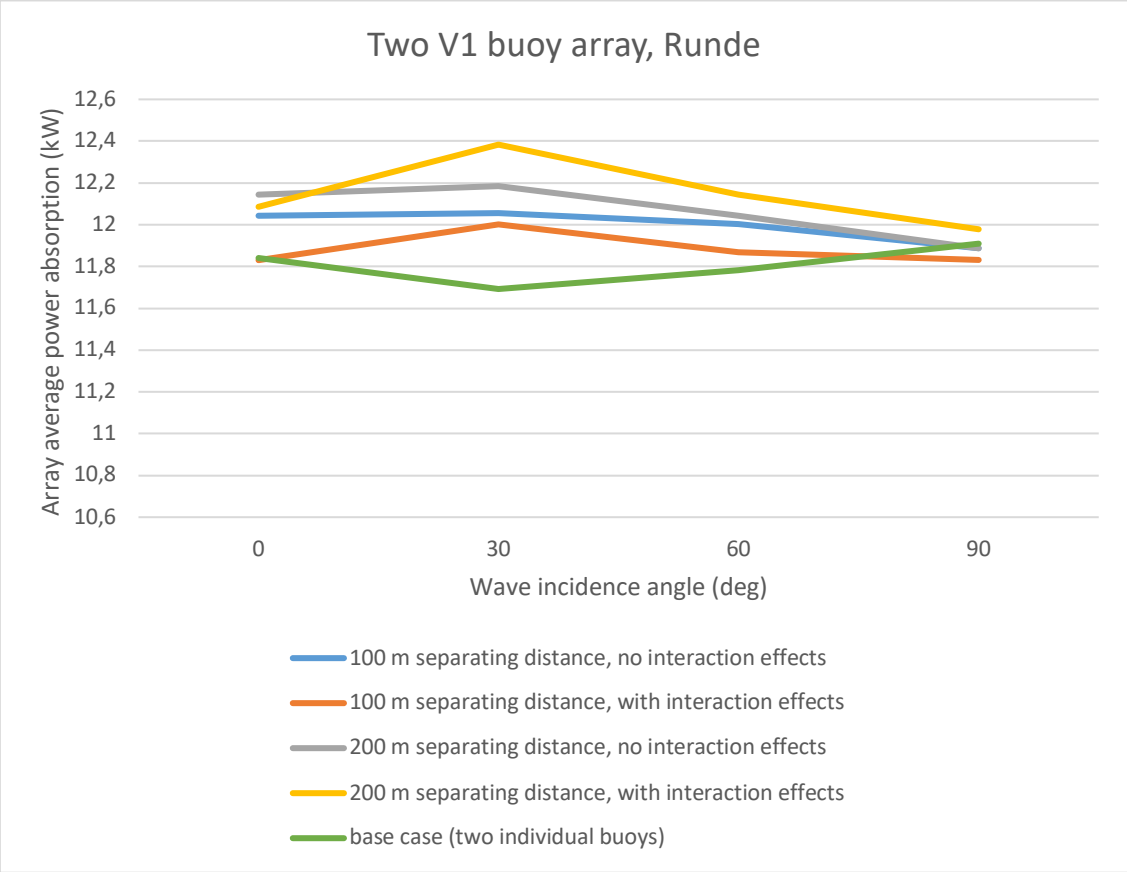

Figure 7.2.2: Relationship between array power absorption, wave incidence angle, separating distance, and the calculation of interaction effects in a two buoy array of V1 buoys in Runde.

7.2.2 TriBuoy, V2

a) Separation distance 173 m

The results of the single buoy simulations at Runde indicated that decreasing the segment ratio between mooring line segments 1 and 2 increases the WEC power absorption. By applying this to the mooring line configuration in the TriBuoy array and reducing the segment ratio from 1.231 in Tri.V2.173.1 to 0.706 in Tri.V2.173.2, WEC power absorption can be increased by 10%. In Tri.V2.173.3, the mooring configuration is changed while keeping the same segment lengths and anchor radius as Tri.V2.173.2. Both power absorption and fatigue life values do not change significantly.

Table 7.22.: Post-processing results of Tribuoy V2 configurations with a WEC separating distance of 173 m.

Design name	Anchor radius (m)	Ratio segment 1/2 length	Total power absorption (kW)	Average power per WEC (kW)	Maximum axial force (kN)	Estimated fatigue life (years)
Tri.V2.173.1	100	1.23	27.39	9.13	170.44	1.09E+07
Tri.V2.173.2	100	0.71	30.19	10.06	149.48	8.96E+07
Tri.V2.173.3	100	0.71	30.19	10.06	150.32	8.13E+07

Table 7.2.3 displays the effect of changing the wave incidence angle on the power absorption and fatigue life in designs Tri.V2.173.2 and Tri.V2.173.3. The array's power absorption is not affected significantly, but the fatigue life of the weakest mooring line is very dependent on the incidence angle. In Tri.V2.173.2, the worst fatigue life is found at a wave incidence angle of 30 deg, while in Tri.V2.173.3, the worst fatigue life is found at a wave incidence angle of 90 deg. In both cases this corresponds to a wave incidence angle that is directly in the direction of the mooring line with the shortest fatigue life.

Table 7.2.3: Effect of wave incidence angle on the power absorption and fatigue life of designs Tri.V2.173.2 and Tri.V2.173.3.
PA = array average power absorption (kW)
FL = estimated fatigue life in weakest mooring line (years)

	Wave Incidence Angle							
	0 deg		30 deg		60 deg		90 deg	
Design Name	PA (kW)	FL (years)	PA (kW)	FL (years)	PA (kW)	FL (years)	PA (kW)	FL (years)
Tri.V2.173.2	30.19	8.96E+07	30.89	8.57E+06	31.10	7.96E+07	31.65	4.45E+09
Tri.V2.173.3	30.19	8.13E+07	31.13	5.52E+09	31.08	6.88E+07	31.43	7.20E+06

b) Separating distance 260 m

It is interesting to note that though separation distance is believed to have a large impact on the power absorption of the array, when increasing the separating distance from 173 to 260 m the power absorption of the array barely changes if the mooring line lengths are kept constant (see Figure 7.2.3). However, with larger separation distances, the mooring line lengths can be increased, which thus significantly increases the power output of the array.

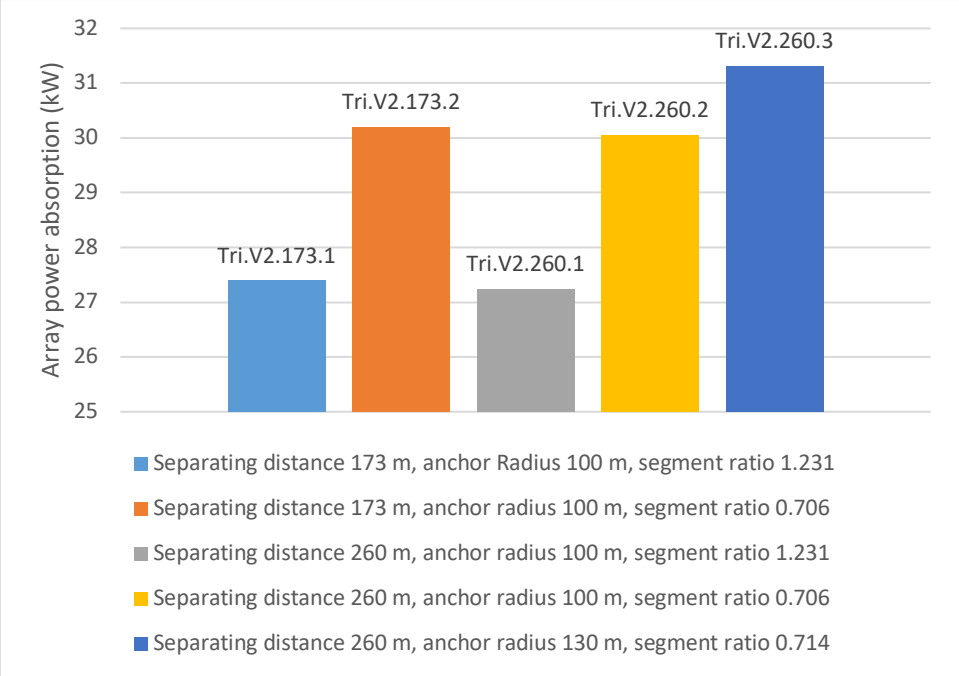

Figure 7.2.3: Comparison of the average power absorption of arrays Tri.V2.173.1, Tri.V2.173.2, Tri.V2.260.1, Tri.V2.260.2 and Tri.V2.260.V3.

As can be seen by comparing Tri.V2.260.3 to Tri.V2.260.1, if the anchor radius is increased to the optimal distance of 130 and the segment ratio is decreased to 0.714, the power absorption can be increased by 15%. As seen in Table 7.2.4, changing the mooring configuration to that of Tri.V2.260.7 further increases the power absorption by 3%. However, this could be due to 0 degrees being the optimal wave incidence angle for that configuration. An increase in mooring line length represented by anchor radius also increases the fatigue life in the weakest line. The shortest fatigue life is found in Tri.V2.260.1, with the shortest simulated anchor radius and largest segment ratio.

Table 7.2.4: Post-processing results of Tribuoy V2 configurations with a WEC separating distance of 260 m.

Design name	Anchor radius (m)	Ratio segment 1/2 length	Total power absorption (kW)	Average power per WEC (kW)	Maximum axial force (kN)	Estimated fatigue life (years)
Tri.V2.260.1	100	1.23	27.24	9.08	169.09	4.87E+06
Tri.V2.260.2	100	0.71	30.05	10.02	161.69	3.93E+07
Tri.V2.260.3	130	0.71	31.31	10.44	157.46	4.55E+07
Tri.V2.260.4	150	1	31.65	10.55	167.69	1.07E+08
Tri.V2.260.5	150	0.73	31.15	10.38	156.06	1.80E+08
Tri.V2.260.6	100	0.71	30.06	10.02	160.50	4.46E+07
Tri.V2.260.7	130	0.71	32.37	10.79	142.81	1.30E+08
Tri.V2.260.8	150	0.73	31.14	10.38	155.85	1.91E+08

c) Separating distance 130 m

A separating distance of 130 m limits the mooring lines to shorter lengths, which decreases the total power absorption and decreases fatigue life substantially compared to the arrays with larger separating distances (see Table 7.2.5).

Table 7.2.5: Post-processing results of TriBuoy V2 configurations with a separating distance of 130 m.

Design name	Anchor Radius (m)	Ratio segment 1/2 length	Total power absorption (kW)	Average power per WEC (kW)	Maximum axial force (kN)	Estimated fatigue life (years)
Tri.V2.130.1	75	0.71	24.49	8.16	197.85	4.89E+05
Tri.V2.130.2	75	0.85	23.79	7.93	197.59	4.86E+05
Tri.V2.130.3	75	1	23.54	7.85	196.46	5.81E+05

7.2.3 TriBuoy, V1

As mentioned in the single buoy simulations, the V1 buoy is less effective in the first sea state assumed at Runde. Nonetheless, the purpose of conducting simulations of an array of V1 buoys is to see if the interaction effects can positively affect the power absorption of the V1 buoys, and how separation distance and wave incidence angle will affect the system. The design specifications for Tri.V1.173.1, Tri.V1.260.1, and Tri.V.130.1 are outlined in Appendix 11.3.

Tables 7.2.6, 7.2.7 and 7.2.8 display the power absorption, maximum axial force, and estimated fatigue life calculations for the TriBuoy V1 configurations of 173 m, 260 m, and 130 m separation distances, respectively. Results are displayed for wave incidence angles 0, 30, 60, and 90 degrees.

Table 7.2.6: Post-processing results of Tri.V1.173.1.

Design name	Wave incidence angle (deg)	Total power absorption (kW)	Average power per WEC (kW)	Maximum axial force (kN)	Estimated fatigue life (years)
Tri.V1.173.1	0	18.47	6.16	145.18	3.82E+08
Tri.V1.173.1	30	18.12	6.04	161.06	3.17E+07
Tri.V1.173.1	60	18.53	6.18	139.57	6.65E+08
Tri.V1.173.1	90	17.79	5.93	119.87	1.12E+10

Table 7.2.7: Post-processing results of Tri.V1.260.1.

Design name	Wave incidence angle (deg)	Total power absorption (kW)	Average power per WEC (kW)	Maximum axial force (kN)	Estimated fatigue life (years)
Tri.V1.260.1	0	19.36	6.45	141.80	7.76E+08
Tri.V1.260.1	30	18.89	6.30	156.18	1.11E+08
Tri.V1.260.1	60	19.46	6.49	141.13	5.77E+08
Tri.V1.260.1	90	19.29	6.43	113.57	1.25E+09

Table 7.2.8: Post-processing results of Tri.V1.130.1.

Design name	Wave incidence angle (deg)	Total power absorption (kW)	Average power per WEC (kW)	Maximum axial force (kN)	Estimated fatigue life (years)
Tri.V1.130.1	0	13.92	4.64	191.31	2.74E+06
Tri.V1.130.1	30	15.03	5.01	216.72	4.36E+05
Tri.V1.130.1	60	14.13	4.71	191.31	2.28E+06
Tri.V1.130.1	90	13.01	4.34	160.30	4.60E+07

The relationship between the three TriBuoy V1 configurations and a reference case can be seen in Figures 7.2.4 and 7.2.5. The reference case refers to 3 individual V1 WEC configurations spaced at a large distance from one another (no interaction effects). The largest power absorption is obtained from the design Tri.V.260.1, followed by Tri.V1.173.1, the reference case, and finally Tri.V1.130.1. In Figure 7.2.4, the results indicate that larger WEC separation distances correspond with larger power absorption. However, this relationship is more so due to an increase in anchor radius, which can be seen in Figure 7.2.5.

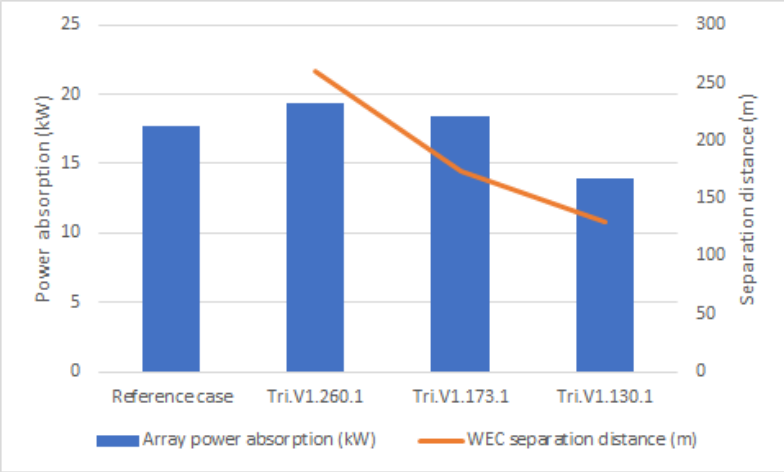

Figure 7.2.4: Comparison of power absorption of TriBuoy V1 configurations and WEC separation distance.

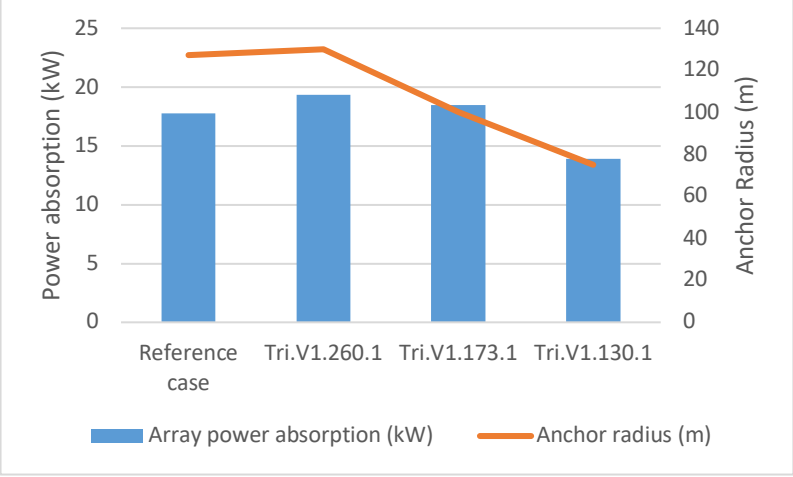

Figure 7.2.5: Comparison of power absorption of TriBuoy V1 configurations and anchor radii.

7.2.4 SquareBuoy, V2

a) Separation distance 141 m

Table 7.2.9 displays the results of the SquareBuoy V2 configurations with a separation distance of 141 m. A separation distance of 141 m limits the anchor radius, even if anchors are shared. Small anchor radii correspond to short mooring lines, which results in a significant reduction in the fatigue life. Anchor radius can be increased by changing the angles of the mooring lines and assuming that the cable and hub configuration is no longer placed in the center of the array, as mentions in the array design selection. Comparing Sq.V2.141.3 to Sq.V2.141.1, increasing the anchor radius by 30 m increases the power absorption by 38%.

Table 7.2.9: Post-processing results of SquareBuoy V2 configurations with a separating distance of 141 m.

Design name	Anchor Radius (m)	Ratio segment 1/2 length	Total power absorption (kW)	Average power per WEC (kW)	Maximum axial force (kN)	Estimated fatigue life (years)
Sq.V2.141.1	70	0.77	30.12	7.53	221.46	6.71E+04
Sq.V2.141.2	75	0.71	32.02	8.01	198.47	5.43E+05
Sq.V2.141.3	100	0.71	41.54	10.39	161.11	3.33E+07
Sq.V2.141.4	100	0.71	41.33	10.33	176.29	4.36E+06
Sq.V2.141.5	100	0.71	41.33	10.33	176.03	4.44E+06

b) Separation distance 282 m

Table 7.2.10 displays the results of the SquareBuoy V2 configurations with a separation distance of 282 m. When using the same anchor radius as in a separating distance of 141 m, a SquareBuoy array configuration with a separating distance of 282 m yields slightly less power absorption. However, like the TriBuoy configuration, increasing the separating distance allows for an increase in anchor radius. When the anchor radius is increased by 30 m, power absorption increases by 7%. In this design, sharing anchors produces the highest power absorption (Sq.V2.282.4), producing 1.3% more power than a design of the same anchor radius sharing no anchors (Sq.V2.282.5).

Table 7.2.10: Post-processing results of SquareBuoy V2 configurations with a separating distance of 282 m.

Design name	Anchor Radius (m)	Ratio segment 1/2 length	Total power absorption (kW)	Average power per WEC (kW)	Maximum axial force (kN)	Estimated fatigue life (years)
Sq.V2.282.1	100	0.71	41.19	10.30	158.58	2.92E+07
Sq.V2.282.2	130	0.70	44.20	11.05	152.60	1.97E+07
Sq.V2.282.3	130	0.70	44.65	11.16	179.98	9.56E+05
Sq.V2.282.4	141	0.71	45.00	11.25	195.26	4.99E+05
Sq.V2.282.5	141	0.71	44.40	11.10	152.92	1.21E+07
Sq.V2.282.6	130	0.71	42.88	10.72	161.36	1.50E+07

7.2.5 Second Sea State

Four configurations, Tri.V2.173.2, Tri.V2.260.3, Tri.V1.260.1 and Sq.V2.141.3, are run using the second most common sea state assumed for Runde, previously defined in Table 7.1.14. These configurations are chosen to represent effective configurations with clearly distinctive design parameters. The first run using the second sea state conditions in all four configurations failed: it was later determined that this was due to the relationship between the anchor radius and mooring line length. Thus, the mooring line configuration needed to be adjusted in all cases. Table 7.2.11 displayed the adjusted mooring line configuration specifications for the second sea state cases, denoted 'ss2'.

Table 7.2.11: Adjusted mooring line configuration specifications for simulations of sea state 2.

Design name	Anchor radius (m)	Length of segment 1 (m)	Length of segment 2 (m)	Ratio segment 1/segment 2 length
Tri.V2.173.2.ss2	100	58	82	0.71
Tri.V2.260.3.ss2	138	70	98	0.71
Tri.V1.260.1.ss2	138	70	98	0.71
Sq.V2.141.3.ss2	100	58	82	0.71

Figure 7.2.6 displays the difference in power absorption between the configurations in sea state 1 and sea state 2. Figure 7.2.7 displays the difference in fatigue life between the configurations in sea state 1 and sea state 2. Like the single buoy configurations, the second sea state increases the power absorption and decreases the fatigue life of the system. It is interesting to note that with the first sea state the Tri.V1.260.1 configuration has the lowest power absorption and highest fatigue life of the configurations graphed, but with the second sea state the Tri.V1.260.1 configuration has the highest power absorption and lowest fatigue life of the configurations. This indicates that the V1 buoy design is very sensitive to changes in sea state.

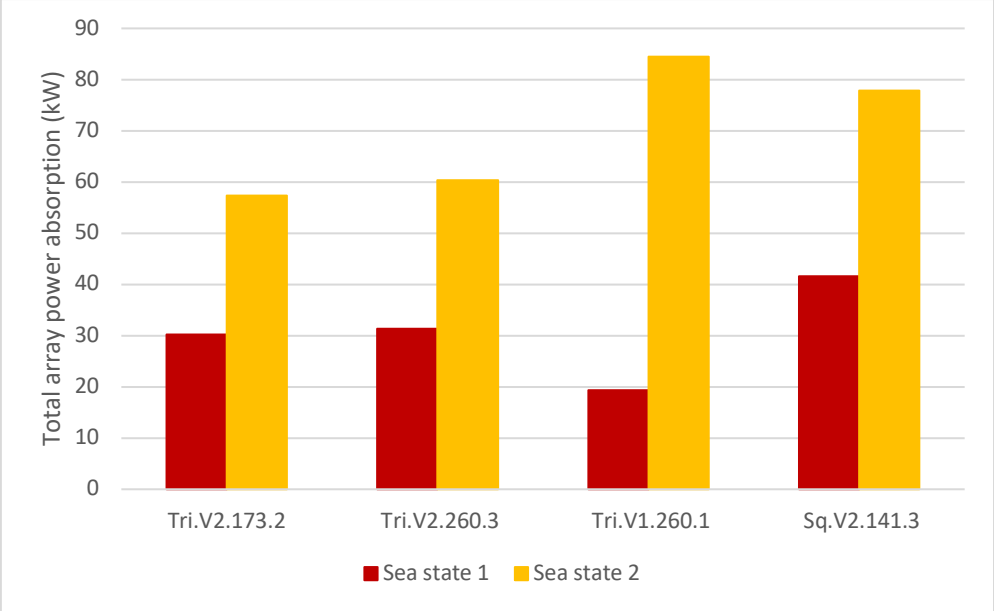

Figure 7.2.6: Comparison between sea states 1 and 2 on the total power absorption of Tri.V2.173.2, Tri.V2.260.3, Tri.V1.260.1 and Sq.V2.141.3 arrays.

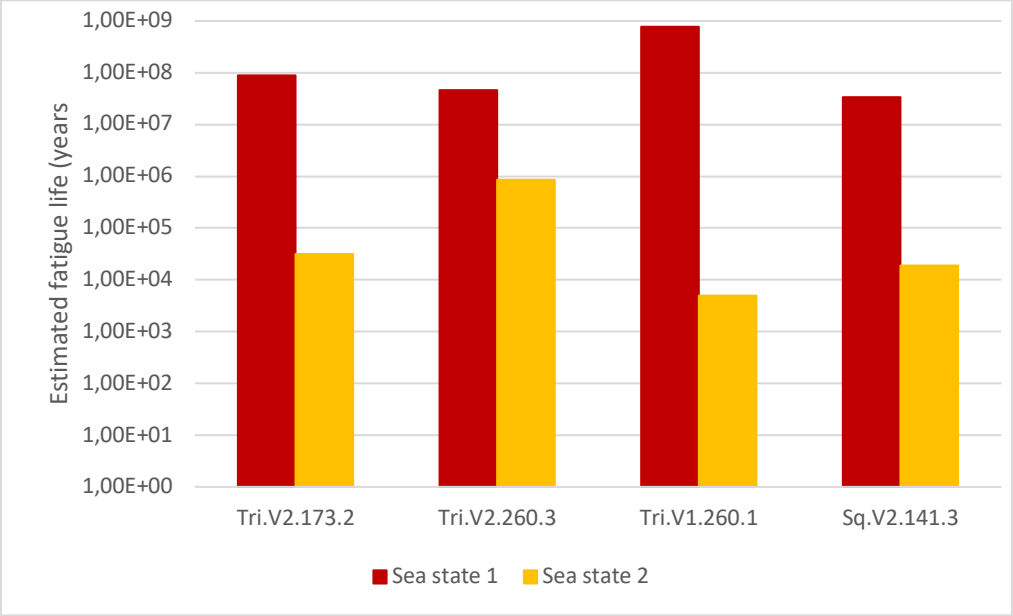

Figure 7.2.7: Comparison between sea states 1 and 2 on the estimated fatigue life in the weakest mooring line of Tri.V2.173.2, Tri.V2.260.3, Tri.V1.260.1 and Sq.V2.141.3 arrays.

7.2.6 Discussion

Figure 7.2.8 displays the relationship between separating distance, anchor radius and power absorption in the TriBuoy V2 configurations assuming sea state 1. Changing the configuration of the mooring lines, such as the ratio between segment lengths, can result in different power absorptions among TriBuoy configurations of the same anchor radius and separating distance. However, Figure 7.2.8 indicates that it is the anchor radius that significantly affects the power absorption of the array. The separating distance itself does not affect power absorption significantly but affects the possibility of choosing the optimal anchor radius. Smaller

separating distances limit anchor radius and thus limit power absorption and fatigue life when considering mooring lines of equal length. However, if interbody moorings such as the configurations explored in the research of Vicente et al. (2009) are considered, the results could be entirely different. This could be explored in future studies.

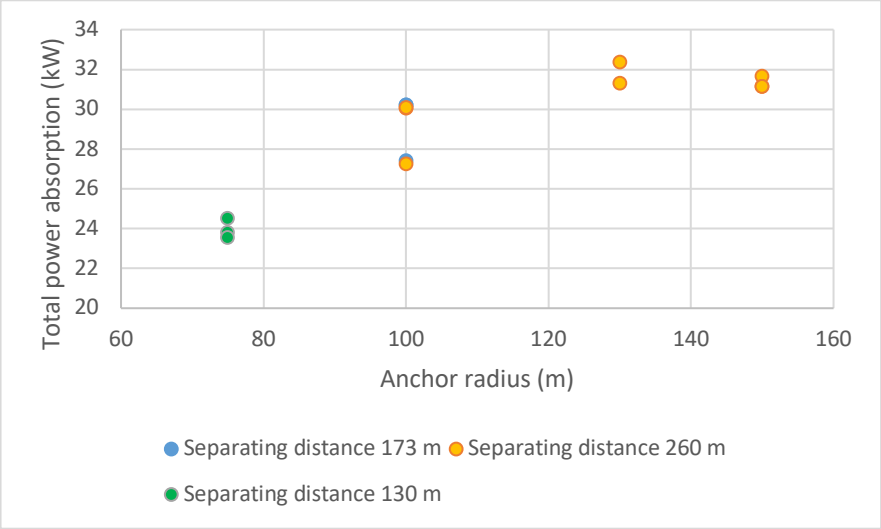

Figure 7.2.8: Comparison of total power absorption of TriBuoy V2 configurations assuming the first sea state.

Figure 7.2.9 displays the relationship between separating distance, anchor radius and power absorption in the SquareBuoy V2 configurations assuming sea state 1. Like in the TriBuoy configurations, it is obvious that anchor radius is a significant parameter in optimizing power absorption in the SquareBuoy configurations. When anchor radius is 100 m for both separating distances, the configuration with the separating distance of 141 m performs slightly better than the configuration with the separating distance of 282 m. However, with the optimal anchor radius applied, the configurations with the larger separating distance outperform the configurations with the separating distance of 141 m.

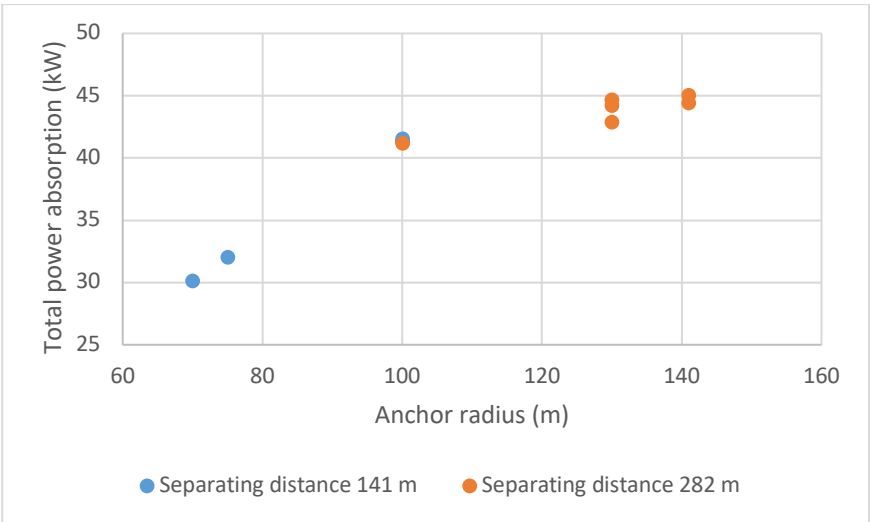

Figure 7.2.9: Comparison of total power absorption of SquareBuoy V2 configurations assuming the first sea state.

The results from the simulations of the second sea state indicate that mooring line configurations assumed in the first sea state cannot be automatically applied to simulations of the second sea state. Because the most common sea state is less extreme than the second most common sea state, it is possible that the configurations designed with consideration of the first sea state cannot withstand the higher forces from the second sea state. Thus, a suggestion for future studies would be to begin with ensuring that simulations of the models designed run effectively with more extreme sea states, and then run simulations using the most common sea state to calculate the power absorption and fatigue life.

7.2.7 Modified Results

Table 7.2.12 displays the power absorption and fatigue life of the weakest mooring line in select configurations after adjustments are made. The selected configurations are the following: Tri.V2.173.2, Tri.V2.260.3, Sq.V2.141.1, Sq.V2.141.3, Sq.V2.282.4, Tri.V1.173.1, Tri.V1.260.1, Tri.V2.173.2.ss2, Tri.V2.260.3.ss2, Sq.V2.141.The original axial forces from the simulation results are multiplied by 1.33, and the fatigue life in each mooring line is recalculated using these values. The calculated power absorption is multiplied by a factor of 1.24. These modifications are done to represent a longer simulation time of 3 hours.

Table 7.2.12: Modified fatigue life and power absorption of the top configuration concepts to be used in the LCOE and LCA calculations.

Design name	Modified fatigue life (years)	Modified array power absorption (kW)
Tri.V2.173.2	1.93E+06	37.44
Tri.V2.260.3	9.79E+05	38.82
Sq.V2.141.1	3955.7	37.35
Sq.V2.141.3	7.17E+05	51.51
Sq.V2.282.4	10733	55.80
Tri.V1.173.1	1.25E+07	22.90
Tri.V1.260.1	8.23E+06	24.00
Tri.V2.173.2.ss2	668.34	71.77
Tri.V2.260.3.ss2	18189	74.83
Tri.V1.260.1.ss2	106.08	104.71
Sq.V2.141.3.ss2	409.85	96.60

7.3 LCOE

The purpose of the LCOE is comparative and thus many costs are not included, such as the concept development cost C1 and the design and development cost C2. The costs are all estimations based on previous research and can be seen in Appendix 11.7. V1 and V2 WEC buoys are assumed to have the same costs. Cable costs are based on the initial cable and hub design, assuming a 135 m length for smaller WEC separation distances and a 190 m and 245 m length for the separation distances of 260 and 282 m, respectively. The cost of anchors is a function of weight and it is assumed that sharing anchors between mooring lines does not decrease the weight required to moor the system, so there is no financial benefit to sharing anchors between mooring lines. The reference case is a single V1 or V2 buoy at the Runde site, assuming a uniform water depth of 86.6 m, with a 0 deg wave, wind and current incidence angle. The fatigue life and power absorption values are the modified versions from section 7.1.2. Percentage of availability and transmission efficiency are assumed to be 1. A low,

medium and high WACC is set as 5%, 10% and 15%. This corresponds to r values of 1.05, 1.10, and 1.15.

The modified fatigue life and power absorption values in section 7.2.7 are used for the array designs. Power absorption is used to estimate the energy produced in the WEC's lifetime, which has been assumed to be 25 years. The fatigue life in the weakest mooring line is used to indicate whether the mooring system will need to be replaced at some point in the WEC system's lifetime. For example, if the fatigue life is under 25 years, a mooring line will be expected to fail at least once during the system's lifetime; thus, the mooring system would need to be replaced at least once. The LCOE results are calculated assuming a wave incidence angle of 0 deg in the TriBuoy arrays and 60 deg in the SquareBuoy arrays. The results of the LCOE calculations are displayed in Table 7.3.1.

Table 7.3.1: Results of the LCOE for select array designs, compared to the reference case.

Design name	Fatigue life (years)	Power absorption (kW)	Length of mooring lines per WEC (m)	LCOE (Euro/MWh)		
				r = 1.05	r = 1.10	r = 1.15
Reference case: V2	1.06E+07	12.47	529.8	8.83E+03	9.02E+03	9.20E+03
Tri.V2.173.2	1.93E+06	37.44	447	7.56E+03	7.72E+03	7.88E+03
Tri.V2.260.3	9.79E+05	38.82	516	7.32E+03	7.51E+03	7.64E+03
Sq.V2.141.1	3955.7	37.35	357	9.83E+03	1.00E+04	1.03E+04
Sq.V2.141.3	7.17E+05	51.51	447	7.18E+03	7.34E+03	7.48E+03
Sq.V2.282.4	10733	55.80	546	6.71E+03	6.86E+03	6.99E+03
Reference case: V1	4.54E+07	7.34	529.8	1.50E+04	1.53E+04	1.56E+04
Tri.V1.173.1	1.25E+07	22.90	447	1.24E+04	1.26E+04	1.29E+04
Tri.V1.260.1	8.23E+06	24.01	516	1.19E+04	1.21E+04	1.24E+04
Tri.V2.173.2.ss2	668.34	71.77	432	3.94E+03	4.02E+03	4.11E+03

Tri.V2.260.3.ss2	18189	74.83	516	3.81E+03	3.89E+03	3.97E+03
Tri.V1.260.1.ss2	106.08	104.71	516	2.72E+03	2.78E+03	2.84E+03
Sq.V2.141.3.ss2	409.85	96.60	432	3.82E+03	3.91E+03	3.99E+03

The lowest LCOE calculated assuming the most common sea state is 6710 Euro/MWh. By contrast, the current LCOE of other renewable energies such as solar PV, onshore wind, and offshore wind is in the range of 40-260 Euro/MWh (Ren21, 2017). Though the LCOE values calculated in this thesis are rough estimates and cannot realistically be compared to other renewable energy technologies, this indicates that for the costs assumed, the deployment of small arrays is not economically competitive at this time.

The SquareBuoy array Sq.V2.282.4 has the lowest LCOE of the simulations run assuming the first sea state. This indicates that the additional energy absorption obtained from this configuration outweighs the additional cost of longer mooring lines and cables. Regarding the designs simulated with the second sea state, the LCOE calculated is much lower because the lifetime energy production is higher. The lowest LCOE of 2720 Euro/MWh is found in TriBuoy array design Tri.V1.260.1.ss2.

Figures 7.3.1 and 7.3.2 display the cost breakdown from the LCOE calculations for Sq.V2.282.4. As can be seen from Figure 7.3.1, the highest costs are associated with the manufacturing phase (C3). Figure 7.3.2 displays the contribution of manufacturing sub-costs to the total manufacturing cost. The largest cost contribution is from the manufacturing of the WEC buoy (C31), followed by the mooring lines (C33), anchors (C34), and cable and hub (C35).

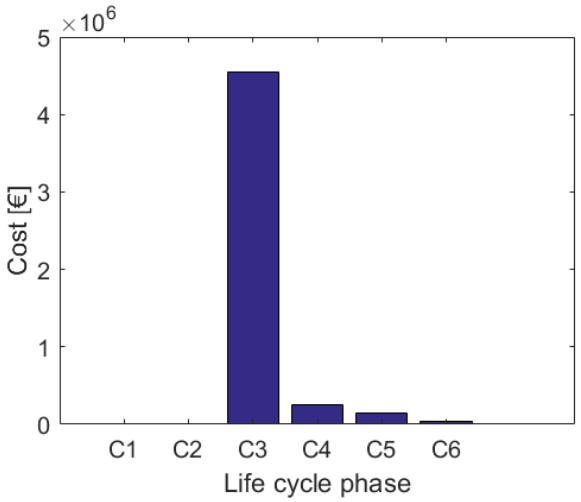

Figure 7.3.1: Cost breakdown by life cycle phase.

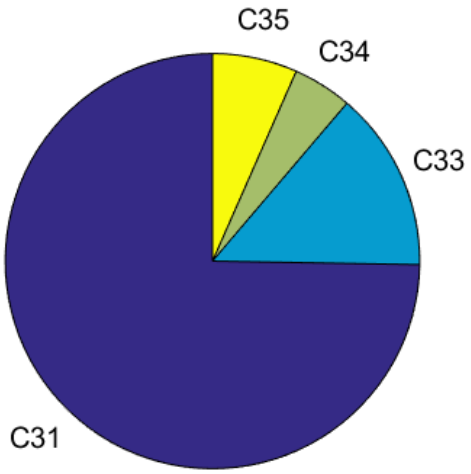

Figure 7.3.2: Manufacturing sub-costs.

1. Including multiple wave incidence angles

In a multidirectional climate, the wave incidence angle cannot be assumed to be constant for the lifetime of the array. Thus, for designs Tri.V2.173.2, Tri.V2.260.3, Sq.V2.141.1, Sq.V2.282.4, Tri.V1.173.1 and Tri.V1.260.1, the power absorption at 0 deg, 30 deg, 60 deg, and 90 deg is calculated, modified and then averaged. It is assumed that averaging the results from these angles is enough to represent the power absorption in a multidirectional climate. LCOE is calculated using the new power absorption values, with a discount factor of 1.10. The results are displayed in Table 7.3.2.

Table 7.3.2: Difference in LCOE in various array designs when calculating power absorption from a single incidence angle or from multiple incidence angles. Single angle refers to wave, wind and current incidence angles of 0 deg in the TriBuoy configurations and 60 deg in the SquareBuoy configurations.

Design name	Single or multiple angle	Power absorption (kW)	LCOE (Euro/MWh)
Tri.V2.173.2	Multiple	38.39	7.53E+03
	Single	37.44	7.72E+03
Tri.V2.260.3	Multiple	39.78	7.33E+03
	Single	38.82	7.51E+03
Sq.V2.141.3	Multiple	50.56	7.47E+03
	Single	51.51	7.34E+03
Sq.V2.282.4	Multiple	55.80	6.86E+03
	Single	55.66	6.87E+03
Tri.V1.173.1	Multiple	22.60	1.28E+04
	Single	22.90	1.26E+04
Tri.V1.260.1	Multiple	23.87	1.22E+04
	Single	24.00	1.21E+04

Calculating LCOE using only one incidence angle in a multidirectional environment has small but identifiable effects. Assuming an incidence angle of 0 deg for the lifetime of TriBuoy arrays generally underestimates the power absorption, while assuming an incidence angle of 60 degrees for the SquareBuoy arrays generally overestimates the power absorption. This leads to higher calculated LCOEs for the TriBuoy arrays and lower LCOEs for the SquareBuoy arrays.

2. Mooring line changes

In the previous LCOE calculations, it is assumed that correctional maintenance is negligible and that the mooring lines will not need to be changed because the fatigue lives of the mooring lines are all over the 25 years expected lifetime of the device. However, as mentioned earlier the fatigue life calculations are not realistic and there is actually a significant risk that the mooring lines in these designs will fail with extreme loading conditions, biofouling, sabotage from fishing vessels or other possible hazards. Thus, two more conditions are tested: changing the mooring lines once in the system's lifetime and changing the mooring lines three times in the system's lifetime. The discount factor used is the more conservative 1.15. The results are displayed in Table 7.3.3.

Table 7.3.3: Effect of changing mooring lines 0, 1 or 3 times on the calculated LCOE of array designs using the second sea state.

Design name	Number of mooring line changes	LCOE (Euro/MWh)
Tri.V2.173.2.ss2	0	4.11E+03
	1	4.12E+03
	3	4.14E+03
Tri.V2.260.3.ss2	0	3.97E+03
	1	3.98E+03
	3	4.01E+03
Tri.V1.260.1.ss2	0	2.84E+03
	1	2.85E+03
	3	2.87E+03
Sq.V2.141.3.ss2	0	3.99E+03
	1	4.00E+03
	3	4.02E+03

Changing the mooring lines does not seem to have a large effect on the overall LCOE, increasing the Euros/MWh by at most 1%. However, the additional engineering and urgency that may go into losing a line may have additional hidden costs not accounted for in this analysis. Further investigation into the subject may involve a risk assessment and the potential costs associated with those risks.

7.4 LCA

Like the LCOE, the reference case for the LCA is a single V1 or V2 buoy at the Runde site, assuming a uniform water depth of 86.6 m, with a 0 deg wave, wind and current incidence angle. The energy absorption is calculated assuming the most common sea state. The cable and hub are not considered. Figure 7.4.1 shows the product system of connected life cycle processes for the reference case with the V2 buoy created in OpenLCA. The input data needed to create the processes and flows for the reference cases is displayed in Appendix 11.8.

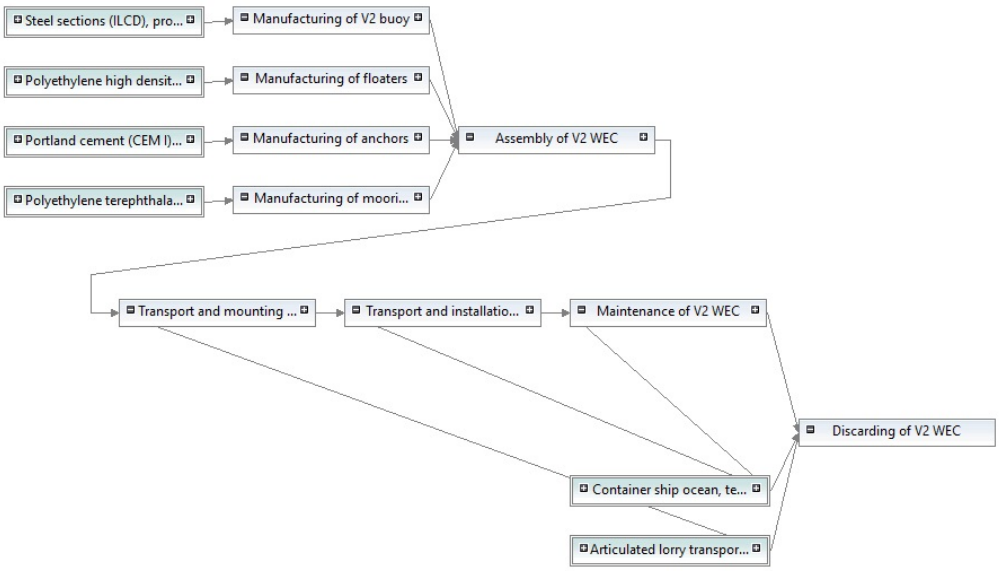

Figure 7.4.1: Product system for reference V2 WEC.

Table 7.4.1 shows the OpenLCA LCIA results for the V1 and V2 reference cases. The impact category values are per MWh of electricity produced. As can be seen, the V1 buoy has a higher impact in all categories. However, it should be noted that the V1 WEC´s higher impacts may be due to the lower power absorption when considering the first sea state. The results may differ if assuming sea state 2.

Table 7.4.1: Comparison of results of LCIA impact categories for the V1 and V2 reference cases.

Impact category	V1 WEC reference	V2 WEC reference	Unit
climate change - GWP 100a	7.22E+0	2.56E+0	kg CO_2-Eq
ecosystem quality - freshwater and terrestrial acidification	1.49E+0	5.85E-1	mol H+-Eq
ecosystem quality - freshwater ecotoxicity	1.26E+1	4.79E+0	CTUh.m3.yr
ecosystem quality - freshwater eutrophication	0.00e+0	0.00e+0	kg P-Eq
ecosystem quality - ionising radiation	0.00e+0	0.00e+0	mol N-Eq
ecosystem quality - marine eutrophication	4.62E-4	2.28E-4	kg N-Eq
ecosystem quality - terrestrial eutrophication	6.73E-2	3.33E-2	mol N-Eq
human health - carcinogenic effects	3.99E-7	1.46E-7	CTUh
human health - ionising radiation	5.70E-1	2.21E-1	kg U235-Eq
human health - non-carcinogenic effects	3.21E-5	1.17E-5	CTUh
human health - ozone layer depletion	1.25E-6	4.88E-7	kg CFC-11-Eq
human health - photochemical ozone creation	2.36E-1	1.03E-1	kg ethylene-Eq
human health - respiratory effects, inorganics	1.14E-1	4.37E-2	kg PM2.5-Eq
resources - land use	0.00E+0	0.00E+0	kg Soil Organic Carbon
resources - mineral, fossils and renewables	-1.53E-9	-4.82E-10	kg Sb-

In this thesis, the impact on the environment as well as human health and safety are quantified mainly through the contribution of the WEC configurations to the climate change impact category. Figures 7.4.2 and 7.4.3 display the process contributions to climate change in the V1 and V2 reference cases. In both cases, the main contribution is the production of the steel sections, which are used in the manufacturing of the WEC buoy. This contribution is larger in the V1 WEC buoy due to its larger size, which requires more material in the manufacturing process. In the V1 reference case, the second and third largest contributors are the container ship transport and lorry transport, while in the V2 reference case the second and third largest

contributors are the production of the PET fibers used in the mooring lines and then container ship transport. This difference is due to the heavier weight of the assembled V1 WEC causing the fuel needs for transport to increase and thus emissions to increase in the reference V1 case.

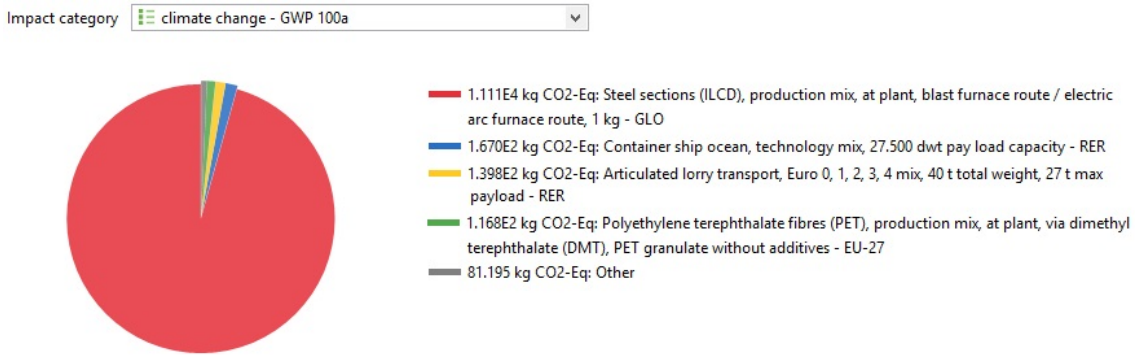

Figure 7.4.2: Lifetime process contributions to climate change impact category in V1 buoy reference case.

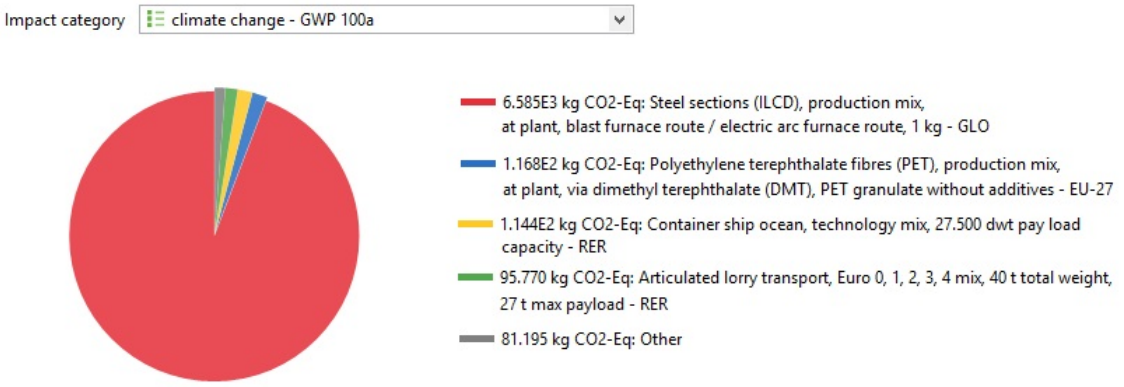

Figure 7.4.3: Lifetime process contributions to climate change impact category in V2 buoy reference case.

Table 7.4.2 displays the LCIA results of the Tri.V2.173.2, Tri.V2.260.3, Tri.V1.260.1, and Sq.V2.141.3 configurations. For each configuration the energy absorption is calculated from the most common sea state. The results show that the configuration with the least environmental impact per MWh in all categories is the Tri.V2.260.3 configuration, followed by Tri.V2.173.2, Sq.V2.141.3 and Tri.V1.260.1. In the climate change impact category, Tri.V1.260.1 has nearly three times the impact as all other configurations assessed.

Table 7.4.2: Comparison of results of LCIA impact categories for select configurations.

Impact category	Sq.V2.141.3	Tri.V1.260.1	Tri.V2.173.2	Tri.V2.260.3	Unit
climate change - GWP 100a	2.52E+0	6.67E+0	2.49E+0	2.41E+0	kg CO_2-Eq
ecosystem quality - freshwater and	5.72E-1	1.38E+0	5.66E-1	5.49E-1	mol H+-Eq

terrestrial acidification					
ecosystem quality - freshwater ecotoxicity	4.66E+0	1.16E+1	4.61E+0	4.50E+0	CTUh.m3.yr
ecosystem quality - freshwater eutrophication	0.00E+0	0.00E+0	0.00E+0	0.00E+0	kg P-Eq
ecosystem quality - ionising radiation	0.00E+0	0.00E+0	0.00E+0	0.00E+0	mol N-Eq
ecosystem quality - marine eutrophication	2.24E-4	4.26E-4	2.22E-4	2.14E-4	kg N-Eq
ecosystem quality - terrestrial eutrophication	3.27E-2	6.21E-2	3.24E-2	3.13E-2	mol N-Eq
human health - carcinogenic effects	1.43E-7	3.68E-7	1.42E-7	1.37E-7	CTUh
human health - ionising radiation	2.13E-1	5.24E-1	2.11E-1	2.07E-1	kg U235-Eq
human health - non-carcinogenic effects	1.15E-5	2.96E-5	1.14E-5	1.10E-5	CTUh
human health - ozone layer depletion	4.71E-7	1.15E-6	4.65E-7	4.57E-7	kg CFC-11-Eq
human health - photochemical ozone creation	9.92E-2	2.17E-1	9.80E-2	9.69E-2	kg ethylene-Eq
human health - respiratory effects, inorganics	4.29E-2	1.05E-1	4.24E-2	4.11E-2	kg PM2.5-Eq
resources - land use	0.00E+0	0.00E+0	0.00E+0	0.00E+0	kg Soil Organic Carbon
resources - mineral, fossils and renewables	-4.85E-10	-1.41E-9	-4.79E-10	-4.55E-10	kg Sb-Eq

8 Conclusions

The thesis work used insights from literature and from hydrodynamic and structural response simulations to identify and analyze the key parameters affecting the efficiency of point absorbing wave energy converter configurations. The efficiency of a point absorbing WEC configuration was analyzed through the power absorption and fatigue life of the system, and in some cases was further analyzed through LCOE and LCA calculations. The analyses considered the WEC buoy and mooring system but not the electricity hub or power cable. Single buoy configurations were simulated at multiple prospective installation sites, while simple array configurations were simulated at a single installation site. Key parametric analyses included comparing installation sites, comparing two versions of the WEC buoy V1 and V2, comparing different mooring configurations, and comparing the first and second most common sea states at a site, determined from the location study.

From analysis of the post-processing results, many conclusions were drawn. The best site out of those studied in the single buoy simulations was found to be Garðskagi, Iceland. This was concluded due to the high power absorption found in the most common sea state. The best mooring configuration was concluded to be the two-segment mooring line connected by a floater. It was also concluded that optimal mooring line geometry depended on the water depth, but that optimizing mooring line geometry could increase the power absorption of single WEC buoys as well as WEC arrays significantly. The mooring line configuration was also found to significantly affect the calculated fatigue life. In array designs, mooring line configuration was found to have a more significant influence on the performance of the system than WEC separation distance. The angle of incidence was found to have a significant effect on power absorption and fatigue life; however, in a multidirectional climate such as Runde the effects were concluded to be less influential. Assuming a different sea state was shown to significantly affect the calculated power absorption and fatigue life. It was found that the buoy that produced more power, V1 or V2, depended entirely on the sea state assumed in the simulations. It was concluded that this was due to the difference in the resonance frequencies of the buoys.

From the analysis of the LCOE calculations, the SquareBuoy array configuration Sq.V2.141.3 was concluded to be the most economic option. The array configurations using the V1 buoy were found to be much less economically attractive due to the low power absorption of the V1 buoy in the first sea state. However, when assuming the second sea state, the LCOE results were affected significantly, and Tri.V1.260.1 had the lowest calculated LCOE of the arrays considered. The manufacturing of the WEC buoy was found to be the biggest contributor to life cycle costs.

From the life cycle assessment, it was found that the V1 buoy has a much higher life cycle impact due to more material needed for the design and lower power absorption assuming sea state 1, and that highest and lowest life cycle impacts were found for the array configurations Tri.V1.260.1 and Tri.V2.260.3, respectively. The process contributing the most to the climate change impact category was found to be the production of steel for use in the manufacturing of the WEC.

The main purpose of this work has been to provide recommendations to future researchers or developers on which parameters have a large effect on WEC performance and should be studied in more detail and which parameters have little to no effect on WEC performance. Furthermore, the methodology of this thesis work could be used by companies such as Waves4Power in making appropriate design decisions that improve the economic, environmental and social

sustainability of their projects. Based on the assumptions made and conclusions drawn from the simulation results and analysis, the main environmental parameters affecting WEC performance are water depth, significant wave height, and wave period, and the main design parameters affecting WEC performance are the WEC buoy geometry, mooring line segment ratio and the anchor radius of the mooring lines. Small arrays with WEC separating distances that allow for optimized mooring configurations are a more sustainable solution than individual WEC buoy configurations and could be employed in the near future. Due to the dependency on water depth, in order to optimize mooring line geometry, data should be obtained for the exact bathymetry of the installation site. Thus, Waves4Power could consider geographical exploration of Runde as well as the site with the greatest power potential, Garðskagi for future development. The thesis also suggests that the V1 buoy should not be installed in the array due to the economic costs and environmental and social impacts associated. Furthermore, uncertainty regarding its resistance to buckling requires more research.

9 Recommendations

Many recommendations could be made for future studies. First, in order to run more precise analyses, it is important to simulate for more sea states, as well as wave directions. With the results from the full distribution of environmental conditions at a given site, weighted averages could be taken depending on the probability of the sea states and conditions, leading to power absorption and fatigue life calculations that are more accurate and reliable.

The variation of some parameters not considered in the simulations could be explored in future studies. For instance, the wave spectrum parameter (described in the location study section) was kept constant at 3.3 for all installation sites. However, according to DNV GL (2017a) recommended practice, different regions have different wave spectra; a wave spectrum parameter of 3.3 is appropriate for the North Sea but should be 1 or 2 in the Gulf of Mexico.

When applying the second sea state in the array configurations, the simulations failed. This was fixed in some cases by changing the anchor radii of the mooring lines. This could be an indication that though some mooring line geometries work in one sea state, the forces in another sea state might not allow for the same geometry. The relationship could be investigated further through more analyses of mooring configurations. Mooring configurations could first be simulated in more extreme sea conditions (high mean significant wave height and wave period). If simulations run successfully, the more common sea states could then be simulated.

The array patterns and mooring configurations chosen in this thesis had very symmetrical designs. For locations with unidirectional climates considered in future research, different array patterns exploiting the directional predictability could be explored, such as long linear arrays or semi-circular arrays.

Exploring different materials for the WEC buoy might be beneficial for reducing the costs and climate change impact of the system by replacing the use of steel. Polyethylene is currently under consideration by Waves4Power (Waves4Power, personal communications, May 2018). The use of a different material may also affect the hydrodynamic and structural response of the buoy, which could be explored in simulations.

Without the simulation of the electricity collection system in the array simulations, the interaction of the mooring lines and WECs with the cable and hub was not captured in the results. This may have had effects on the calculated fatigue life in the mooring lines and power absorption of the WEC. Furthermore, a change in the electricity collection system may include changes in cost and material use, which would affect both the LCOE and LCA calculations. Thus, in future studies the cable and hub design and modelling can be considered.

In the future, the deployment of hybrid or fully electric offshore vessels may significantly increase (Bellona Europa, 2017). For the electrification of larger ships travelling farther from shore, installing WECs in deeper waters may become interesting. WEC mooring systems for deep waters may require dramatically different design and engineering. Furthermore, optimal buoy geometries may differ in deeper waters. Future research could investigate these unknowns.

Through more research into the WaveEL system's processes, flows, and costs, the LCOE and LCA analyses could be improved significantly. To study the potential risks of the suggested array designs or locations, a risk assessment could also be performed. A risk assessment could identify areas of weakness in the design of the system and attention could be given to that area. With sufficient resources and data, the methodology highlighted in this thesis could be applied to many applications. The results of this thesis could be adapted to analyze other wave energy projects, including other point absorbing single WEC and WEC array designs, mooring systems of different materials and dimensions, and even other offshore products.

10 References

Acero, A. P., Rodríguez, C. & Ciroth, A. (2015). LCIA methods: Impact assessment methods in Life Cycle Assessment and their impact categories. v.1.5.4. *GreenDelta GmbH.* Berlin, Germany.

Bellona Europa (2017). An emerging race in marine transport electrification. Available at: http://bellona.org/news/arctic/arctic-transport-and-shipping/2017-06-23598 [Accessed 25 May 2018].

Borgarino, B., Babarit, A., & Ferrant, P. (2012). Impact of wave interactions effects on energy absorption in large arrays of wave energy converters. *Ocean Engineering* 41: p. 79-88. http://dx.doi.org/10.1016/j.oceaneng.2011.12.025

Castro-Santos, L., Martins, E., & Soares, C. G. (2016). Methodology to calculate the costs of a floating offshore renewable energy farm. *Energies* 9: p. 324-351. http://dx.doi.org/10.3390/en9050324

de Andres, A. D., Guanche, R., Meneses, L., Vidal, C., & Losada, I. J. (2014). Factors that influence array layout on wave energy farms. *Ocean Engineering* 82: p. 32-41. http://dx.doi.org/10.1016/j.oceaneng.2014.02.027

DNV GL (2015). Position mooring. DNVGL-OS-E301. *DNV GL AS.* Hövik, Norway.

DNV GL (2017a). Environmental conditions and environmental loads. DNVGL-RP-C205. *DNV GL AS.* Hövik, Norway.

DNV GL (2017b). Sesam HydroD V4.9-02. *DNV GL AS.* Hövik, Norway.

DNV GL (2017c). Sesam Sima64 V3.4-01. *DNV GL AS.* Hövik, Norway.

DNV GL (2018a). Strength assessment of offshore structures - Sesam software. Available at: https://www.dnvgl.com/services/strength-assessment-of-offshore-structures-sesam-software-1068 [Accessed 30 April 2018].

DNV GL (2018b). Stability analysis tool - HydroD. Available at: https://www.dnvgl.com/services/stability-analysis-tool-hydrod-14492 [Accessed 30 April 2018].

DNV GL (2018c). Simulation of marine operations - Sima. Available at: https://www.dnvgl.com/services/simulation-of-marine-operations-sima-2324 [Accessed 30 April 2018].

DNV GL (2018d). Conceptual modelling of offshore and maritime structures - GeniE. Available at: https://www.dnvgl.com/services/conceptual-modelling-of-offshore-and-maritime-structures-genie-89128 [Accessed 30 April 2018].

DNV GL (2018e). Frequency domain hydrodynamic analysis of stationary vessels - Wadam. Available at: https://www.dnvgl.com/services/frequency-domain-hydrodynamic-analysis-of-stationary-vessels-wadam-2412 [Accessed 30 April 2018].

DNV GL (2018f). Engineering analysis of fixed and floating OWT structures - Sesam for offshore wind. Available at: https://www.dnvgl.com/services/engineering-analysis-

of-fixed-and-floating-owt-structures-sesam-for-offshore-wind-2438 [Accessed 30 April 2018].

European Commission (2017). Life cycle impact assessment. *European Commission Joint Research Centre*, [online]. Available at: http://eplca.jrc.ec.europa.eu/?page_id=1159 [Accessed 17 May 2018].

European Environment Agency (2017). Climate change, impacts and vulnerability in Europe 2016: An indicator-based report. EEA Report No 1/2017. Available at: https://www.eea.europa.eu/publications/climate-change-impacts-and-vulnerability-2016

GreenDelta (2016). *OpenLCA 1.5.0.* Berlin: GreenDelta. Available at: http://www.openlca.org/.

Gunn, K. & Stock-Williams, C. (2012). Quantifying the global wave power resource. *Renewable Energy* 44: p. 296-304. https://doi.org/10.1016/j.renene.2012.01.101

Göteman, M., Engström, J., Eriksson, M., Isberg, J., Leijon, M. (2014). Methods of reducing power fluctuations in wave energy parks. *Journal of Renewable and Sustainable Energy* 6: 043103. http://dx.doi.org/10.1063/1.4889880

Göteman, M. (2017). Wave energy parks with point-absorbers of different dimensions. *Journal of Fluids and Structures* 74: p. 142-157. http://dx.doi.org/10.1016/j.jfluidstructs.2017.07.012

International Energy Agency [IEA] (2017). Key world energy statistics. Available at: http://www.iea.org/publications/freepublications/publication/KeyWorld2017.pdf

Isee systems (2013). *STELLA v10.0.3.* Lebanon, New Hampshire: isee systems inc.

Jansson, H. & Örgård, M. (2017). Design of mooring system for point absorbing wave energy devices in an array system. http://studentarbeten.chalmers.se/publication/252402-design-of-mooring-system-for-point-absorbing-wave-energy-devices-in-an-array-system.

Kim, J., Kweon, H.-M., Jeong, W.-M., Cho, I.-H., & Cho, H.Y. (2015). Design of the dual-buoy wave energy converter based on actual wave data of East Sea. *Int. J. Nav. Archit. Ocean Eng.* 7: 739-749. http://dx.doi.org/10.1515/ijnaoe-2015-0052

MathWorks Inc. (2016). *MATLAB R2016b Documentation.* Natick, Massachusetts: Mathworks Inc.

Myhr, A., Bjerkseter, C., Ågotnes, A., & Nygaard, T. A. (2014). Levelised cost of energy for offshore floating wind turbines in a life cycle perspective. *Renewable Energy* 66: 714-728. http://dx.doi.org/10.1016/j.renene.2014.01.017

National Oceanic and Atmospheric Administration (2018). National buoy data center. Available at: http://www.ndbc.noaa.gov/ [Accessed 6 February 2018].

NBC (2017). Two months after hurricane maria, puerto rico is still in crisis. Available at: https://www.nbcnews.com/storyline/puerto-rico-crisis/two-months-after-hurricane-maria-puerto-rico-still-crisis-mode-n822536 [Accessed 23 March 2018].

Norwegian Meteorological Institute and Norwegian Broadcasting Corporation (2018). Ocean forecast for 62.41847 5.58153. Available at: https://www.yr.no/place/Ocean/62.41847_5.58153/ [Accessed February – April 2018]

Ocean Energy Forum (2016). Ocean Energy Strategic Roadmap 2016, building ocean energy for Europe. Available at: https://www.oceanenergy-europe.eu/wp-content/uploads/2017/10/OEF-final-strategic-roadmap.pdf

Paredes, G. M., Palm, J., Eskilsson, C., Bergdahl, L. & Taveira-Pinto, F. (2016). Experimental investigation of mooring configurations for wave energy converters. *International Journal of Marine Energy* 15: p. 56-67. http://dx.doi.org/10.1016/j.ijome.2016.04.009

Swedish Meteorological and Hydrological Institute (2018a). Oceanografiska observationer. Available at: http://opendata-download-ocobs.smhi.se/explore/ [Accessed 7 February 2018].

Swedish Meteorological and Hydrological Institute (2018b). Meteorologiska observationer. Available at: http://opendata-download-metobs.smhi.se/explore [Accessed 7 February 2018].

Swedish Maritime Administration. (2018). Swedish oceanographic stations. Available at: https://www.google.com/maps/d/u/0/viewer?hl=en&mid=14luDl4C9qKoi0klec7P3PgnEQ_k&ll=57.70358641414199%2C12.604555078125031&z=7

Thomson, C, Harrison, G. & Chick, J. (2011). Full Life Cycle Assessment of a Wave Energy Converter. *IET Renewable Power Generation Conference, Edinburgh, September 2011*. http://dx.doi.org/10.1049/cp.2011.0124

Uihlien, A. (2016). Life cycle assessment for ocean energy technologies. *The International Journal of Life Cycle Assessment* 21: 1425–1437. http://dx.doi.org/10.1007/s11367-016-1120-y

United Nations (2015a). Paris agreement. Available at: https://unfccc.int/sites/default/files/english_paris_agreement.pdf.

United Nations (2015b). Transforming our world: the 2030 agenda for sustainable development. Available at: http://www.un.org/ga/search/view_doc.asp?symbol=A/RES/70/1&Lang=E

Vegagerðin (2018a). Forecasts: Tides. Available at: http://www.vegagerdin.is/vs/ArealDetails.aspx?type=tides

Vegagerðin (2018b). Measurements: Wave buoys. Available at: http://www.vegagerdin.is/vs/Stations.aspx?st=1

Vegagerðin (2018c). Other information: Wave buoys. Available at: http://www.vegagerdin.is/vs/Content_1012.aspx?la=en

Vegagerðin (2018d). Weather stations: Garðskagi. Available at: http://www.vegagerdin.is/vs/Stationsdetails.aspx?ID=117

Vegagerðin (2018e). Weather stations: Grimsey. Available at: http://www.vegagerdin.is/vs/Stationsdetails.aspx?ID=120

Vicente, P. C., Falcão, A. F., Gato, L. M. C., & Justino, P. A. P. (2009). Dynamics of arrays of floating point-absorber wave energy converters with inter-body and bottom slack-mooring connections. *Applied Ocean Research* 31: p. 267-281. http://dx.doi.org/10.1016/j.apor.2009.09.002

WAFO-group (2017). *WAFO - a MATLAB toolbox for analysis of random waves and loads – a tutorial.* Sweden: Math. Stat., Center for Math. Sci., Lund Univ.

Waves4Power (2018a). Waves4Power – the solution. Available at: https://www.waves4power.com/waves4power-the-solution/ [Accessed 23 January 2018].

Waves4Power (2018b). Demonstration site at Runde, Norway. Available at: https://www.waves4power.com/demo-runde/ [Accessed 23 January 2018].

Windfinder (2018). Wind & weather statistics: Fosnavåg. Available at: https://www.windfinder.com/windstatistics/fosnavag [Accessed 27 February 2018].

World Commission on Environment and Development. (1987). Our Common Future. Available at: http://www.un-documents.net/our-common-future.pdf

World Energy Council. (2016). World Energy Resources: Marine Energy. Available at: https://www.worldenergy.org/wp-content/uploads/2017/03/WEResources_Marine_2016.pdf

Yang, S.-H., Ringsberg, J. W., Johnson, E., Hu, Z., & Palm, J. (2016). A comparison of coupled and de-coupled simulation procedures for the fatigue analysis of wave energy converter mooring lines. *Ocean Engineering* 117, p. 332-345. http://dx.doi.org/10.2016/j.oceaneng.2016.03.018

Yang, S.-H., Ringsberg, J. W., Johnson, E., & Hu, Z. (2017). Biofouling on mooring lines and power cables used in wave energy converter systems - analysis of fatigue life and energy performance. *Applied Ocean Research* 65: p. 166-177. http://dx.doi.org/10.1016/j.apor.2017.04.002

11 Appendix

Appendix 11.1: Frequency of Observed Wave, Wind and Current Directions

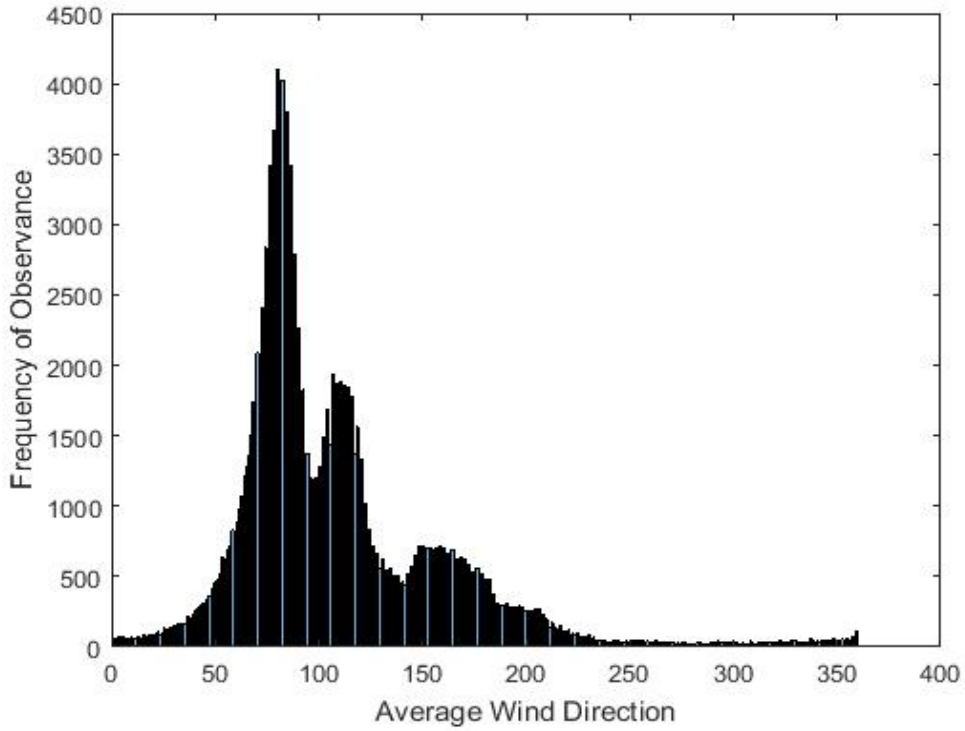

Figure 11.1.1: Frequency of average wind direction observances at San Juan site.

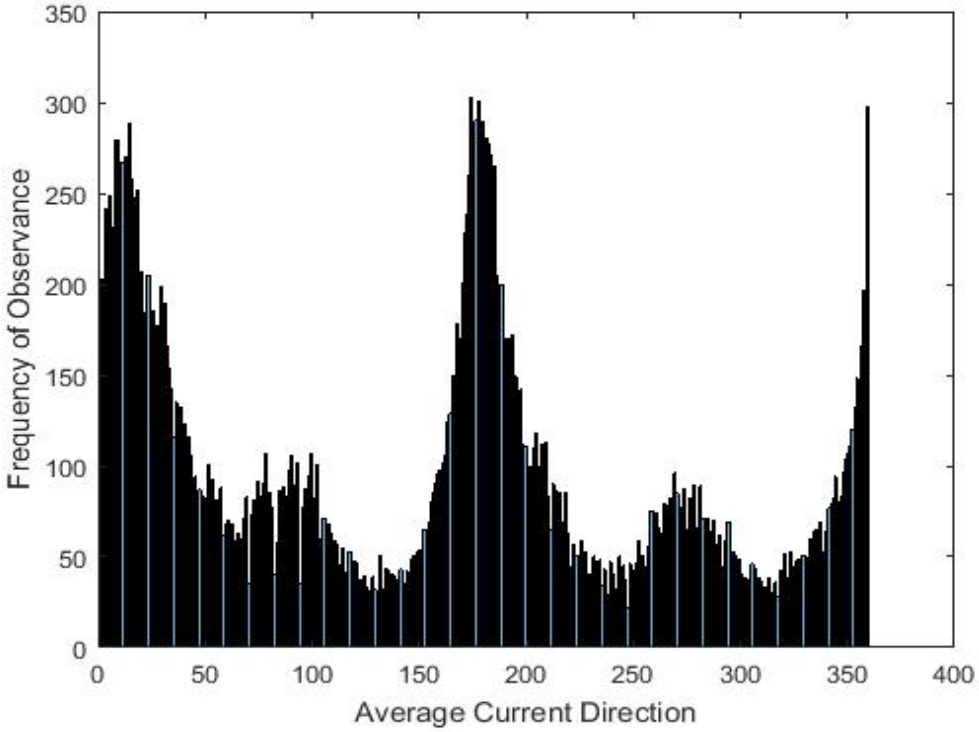

Figure 11.1.2: Frequency of average current direction observances at San Juan site.

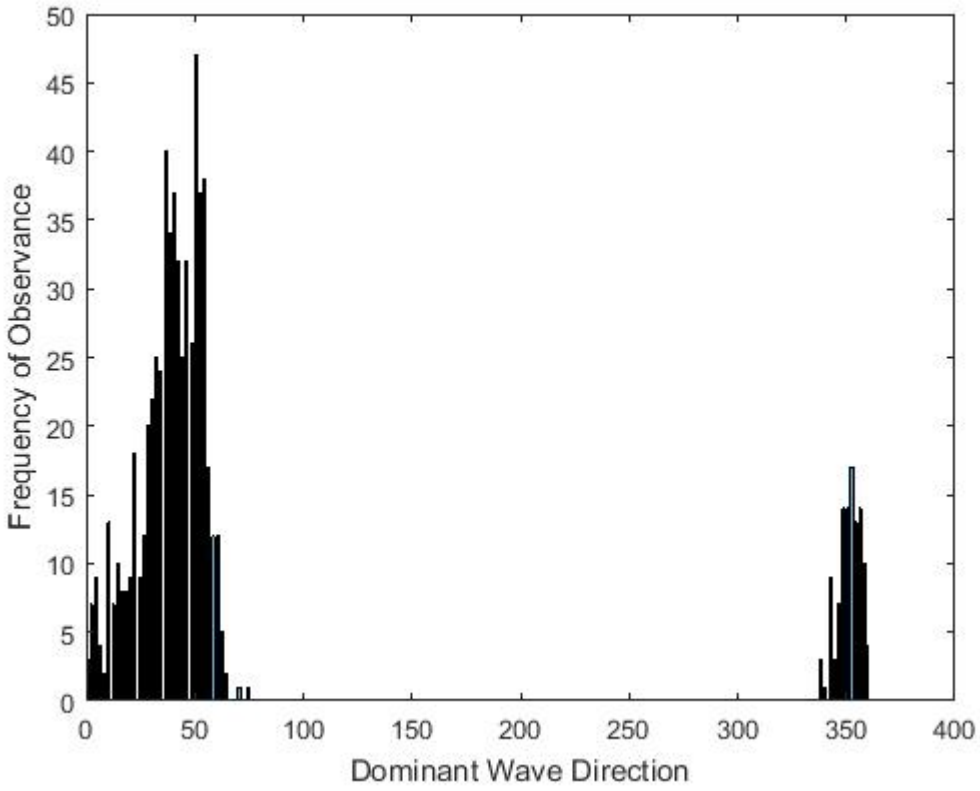

Figure 11.1.3: Frequency of average wave direction observances at San Juan site in September 2017.

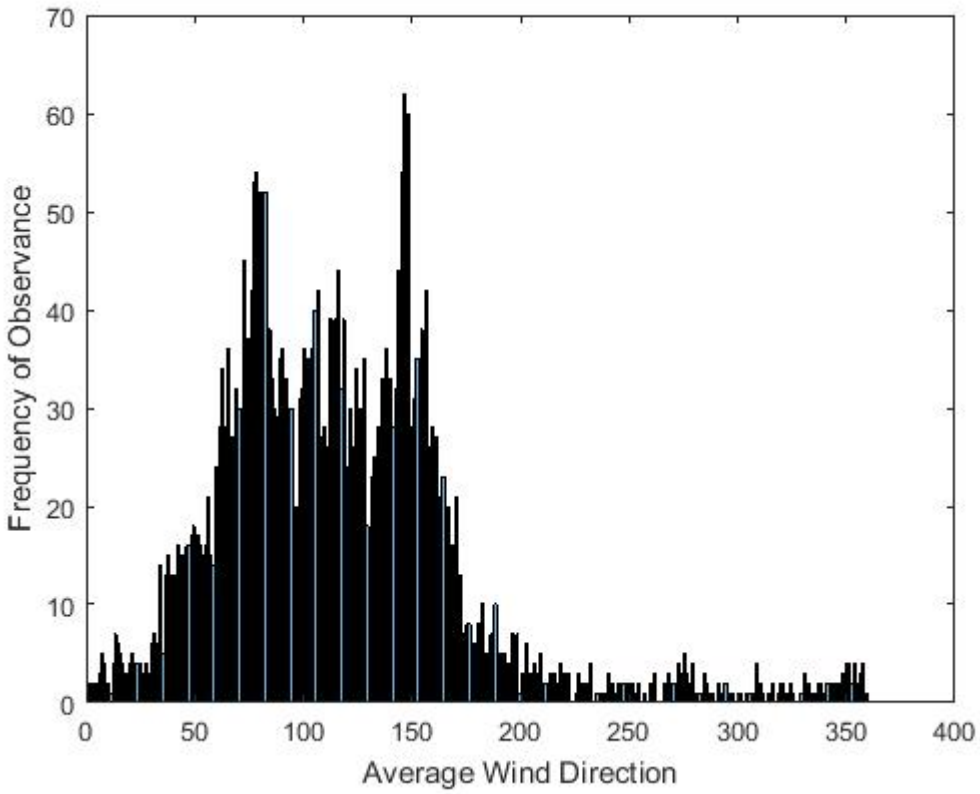

Figure 11.1.4: Frequency of average wind direction observances at San Juan site in September 2017.

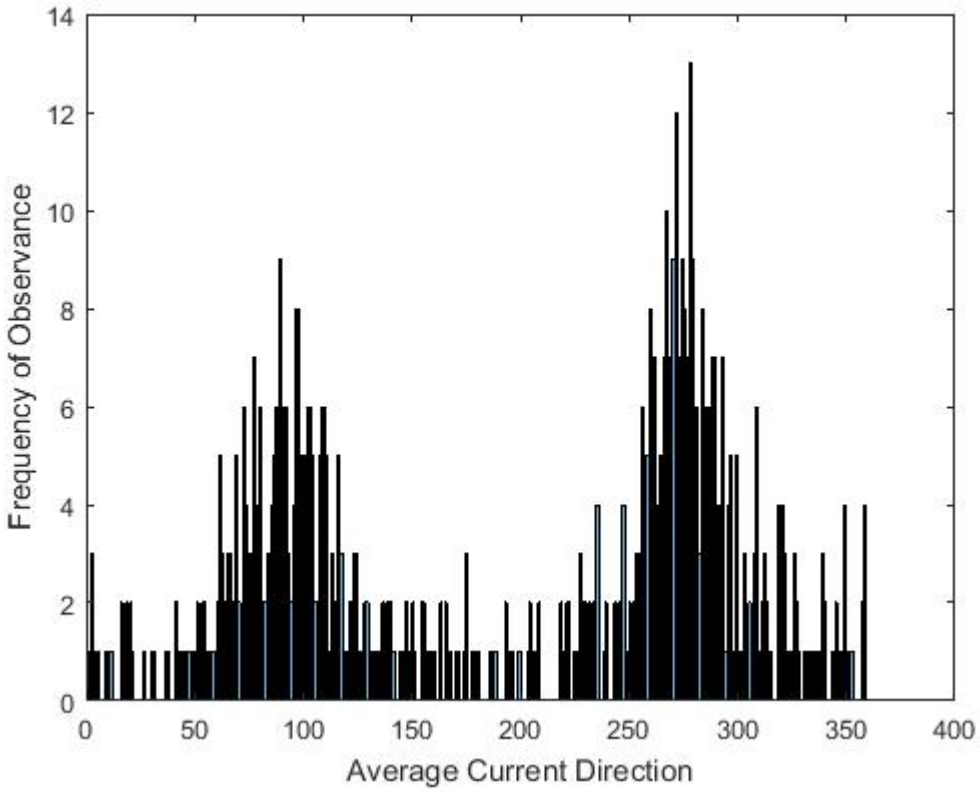

Figure 11.1.5: Frequency of average current direction observances at San Juan site in September 2017.

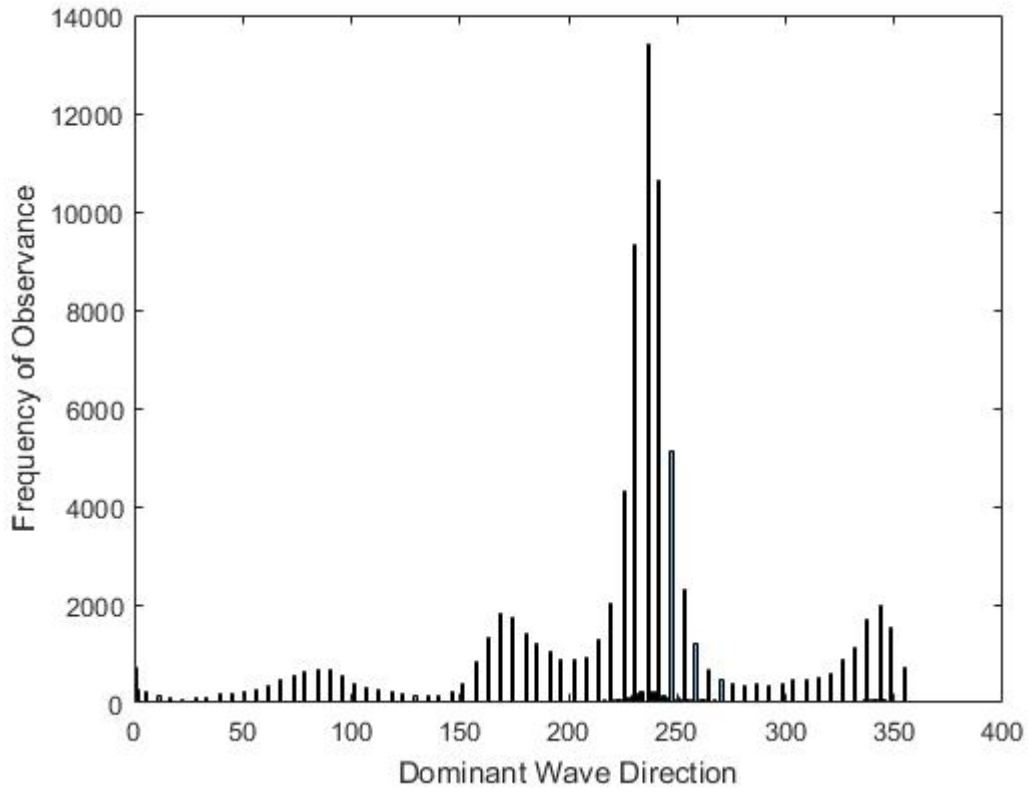

Figure 11.1.6: Dominant wave direction observed at Väderöarna site.

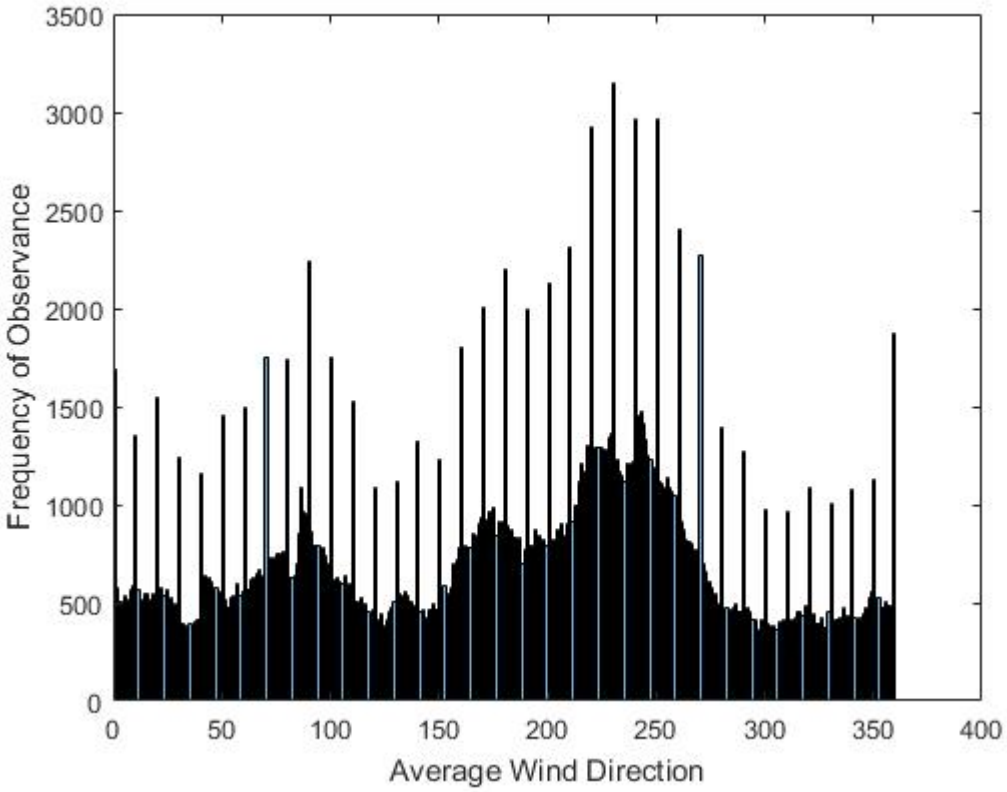

Figure 11.1.7: Dominant wind direction observed at Väderöarna site.

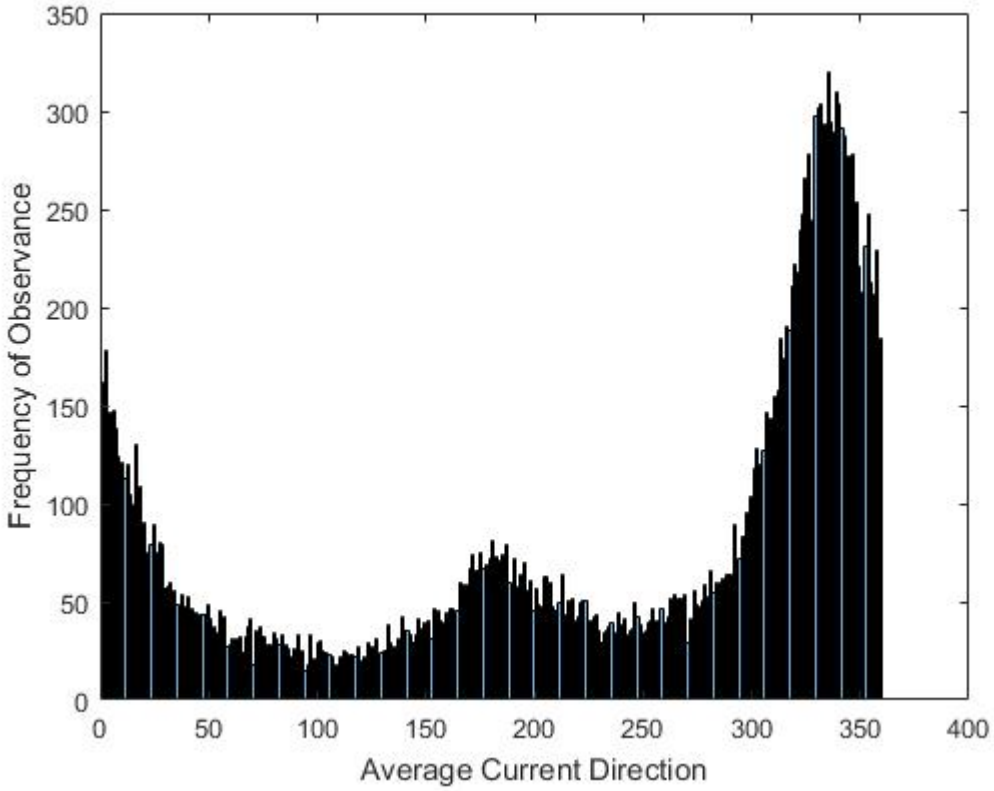

Figure 11.1.8: Dominant current direction observed at Väderöarna site.

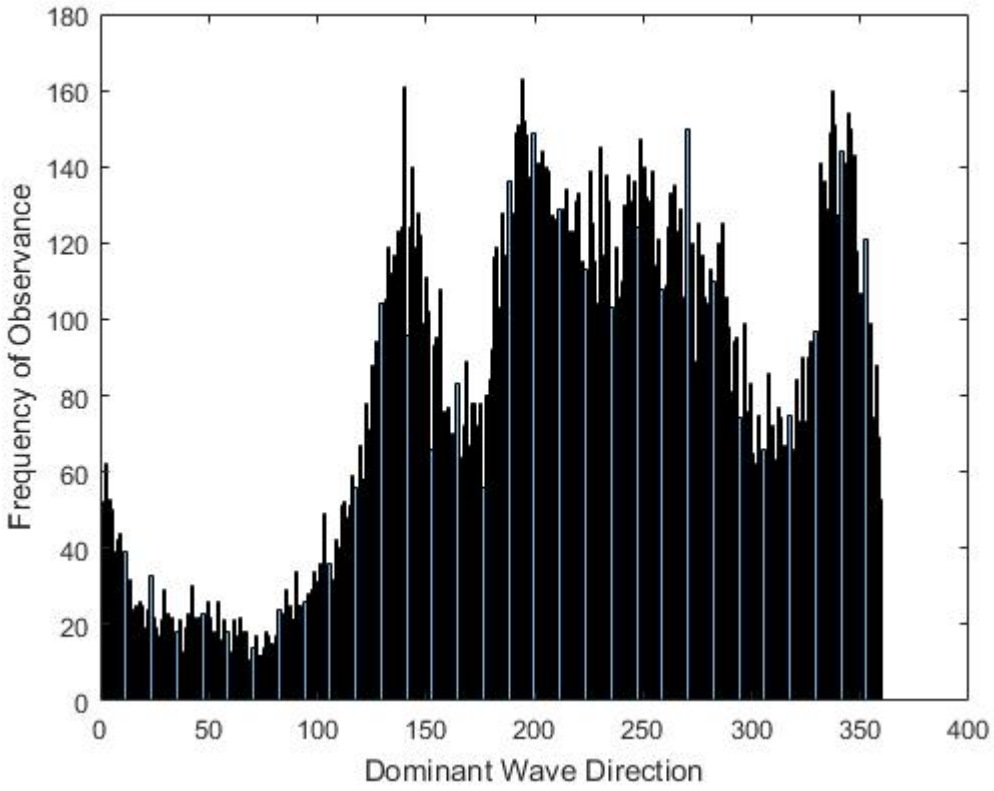

Figure 11.1.9: Dominant wave direction observed at Läsö Ost location.

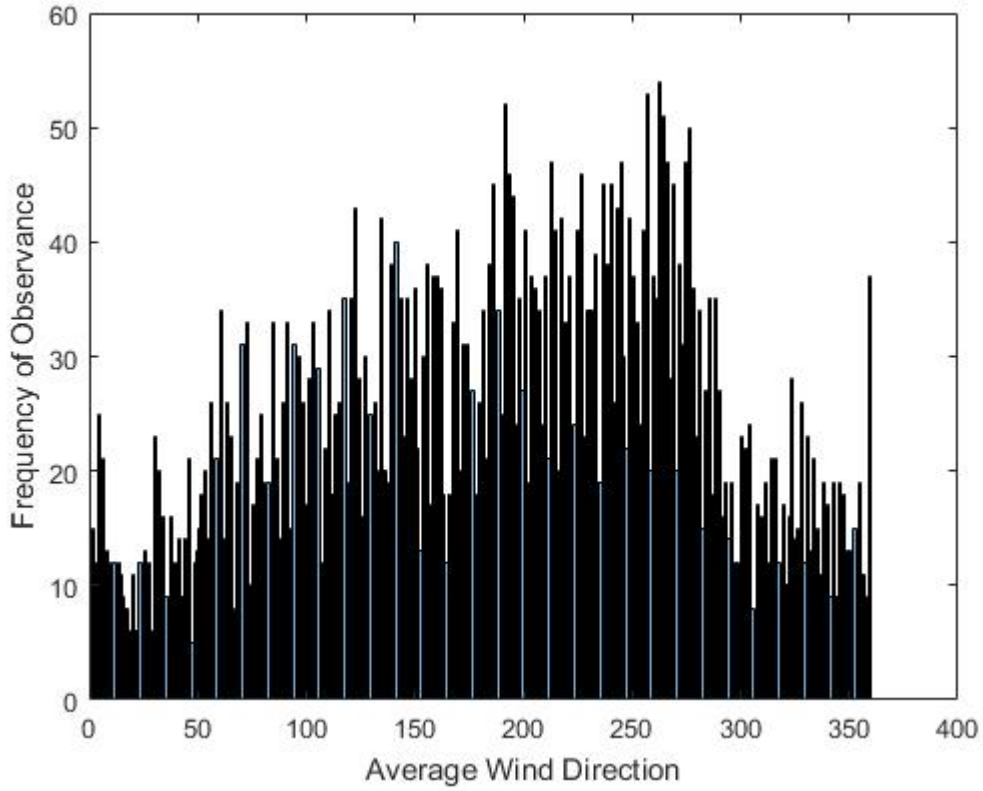

Figure 11.1.10: Dominant wind direction observed at Läsö Ost location.

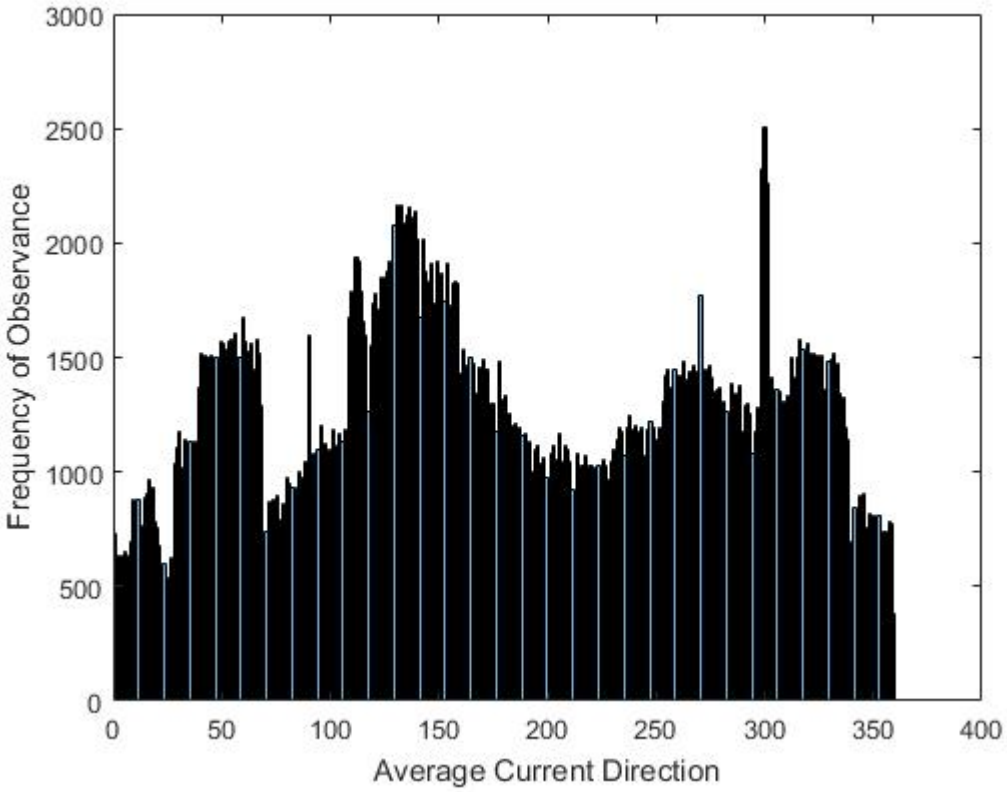

Figure 11.1.11: Dominant current direction observed at Läsö Ost location.

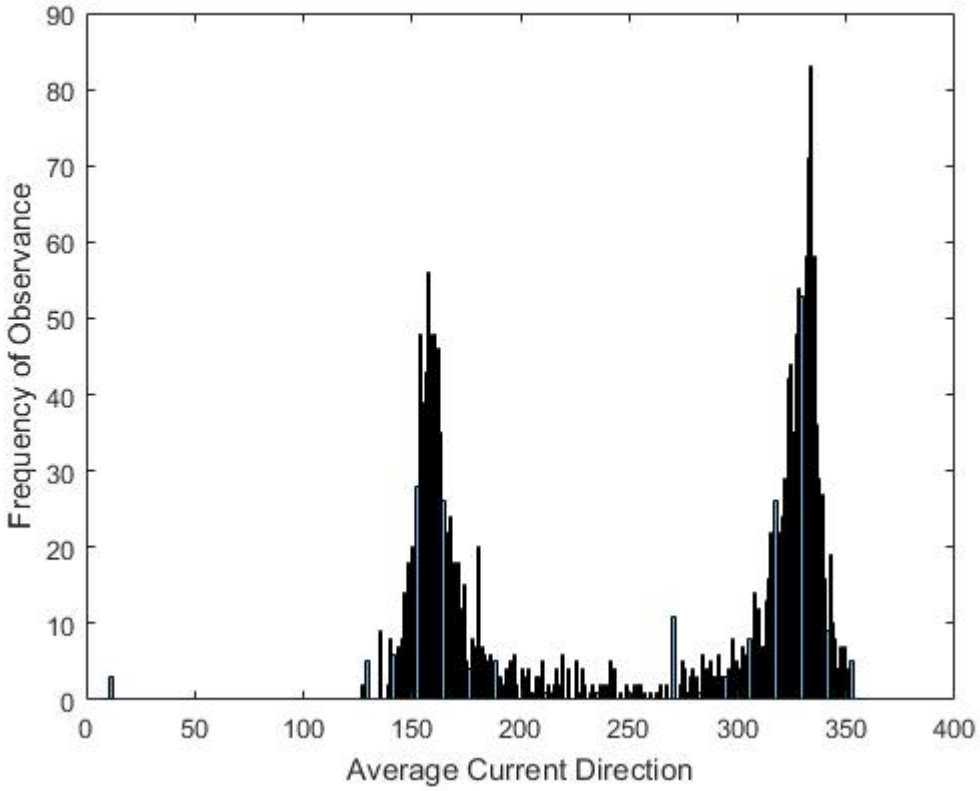

Figure 11.1.12: Dominant current direction observed at Garðskagi location.

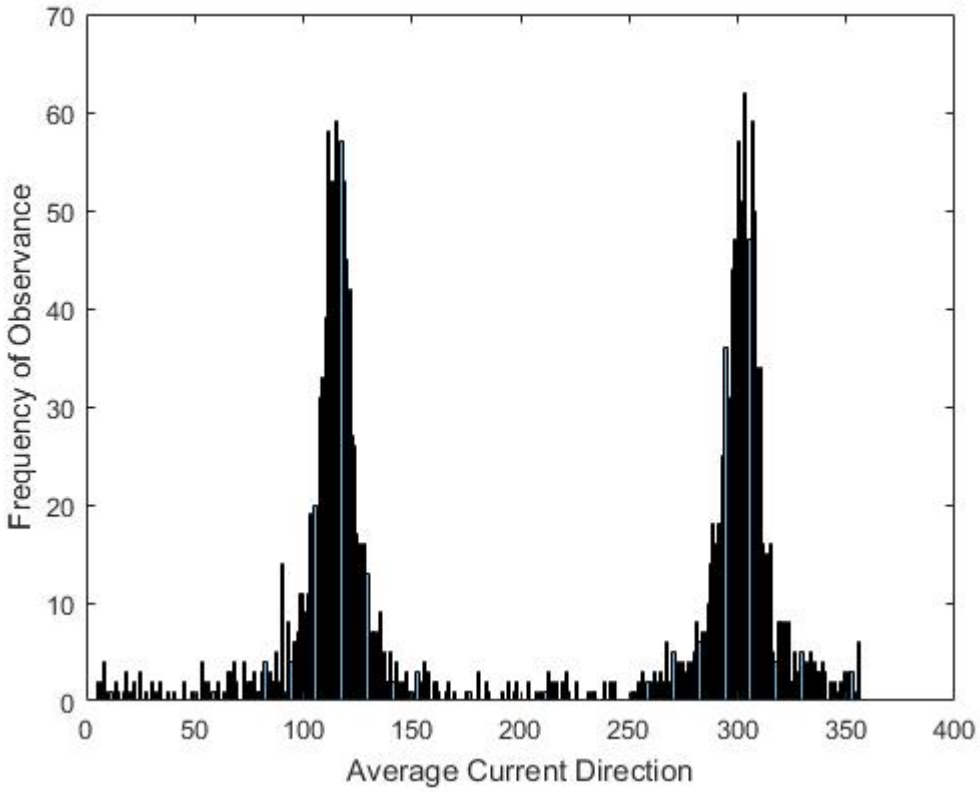

Figure 11.1.13: Dominant current direction observed at Grimseyjarsund location.

Appendix 11.2: Mooring Design Specifications for Single Buoy Configurations

11.2.1. V2 buoy models

Location	Mooring configuration number	Water depth (m)	Anchor radius (m)	Length of segment 1 (m)	Length of segment 2 (m)	Ratio segment 1/2 length
Runde	4	86.6	127.3	117	55	2.13
Runde	2	86.6	127.3	110	60	1.83
Runde	3	86.6	127.3	102	70	1.46
Runde	1	86.6	127.3	96	76.6	1.25
Runde	8	86.6	127.3	90	82	1.10
Runde	15	86.6	127.3	86	86	1
Runde	16	86.6	127.3	82	90	0.91
Runde	17	86.6	130	78	94	0.83
Runde	18	86.6	85	55	68	0.81
Runde	9	86.6	85	65	60	1.08
Runde	10	86.6	85	70	55	1.27
Runde	11	86.6	85	75	50	1.50
Runde	12	86.6	90	60	65	0.92
Runde	13	86.6	100	75	70	1.07
Runde	19	86.6	100	70	75	0.93

Runde	20	86.6	100	60	85	0.71
Runde	6	86.6	92	125	0	-
Runde	14	86.6	100	131	0	-
Runde	5	86.6	151	172	0	-
Runde	7	86.6	194	210	0	-
Runde	21	86.6	130	70	98	0.71
Runde	22	86.6	141	74	104	0.71
San Juan	1	32	75	50	35	1.43
San Juan	7	32	75	48	38	1.26
San Juan	6	32	75	45	40	1.13
San Juan	2	32	80	35	50	0.70
San Juan	8	32	80	50	40	1.25
San Juan	3	32	72	60	20	3
San Juan	14	32	70	55	25	2.20
San Juan	11	32	70	50	30	1.67
San Juan	12	32	70	48	32	1.50
San Juan	13	32	70	45	35	1.29
San Juan	15	32	70	40	40	1
San Juan	9	32	85	55	40	1.40

San Juan	10	32	90	60	40	1.50
San Juan	4	32	83	85	0	-
San Juan	16	32	70	75	0	-
San Juan	5	32	55	60	0	-
Väderöarna	1	75	125	80	80	1
Väderöarna	2	75	125	90	70	1.29
Väderöarna	3	75	125	70	90	0.78
Läsö Ost	1	70	125	78	78	1
Garðskagi	1	60	80	60	50	1.20
Garðskagi	2	60	80	54	54	1
Garðskagi	3	60	80	48	58	0.83
Garðskagi	4	60	100	62	62	1
Garðskagi	5	60	100	70	56	1.25
Garðskagi	6	60	100	76	50	1.52
Garðskagi	7	60	100	82	46	1.78
Garðskagi	8	60	120	72	70	1.03
Garðskagi	10	60	120	78	66	1.18
Garðskagi	9	60	120	82	62	1.32
Grimsey	3	96	120	72	86	0.84

Grimsey	1	96	120	78	82	0.95
Grimsey	2	96	120	86	76	1.13
Grimsey	4	96	120	94	70	1.34

11.2.2. V1 buoy models

Location	Mooring configuration number	Water depth (m)	Anchor radius (m)	Length of segment 1 (m)	Length of segment 2 (m)	Ratio segment 1/2 length
Runde	1	86.6	127.3	96	76.6	1.25
Runde	2	54.1	80	58	46	1.26
Runde	4	54.1	132	113	44	2.57
Runde	3	150	220.5	162	130	1.25
Runde	5	150	130	100	110	0.91
Runde	2	86.6	127.3	110	62	1.77
Runde	3	86.6	127.3	100	72	1.39
Runde	1	86.6	127.3	96	76.6	1.25
Runde	4	86.6	127.3	90	82	1.10
Runde	5	86.6	127.3	86	86	1
Runde	10	86.6	127.3	74	94	0.79
Runde	14	86.6	85	50	73	0.69
Runde	9	86.6	85	55	68	0.81

Runde	6	86.6	85	65	60	1.08
Runde	7	86.6	85	70	55	1.27
Runde	8	86.6	85	75	50	1.50
Runde	13	86.6	140	90	90	1
Runde	12	86.6	140	82	96	0.85
Runde	11	86.6	140	75	100	0.75
Garðskagi	1	60	120	72	70	1.03
Grimsey	1	96	120	78	82	0.95

Appendix 11.3: Mooring Design Specifications and Simulation Model for Each Array Configuration

11.3.1. Naming system

Design name: 1.2.3.4

1. Array type (“Tri” for TriBuoy, “Sq” for SquareBuoy)
    2. Buoy type (“V2” or “V1”)
        3. WEC separating distance
            4. Mooring configuration design number

Example: Tri.V2.173.1

11.3.2. Mooring design specifications

Design name	Anchor radius (m)	Mooring line segment 1 length (m)	Mooring line segment 2 length (m)	Ratio segment 1/2 length	Number of anchors to number of WECs
Tri.V2.173.1	100	80	65	1.23	6:3
Tri.V2.173.2	100	60	85	0.71	6:3
Tri.V2.173.3	100	60	85	0.71	7:3
Tri.V2.260.1	100	80	65	1.23	9:3
Tri.V2.260.2	100	60	85	0.71	9:3
Tri.V2.260.3	130	70	98	0.71	9:3
Tri.V2.260.4	150	92	92	1	6:3

Tri.V2.260.5	150	76	104	0.73	6:3
Tri.V2.260.6	100	60	85	0.71	9:3
Tri.V2.260.7	130	70	98	0.71	9:3
Tri.V2.260.8	150	76	104	0.73	7:3
Tri.V2.130.1	75	50	70	0.71	6:3
Tri.V2.130.2	75	55	65	0.85	6:3
Tri.V2.130.3	75	60	60	1	6:3
Tri.V1.173.1	100	60	85	0.71	6:3
Tri.V1.260.1	130	70	98	0.71	9:3
Tri.V1.130.1	75	50	70	0.71	6:3
Sq.V2.141.1	70	50	65	0.77	8:4
Sq.V2.141.2	75	50	70	0.71	12:4
Sq.V2.141.3	100	60	85	0.71	11:4
Sq.V2.141.4	100	60	85	0.71	9:4

Sq.V2.141.5	100	60	85	0.71	11:4
Sq.V2.282.1	100	60	85	0.71	12:4
Sq.V2.282.2	130	70	100	0.70	12:4
Sq.V2.282.3	130	70	100	0.70	12:4
Sq.V2.282.4	141	74	104	0.71	8:4
Sq.V2.282.5	141	74	104	0.71	12:4
Sq.V2.282.6	130	70	98	0.71	12:4

11.3.3. Top view of array models

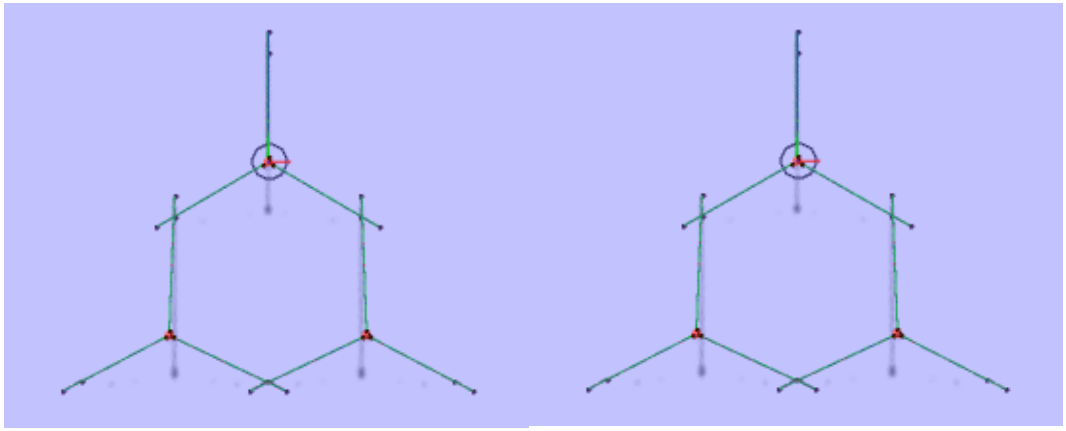

Tri.V2.173.1 Tri.V2.173.2

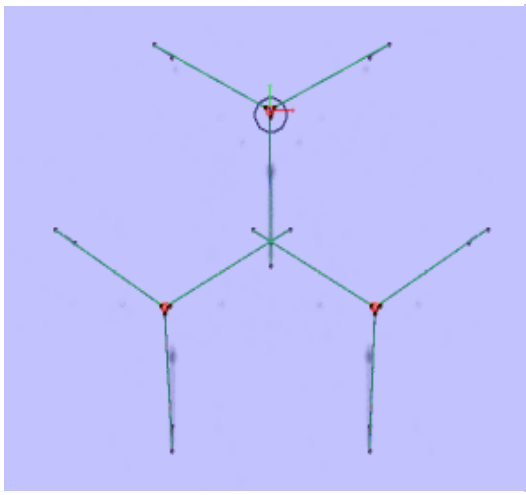

Tri.V2.173.3

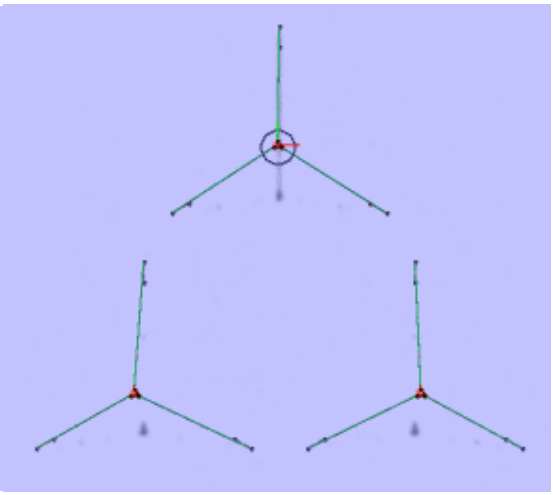

Tri.V2.260.1

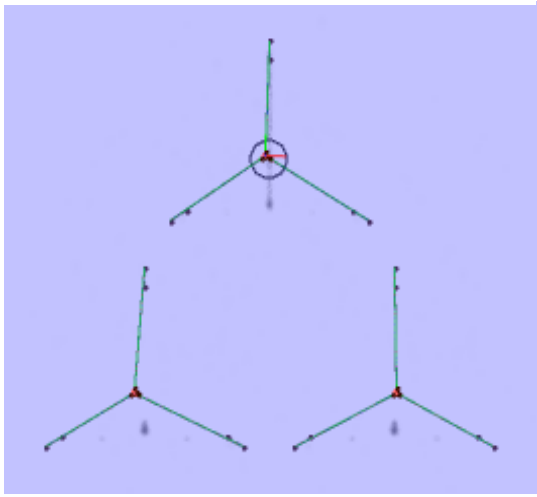

Tri.V2.260.2

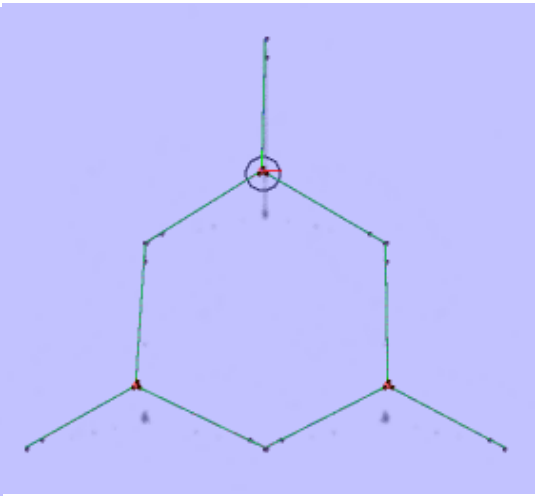

Tri.V2.260.3

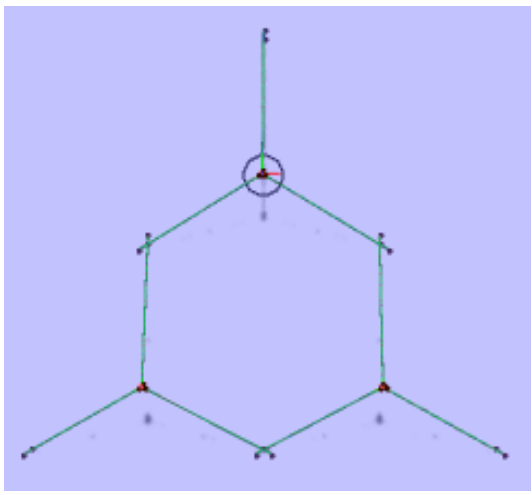

Tri.V2.260.4

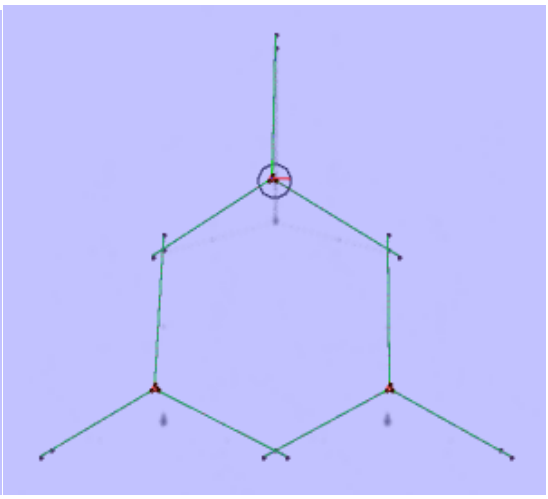

Tri.V2.260.5

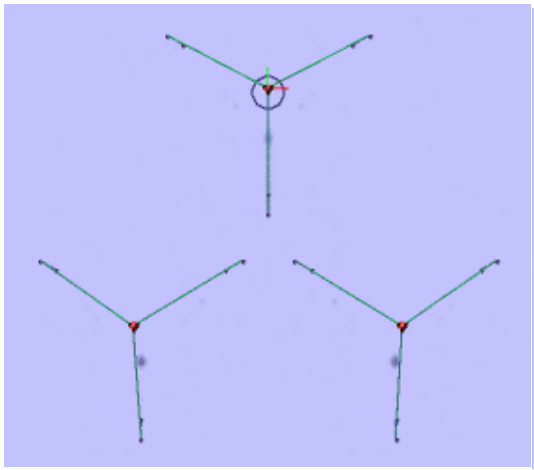

Tri.V2.260.6

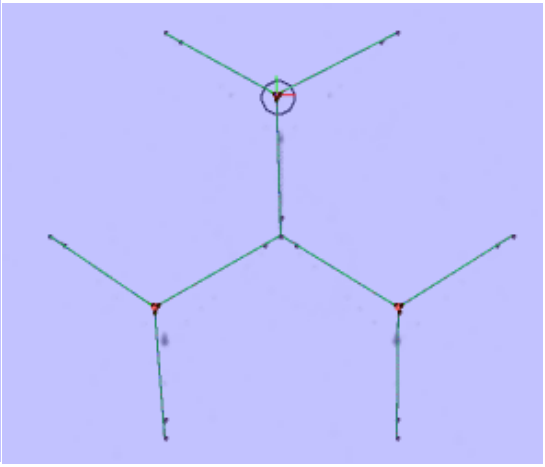

Tri.V2.260.7

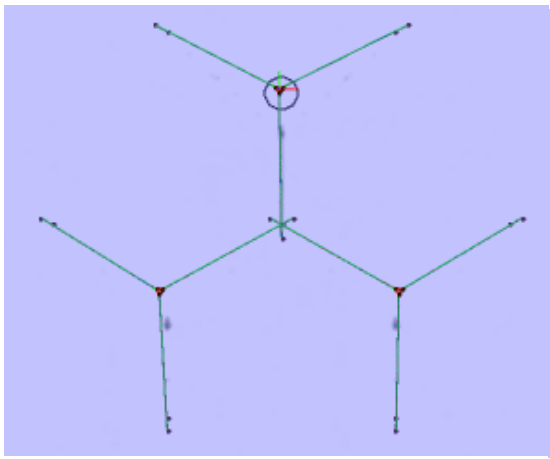

Tri.V2.260.8

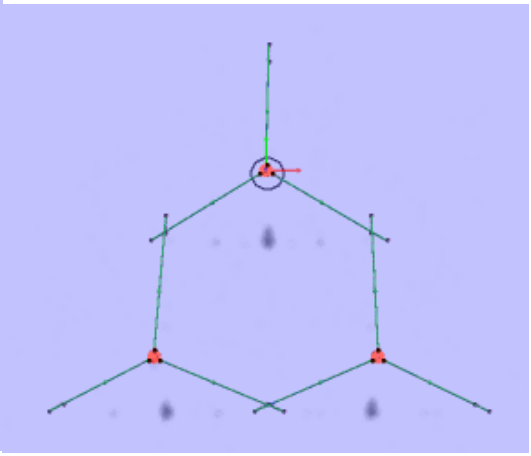

Tri.V2.130.1

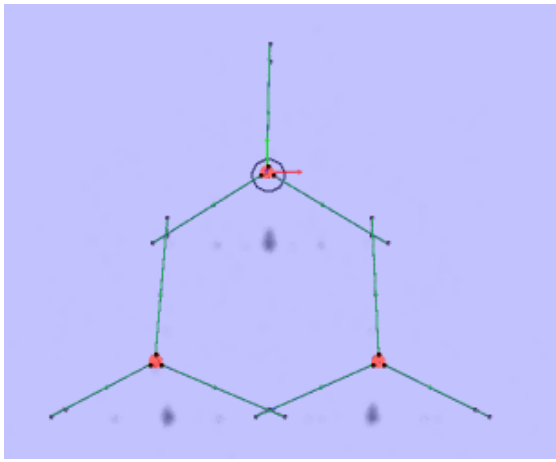

Tri.V2.130.2

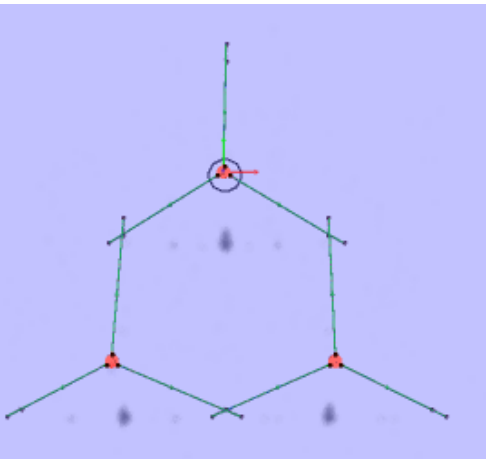

Tri.V2.130.3

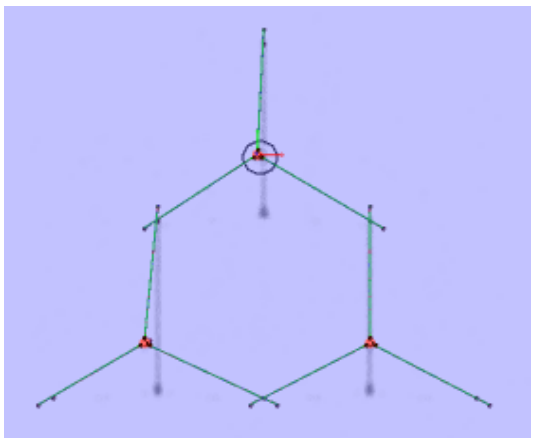

Tri.V1.173.1

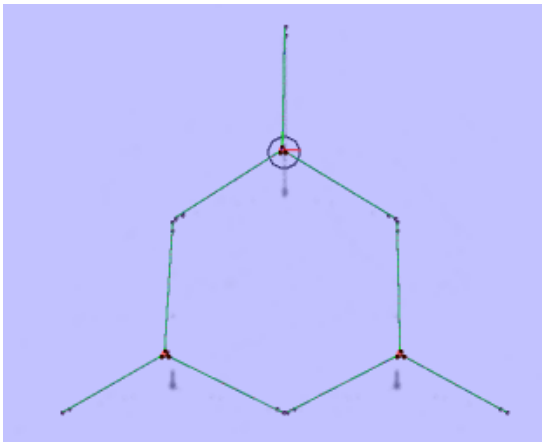

Tri.V1.260.1

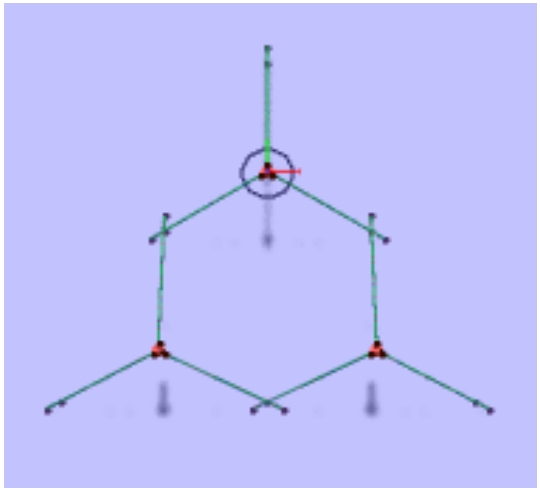

Tri.V1.130.1

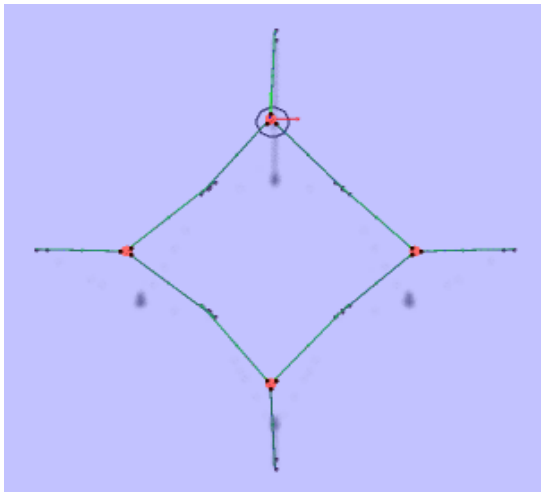

Sq.V2.141.1

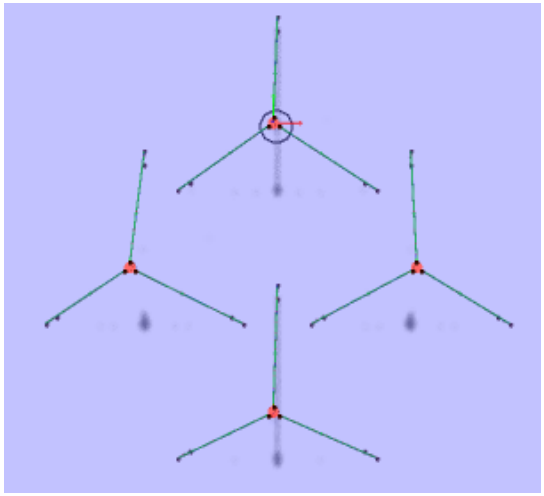

Sq.V2.141.2

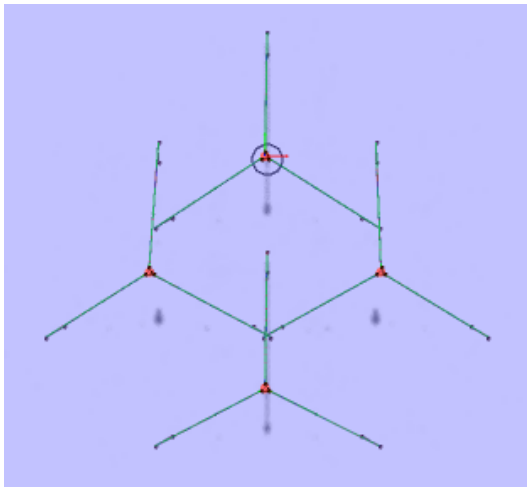

Sq.V2.141.3

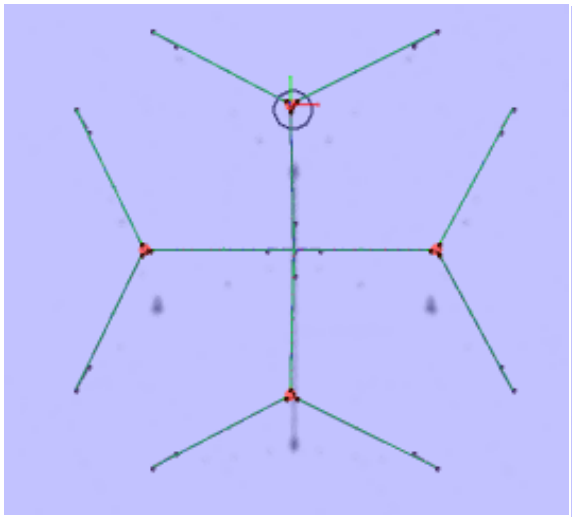

Sq.V2.141.4

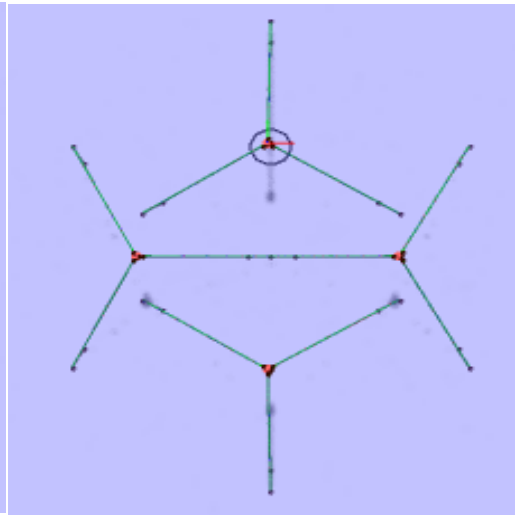

Sq.V2.141.5

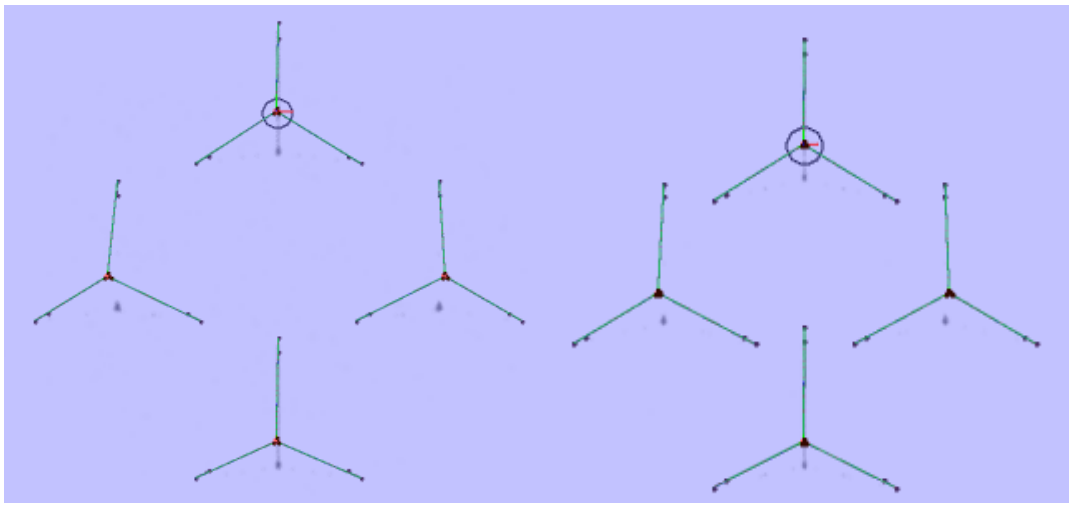

Sq.V2.282.1

Sq.V2.282.2

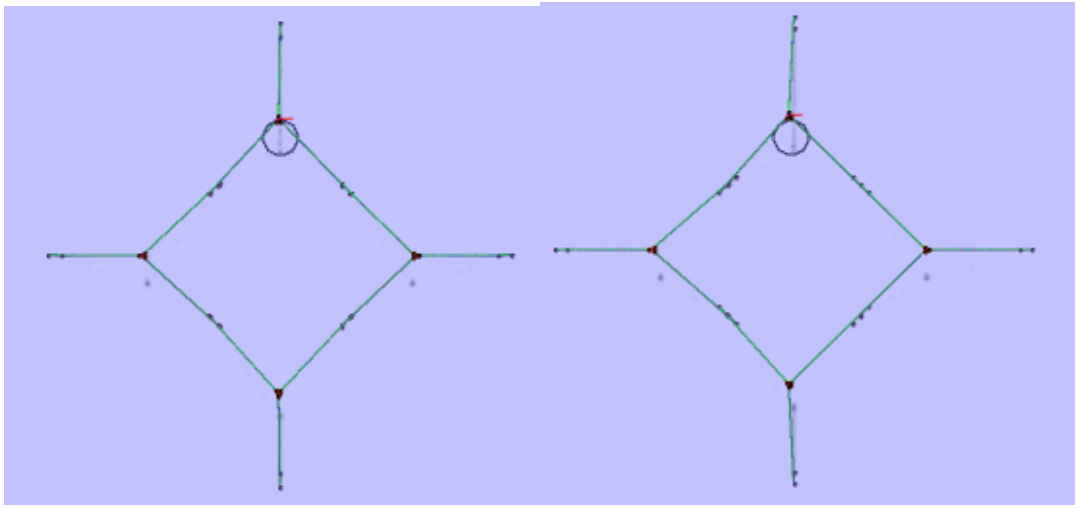

Sq.V2.282.3

Sq.V2.282.4

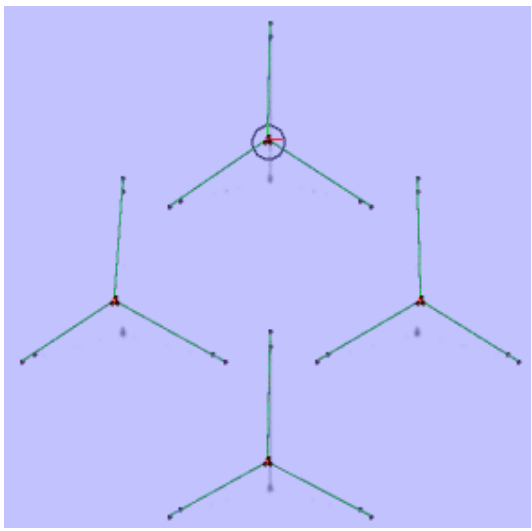

Sq.V2.282.5

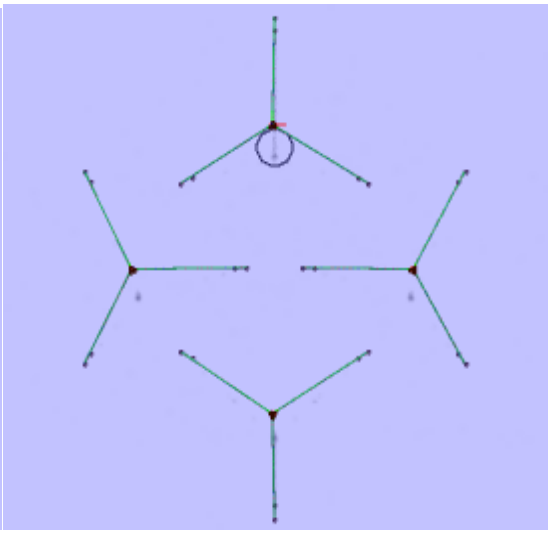

Sq.V2.282.6

Appendix 11.4: Static and Dynamic Calculation Parameters for Base Case Scenario

11.4.1 Static calculation parameters: Loading sequence

Load type	Run with previous?	N step	Max iterations	Accuracy
Volume forces	no	100	100	1E-06
Specified forces	Yes	100	100	1E-06
Specified displacements	No	100	100	1E-06
Boundary change	No	10	10	1E-06
Body forces	No	100	100	1E-06
Current forces	No	20	100	1E-06
Activate bottom friction forces	Yes	20	100	1E-06

11.4.2: Dynamic calculation parameters: Irregular analysis

Simulation length	Time step	Requested time series length	Time increment	Wave seed	Wind seed
10800	0.1	10800	0.2	4	4

11.4.3: Dynamic calculation parameters: Storage

Line	Line Type	Segment	Element Number	All Elements
w1Moor1	ltypMoor1	1	1	☐
w1Moor1	ltypMoor1	1	2	☐
w1Moor1	ltypMoor1	1	3	☐
w1Moor1	ltypMoor1	1	18	☐
w1Moor1	ltypMoor1	1	33	☐
w1Moor1	ltypMoor1	1	48	☐
w1Moor1	ltypMoor1	1	63	☐
w1Moor1	ltypMoor1	1	78	☐
w1Moor1	ltypMoor1	1	93	☐
w1Moor1	ltypMoor1	1	94	☐
w1Moor1	ltypMoor1	1	95	☐
w1Moor1	ltypMoor1	1	96	☐
w1Moor1	ltypMoor1	2	1	☐
w1Moor1	ltypMoor1	2	2	☐
w1Moor1	ltypMoor1	2	3	☐
w1Moor1	ltypMoor1	2	18	☐
w1Moor1	ltypMoor1	2	33	☐
w1Moor1	ltypMoor1	2	48	☐
w1Moor1	ltypMoor1	2	63	☐
w1Moor1	ltypMoor1	2	75	☐
w1Moor1	ltypMoor1	2	76	☐
w1Moor1	ltypMoor1	2	77	☐
w1Moor2	ltypMoor2	1	1	☐
w1Moor2	ltypMoor2	1	2	☐
w1Moor2	ltypMoor2	1	3	☐
w1Moor2	ltypMoor2	1	18	☐
w1Moor2	ltypMoor2	1	33	☐
w1Moor2	ltypMoor2	1	48	☐
w1Moor2	ltypMoor2	1	63	☐
w1Moor2	ltypMoor2	1	78	☐
w1Moor2	ltypMoor2	1	93	☐
w1Moor2	ltypMoor2	1	108	☐
w1Moor2	ltypMoor2	1	111	☐
w1Moor2	ltypMoor2	1	112	☐
w1Moor2	ltypMoor2	1	113	☐
w1Moor2	ltypMoor2	2	1	☐
w1Moor2	ltypMoor2	2	2	☐
w1Moor2	ltypMoor2	2	3	☐
w1Moor2	ltypMoor2	2	18	☐
w1Moor2	ltypMoor2	2	33	☐
w1Moor2	ltypMoor2	2	42	☐
w1Moor2	ltypMoor2	2	43	☐
w1Moor2	ltypMoor2	2	44	☐

w1Moor3	ltypMoor3	1	1	☐
w1Moor3	ltypMoor3	1	2	☐
w1Moor3	ltypMoor3	1	3	☐
w1Moor3	ltypMoor3	1	18	☐
w1Moor3	ltypMoor3	1	33	☐
w1Moor3	ltypMoor3	1	48	☐
w1Moor3	ltypMoor3	1	63	☐
w1Moor3	ltypMoor3	1	78	☐
w1Moor3	ltypMoor3	1	93	☐
w1Moor3	ltypMoor3	1	96	☐
w1Moor3	ltypMoor3	1	97	☐
w1Moor3	ltypMoor3	1	98	☐
w1Moor3	ltypMoor3	2	1	☐
w1Moor3	ltypMoor3	2	2	☐
w1Moor3	ltypMoor3	2	3	☐
w1Moor3	ltypMoor3	2	18	☐
w1Moor3	ltypMoor3	2	33	☐
w1Moor3	ltypMoor3	2	48	☐
w1Moor3	ltypMoor3	2	55	☐
w1Moor3	ltypMoor3	2	56	☐
w1Moor3	ltypMoor3	2	57	☐

Appendix 11.5: Graphical Representation of Forces in Mooring Lines from Base Case Scenario

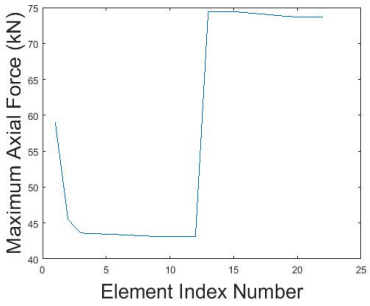

Figure 11.5.1a : Moor1

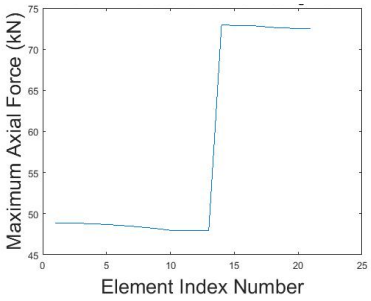

Figure 11.5.1b: Moor 2

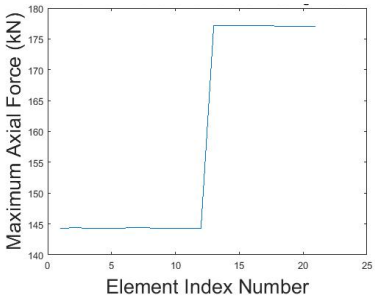

Figure 11.5.1c: Moor 3

Figures 11.5.1a-c: Maximum axial force per element in mooring lines 1, 2, and 3 in base case simulation results.

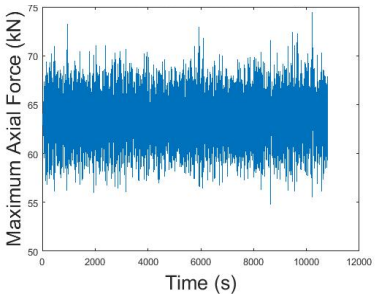

Figure 11.5.2a: Moor 1

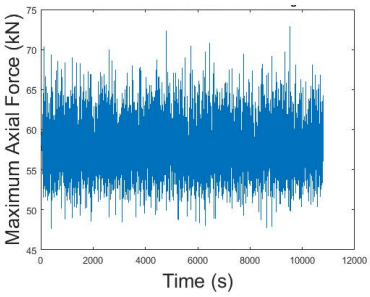

Figure 11.5.2b: Moor 2

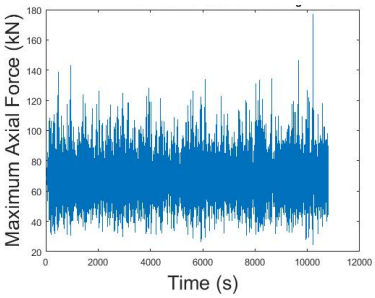

Figure 11.5.2c: Moor 3

Figures 11.5.2a-c: Maximum axial force per second in mooring lines 1, 2, and 3 in base case simulation results.

Appendix 11.6: Graphical Representation of Forces in Mooring Line 3 from Simulation Time Variation

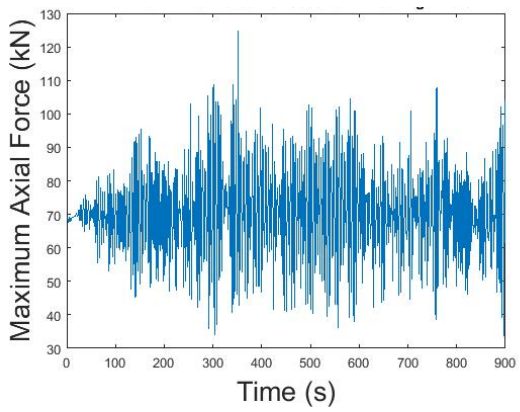

Figure 11.6.1a: Maximum axial force

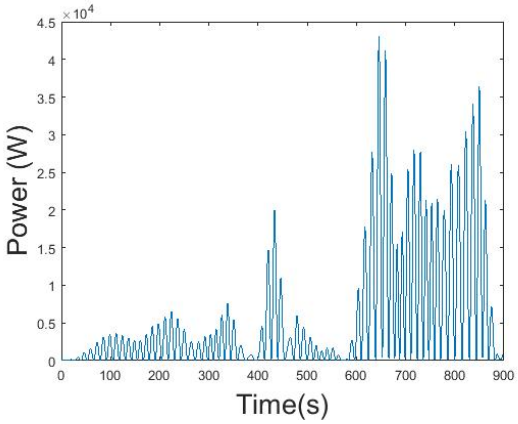

Figure 11.6.1b: Instantaneous power

Figure 11.6.1a-b: Maximum axial force per time step and instantaneous power per time step in 15 minute simulation.

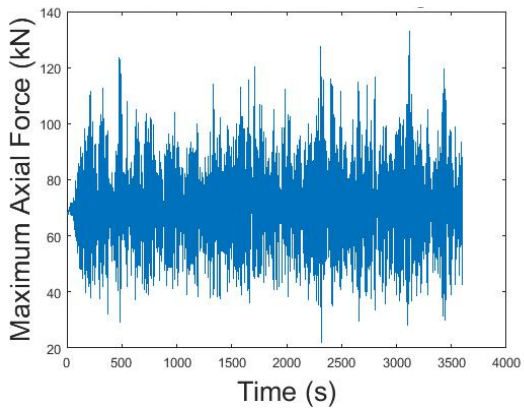

Figure 11.6.2a: Maximum axial force

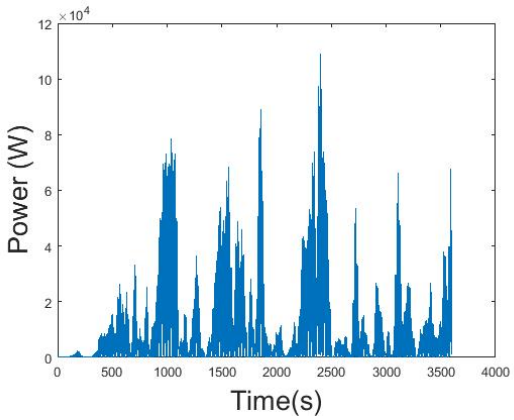

Figure 11.6.2b: Instantaneous power

Figure 11.6.2a-b: Maximum axial force per time step and instantaneous power per time step in 1 hour simulation.

Appendix 11.7: LCOE Input Data (MATLAB)

```
% System parameters

N=1; % Number of devices in the array

Nts=1; % Number of transformers in the array

N_hub=1; % Number of hubs in array

N_farm=25; % Lifetime of wave power farm

N_anc=3; % Number of anchors per device

mass_anc=40000*N_anc; % total mass of anchors in kg per device

N_float=3; % Number of floaters per device

N_lines=3; % number of mooring lines per device

length_moor=(4+58+82)*N_lines; % Total length of mooring lines per device
(fairlead radius + segment 1 + segment 2)


P=12.81; % Average power produced per array (kW)

eta_avi=1; % percentage of availability

eta_trans=1; % transmission efficiency

r=1.10; % capital cost of project


% Cable data - electric cables

Nb=1*N; % Number of electric cables from buoy to hub

db=135; % length of electric cables from buoy to hub

cb=60; % Cost in euro per meter of electric cables from buoy to hub


Nd=1; % Number of electric cables from hub to land

dd=926; % length of electric cables from hub to land

cd=100; % Cost in euro per meter of electric cables from hub to land


% C1 Concept development cost

C11 = 0; % market study cost

C12 = 0; % legislative factors cost

Cemet = 0; % sea conditions study

Csmet = 0; % sea conditions study

Csamet = 0; % sea conditions study
```

```
Clm = 0; % geotechnical characteristic study
C13 = (Cemet+Csmet+Csamet) + (Clm*P); % location study
C1 = C11 + C12 + C13;

% C2 Design and development cost
Cga = 0; % cost of design and development per unit
C2 = Cga*P;

% C3 Manufacturing cost
Cmw = 8.5*10^5; % cost of WEC in euros
C31 = Cmw*N; % cost of fabricating the device generators
C32 = 0; % cost of fabricating floating platforms
Cmoor = 86.3; % cost in euro per meter of mooring line
C331 = Cmoor*length_moor*N; % cost of fabricating mooring lines
Cfloater = 37500; %cost in euro per floater
C332 = Cfloater*N_float*N; % cost of fabricating floaters
C33 = C331 + C332;
Canc = 0.4375; % cost of anchor in euro/kg;
C34 = Canc*mass_anc*N; % cost of fabricating anchors
C351 = db*cb*Nb + dd*cd*Nd; % cost of fabricating cables
Chub = 150000; % cost of fabricating hub
C352 = Chub;
C35 = C351 + C352; % cost of fabricating the cable and hub
C3 = C31 + C32 + C33 + C34 + C35;

% C4 Installation cost
C41 = 10000*N; % cost of installing device
C42 = 0; % cost of installing floating platforms
C43 = 5000*N_lines*N; % cost of installing mooring lines
C44 = 8333*N_anc*N; % cost of installing anchors
C45 = 50000; % cost of installing the cable and hub
C4 = C41 + C42 + C43 + C44 + C45;
```

```
% C5 Exploitation cost
% Change of mooring lines X times per life, 25k euro/system
C_inspect=500*N; %for system
n_inspect=2; %Number of planned inspections per year
C_change_moor=25000; % For one wec
N_change=0; %number of change of mooring lines during farms life
C51 = 0.01*(C1+C2+C3+C4); % insurance cost
C52 = 0; % business and administration cost
C531 = N_farm*n_inspect*C_inspect; % preventative maintenance cost
C532 = N_change*(C_change_moor*N+C33+C34); % corrective maintenance cost
C53 = C531+C532; % operation and maintenance (O&M) cost
C5 = C51 + C52 + C53;

% Dismantling
C6=10000*N;

% LCOE
C=C1+C2+C3+C4+C5+C6;

% Energy produced
E=P*eta_avi*eta_trans*365*24/1000;

% First year
LCS_0=C-C5-C6;
LCOE_0t=(LCS_0/((1+r)^0));
LCOE_0n=(E/(1+r)^0);

% Last year
LCS_N=C5/N_farm+C6;
LCOE_Nt=(LCS_N/((1+r)^N_farm));
LCOE_Nn=(E/(1+r)^N_farm);
```

```
% Operational years
LCS=C5/N_farm;
LCOEt=0;
LCOEn=0;

for n=2:N_farm-1
   LCOEt=LCOEt+(LCS/((1+r)^n));
   LCOEn=LCOEn+(E/((1+r)^n));
end

% LCOE considering the full life time
LCOE=(LCOE_0t+LCOEt+LCOE_Nt)/(LCOE_0n+LCOEn+LCOE_Nn)
```

Appendix 11.8: LCA Input Data (OpenLCA)

Process: manufacturing V2 WEC	
Material	Steel sections
Weight	268416 kg
Process: manufacturing V1 WEC	
Material	Steel sections
Weight	452898 kg
Process: manufacturing mooring lines	
Material	Polyester (polyethylene terephthalate fibers)
Weight/length	8.55 kg/m
Number of mooring lines per WEC	3
Length per WEC	529.8 m
Total weight per WEC	4527 kg
Process: manufacturing anchors	
Material	Concrete (Portland cement)
Weight	40000 kg
Number of anchors per WEC	3
Total weight per WEC	120000 kg
Process: manufacturing floaters	
Material	Polyethylene
Weight	2700 kg
Number of floaters per WEC	3
Total weight per WEC	8100 kg
Process: mounting	
Distance to mounting location	911 km
Type of transport	Lorry
Process: installation	
Distance to installation location	1500 km
Type of transport	Oceanic ship
Process: maintenance	
Distance travelled per maintenance trip	5.56 km
Number of times per year	2
Number of times in lifetime	50
Distance travelled in lifetime	278 km
Type of transport	Oceanic ship
Process: discarding	
Distance to shore	1500 km
Type of transport	Oceanic ship
Distance to scrapyard	911 km
Type of transport	Lorry